Structures and Materials Research Report No. 92-1 December 1992
DRAFT FINAL PROJECT REPORT

UF Project No. 4910450436812
State Project No. 99700-7541-119
WPI No. 0510585

Contract No. C-4072
HPR Study No. 0585

EVALUATION OF A POST-TENSIONED FLAT-SLAB BRIDGE SYSTEM FOR FATIGUE AND ULTIMATE LOAD

Ronald A. Cook
Fernando E. Fagundo
Adrian D. Rozen
Haskel Mayer
D. E. Richardson

Department Of Civil Engineering
College of Engineering
UNIVERSITY OF FLORIDA
Gainesville

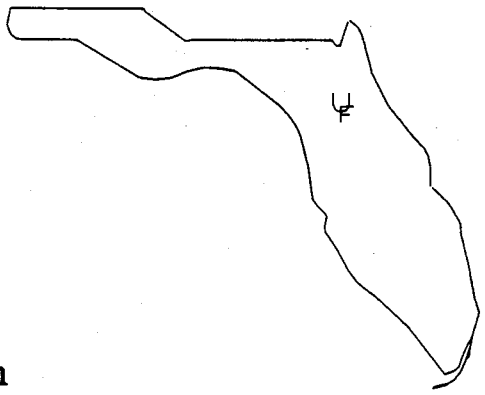

Engineering and Industrial Experiment Station

Technical Report Documentation Page

1. Report No.	2. Government Accession No.	3. Recipient's Catalog No.
FL/DOT/RMC/0585-4072		

4. Title and Subtitle	5. Report Date
EVALUATION OF A POST-TENSIONED FLAT-SLAB BRIDGE SYSTEM FOR FATIGUE AND ULTIMATE LOAD	December 1992
	6. Performing Organization Code
7. Author(s) R.A. Cook, F.E. Fagundo, A.D. Rozen, H. Mayer D.E. Richardson	8. Performing Organization Report No. 4910450436812
9. Performing Organization Name and Address University of Florida Department of Civil Engineering 345 Weil Hall Gainesville, FL 32611-2083	10. Work Unit No. (TRAIS)
	11. Contract or Grant No. HPR 0585
12. Sponsoring Agency Name and Address Florida Department of Transportation Research Management Center 605 Suwannee Street, M.S. 30 Tallahassee, FL 32301-8064	13. Type of Report and Period Covered Final Draft Report 10/1/91 - 12/30/92
	14. Sponsoring Agency Code 99700-7541-119

15. Supplementary Notes

Prepared in cooperation with the Federal Highway Administration

16. Abstract

A new type of short-span bridge system for traversing wetlands and shallow waters (i.e., a trestle-type bridge) has been developed and implemented over the Albemarle Sound south of Edenton, North Carolina. The new system incorporates precast flat-slab sections that are post-tensioned for continuity. The new system has the potential to replace traditional trestle-type bridges constructed using simple-span prestressed beams with a cast-in-place deck.

A continuous two-span, half-scale model of this precast, post-tensioned, flat-slab bridge system was built and tested under various load conditions. The bridge was evaluated analytically and experimentally for the transfer load case (dead load plus prestress), the maximum negative moment service load case, the maximum positive moment service load case, fatigue load, cracking load, and ultimate load. Results for the transfer load case, the maximum negative moment service load case, and the maximum positive moment service load case have been presented in a previous test. This report provides the results of the fatigue load test, the cracking load test, and the ultimate load test.

The model bridge performed as predicted for all load cases. Comparisons between analytical and physical models showed good correlation for all types of tests. At service load levels the bridge exhibited an elastic response with no evidence of cracking. The results of the fatigue load tests showed no degradation of stiffness. The ultimate load and deflections of the new bridge system were readily predicted by standard behavioral models for prestressed concrete.

17. Key Words	18. Distribution Statement
Bridges, Concrete, Precast, Prestressed, Post-Tensioned, Flat Slab, Segmental	No restrictions. This document is available to the public through the National Technical Information Service, Springfield VA, 22161

19. Security Classif. (of this report)	20. Security Classif. (of this page)	21. No. of Pages	22. Price
Unclassified	Unclassified	115	

Approximate Conversions to Metric Measures

Symbol	When You Know	Multiply by	To Find	Symbol
		LENGTH		
in	inches	*2.5	centimeters	cm
ft	feet	30	centimeters	cm
yd	yards	0.9	meters	m
mi	miles	1.6	kilometers	km
		AREA		
in^2	square inches	6.5	square centimeters	cm^2
ft^2	square feet	0.09	square meters	m^2
yd^2	square yards	0.8	square meters	m^2
mi^2	square miles	2.6	square kilometers	km^2
	acres	0.4	hectares	ha
		MASS (weight)		
oz	ounces	28	grams	g
lb	pounds	0.45	kilograms	kg
	short tons (2000 lb)	0.9	tonnes	t
		VOLUME		
tsp	teaspoons	6	milliliters	ml
Tbsp	tablespoons	15	milliliters	ml
fl oz	fluid ounces	30	milliliters	ml
c	cups	0.24	liters	l
pt	pints	0.47	liters	l
qt	quarts	0.95	liters	l
gal	gallons	3.8	liters	l
ft^3	cubic feet	0.03	cubic meters	m^3
yd^3	cubic yards	0.76	cubic meters	m^3
		TEMPERATURE (exact)		
°F	Fahrenheit temperature	5/9 (after subtracting 32)	Celsius temperature	°C

* 1 in. = 2.54 (exactly). for other exact conversions and more detailed tables, see NBS Misc. Publ. 286, Units of Weights and Measures, Price $2.25, SD Catalog No. C13.10.286.

Approximate Conversions from Metric Measures

Symbol	When You Know	Multiply by	To Find	Symbol
		LENGTH		
mm	millimeters	0.04	inches	in
cm	centimeters	0.4	inches	in
m	meters	3.3	feet	ft
m	meters	1.1	yards	yd
km	kilometesr	0.6	miles	mi
		AREA		
cm^2	square centimeters	0.16	square inches	in^2
m^2	square meters	1.2	square yards	yd^2
km^2	square kilometers	0.4	square miles	mi^2
ha	hectares (10,000 m^2)	2.5	acres	
		MASS (weight)		
g	grams	0.035	ounces	oz
kg	kilograms	2.2	pounds	lb
t	tonnes (1000 kg)	1.1	short tons	
		VOLUME		
ml	milliters	0.03	fluid ounces	fl oz
l	liters	2.1	pints	pt
l	liters	1.06	quarts	qt
l	liters	0.26	gallons	gal
m^3	cubic meters	35	cubic feet	ft^3
m^3	cubic meters	1.3	cubic yards	yd^3
		TEMPERATURE (exact)		
°C	Celsius temperature	9/5 (then add 32)	Fahrenheit temperature	°F

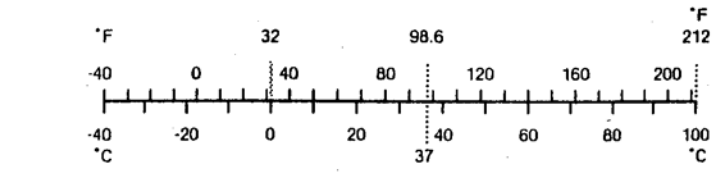

METRIC CONVERSION FACTORS

DISCLAIMER

"The opinions, findings and conclusions expressed in this publication are those of the authors and not necessarily those of the Florida Department of Transportation or the U.S. Department of Transportation.

Prepared in cooperation with the State of Florida Department of Transportation and the U.S. Department of Transportation."

SUMMARY

A new type of short-span bridge system for traversing wetlands and shallow waters (i.e., a trestle-type bridge) has been developed and implemented over the Albemarle Sound south of Edenton, North Carolina. The new system incorporates precast flat-slab sections that are post-tensioned for continuity. The new system has the potential to replace traditional trestle-type bridges constructed using simple-span prestressed beams with a 'cast-in-place deck.

A continuous two-span, half-scale model of this precast, post-tensioned, flat-slab bridge system was built and tested under various load conditions. The bridge was evaluated analytically and experimentally for the transfer load case (dead load plus prestress), the maximum negative moment service load case, the maximum positive moment service load case, fatigue load, cracking load, and ultimate load. Results for the transfer load case, the maximum negative moment service load case, and the maximum positive moment service load case have been presented in a previous test. This report provides the results of the fatigue load test, the cracking load test, and the ultimate load test.

The model bridge performed as predicted for all load cases. Comparisons between analytical and physical models showed good correlation for all types of tests. At service load levels the bridge exhibited an elastic response with no

evidence of cracking. The results of the fatigue load tests showed no degradation of stiffness. The ultimate load and deflections of the new bridge system were readily predicted by standard behavioral models for prestressed concrete.

With the apparent cost savings, short erection time, and multi-span continuity of this system it should be considered as a viable alternative to the standard girder systems available.

EVALUATION OF A POST-TENSIONED FLAT-SLAB BRIDGE SYSTEM FOR FATIGUE AND ULTIMATE LOAD

B_y
Ronald A. Cook, P.E.
Fernando E. Fagundo, P.E.
Adrian D. Rozen
Haskel Mayer
Daniel E. Richardson

Department of Civil Engineering
College of Engineering
University of Florida
Gainesville, Florida

TABLE OF CONTENTS

CHAPTERS

CHAPTER 1

INTRODUCTION

1.1 General

The selection of a bridge system for any particular application is linked to the site's physical constraints such as; clearances and location, the availability of materials and labor, and the availability of funding. Even with these constraints, a number of options still remain to the designer with the final selection usually dictated by cost and aesthetics.

Much work has been done in the area of standard prestressed girders with cast-in-place bridge decks. These systems are currently being used as efficiently as possible. To realize any further savings, new systems must be explored.

One new system consisting of a pie-cast segmental flat-slab bridge, post-tensioned for continuity, has the potential to replace most low, short-span bridges such as those that traverse wetlands and relatively shallow waters. This system has been used successfully over the Albemarle Sound south of Edenton, NC (see Figure 1.1). A significant cost savings could be obtained with this system for certain applications [1].

The cost savings is realized through an efficiently designed cross-section and decreased labor costs through assembly-line production of individual

segments. Another advantage of this system is an integrally cast pile cap in the bent segment. This allows for the segment to be placed directly on piles without the need for a bent to be formed and cast in the field. As with any standardized system, the savings are proportional to the repetition of the application.

1.2 Objectives

In order to obtain sufficient confidence in the new bridge system, an experimental and analytical research program was undertaken to evaluate the behavior of the system.

The objectives of this research program were:

1) Develop and construct a physical scale model of the bridge system.
2) Test the model bridge system for service, fatigue, and ultimate loads.
2) Develop analytical models to predict the performance of the system.
4) Verify the analytical results by comparing them with those obtained from experimental data in order to develop a degree of confidence in the new system.

In order to accomplish these overall objectives, the research program was divided into two phases. This report addresses the second phase. The individual objectives of both phases are discussed below.

1.2.1 Phase I Objectives

The objectives of the first phase of the research program were:

1) Develop a physical scale model of the bridge system that accurately represents the existing bridge system and test this model under service loading.
2) Develop an analytical model to predict the service load performance of the post-tensioned flat-slab bridge, using commercially available computer programs.
3) Verify the analytical results by comparing them with those obtained from experimental data for service load testing.

Complete results of Phase I of the project are provided by Cook et al. [2].

1.2.2 Phase II Objectives

The objectives of the second phase of the research program were:

1) Test the experimental model for fatigue load and ultimate load.
2) Determine the expected cracking and ultimate load capacity of the model using conventional prestressed concrete beam theory.
3) Compare experimental data to predicted values.
4) Evaluate the overall performance of the bridge system.

1.3 Scope

The scope of Phase II of this research project included the following:

1) Determining the critical load configurations for fatigue, cracking, and ultimate load testing.
2) Performing fatigue load testing.
3) Comparing the stiffness of the model bridge before and after fatigue load testing to determine if any degradation occurred.
4) Determining the expected cracking load and ultimate capacity of the model bridge.
5) Performing cracking and ultimate load tests.
6) Comparing test results with values predicted from the analytical models for cracking and ultimate loads.
7) Comparing test results with AASHTO requirements.

1.4 Summary of Previous Work

1.4.1 General

The original structure used as a basis for this study is a bridge over Albemarle Sound between Washington and Chowan Counties in north-eastern North Carolina on State Highway 32. This post-tensioned flat-slab concrete bridge system consists of precast segments that range from 15 to 20 feet in length with: a 34'-3" wide cross-section and a center slab thickness of 16 1/4". The crown5 slope is 1/4"

per foot, and the edge slab thickness is 8". The segments were placed on temporary steel erection girders which spanned between piles. Concrete was then placed in one foot closure joints between each segment and in voids shaped like truncated pyramids directly over each pile to create a 260 foot long section (see Figure 1.1). Each 260 foot section had five interior spans of 40 feet each and two end spans of 30 feet each. The total length of the original project was approximately 3.5 miles. In the original structure, three different types of segments were employed to make up each 260 foot section. An expansion joint segment to begin and end each section, a bent segment with an integrally cast pile cap placed on sets of three piles, and finally, a middle segment to connect the bent segments together. These segment were precast in a casting yard and transported to the erection site by barge. The one foot closure joint between each segment eliminated the need for accurate match-casting, speeding production and reducing the possibility of construction errors.

1.4.2 Design Considerations

The experimental model was developed to provide a suitable structure for evaluation of the bridge system. As discussed previously [2], a two-span structure was selected as the prototype structure since it is the configuration that yields the highest positive and negative moments for standard AASHTO truck loads [3]. A one-half scale model was chosen based on physical limitations of the laboratory.

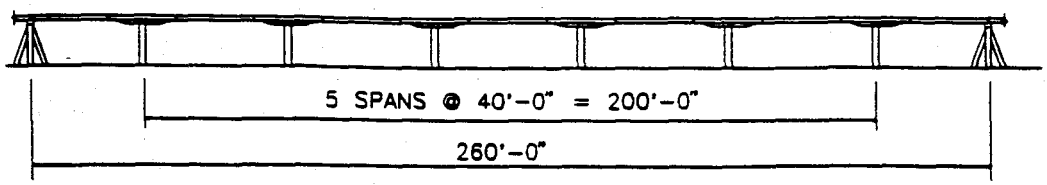

Figure 1.1 Typical Seven Span Bridge Section.

The half-scale, two-span model consisted of two 9'-9" end segments flanking a bent segment with two six-inch construction joints separating them. Figure 1.2 shows a plan view of the model; the elevation and cross-section of the model are shown in Figure 13. Details of reinforcing are given by Cook et al. [2].

1.4.3 Construction

The model bridge was constructed using the same type of erection procedures as used for the existing structure. The bridge segments were cast in line on the floor of the laboratory to facilitate the alignment of the prestress tendon ducts. Six-inch dividers were placed between segments. In addition to the deck segments, concrete support walls were constructed which included three 10" square piers at the middle support and three bearing pads at the end supports. After curing, the segments were placed on temporary shoring located between the two end supports and the center pier support. Closure pours were then made between the segments and in the three voids over the piers at the center support. The bridge was then post-tensioned and the temporary supports removed Complete details of the construction procedure are given by Cook et al. [2].

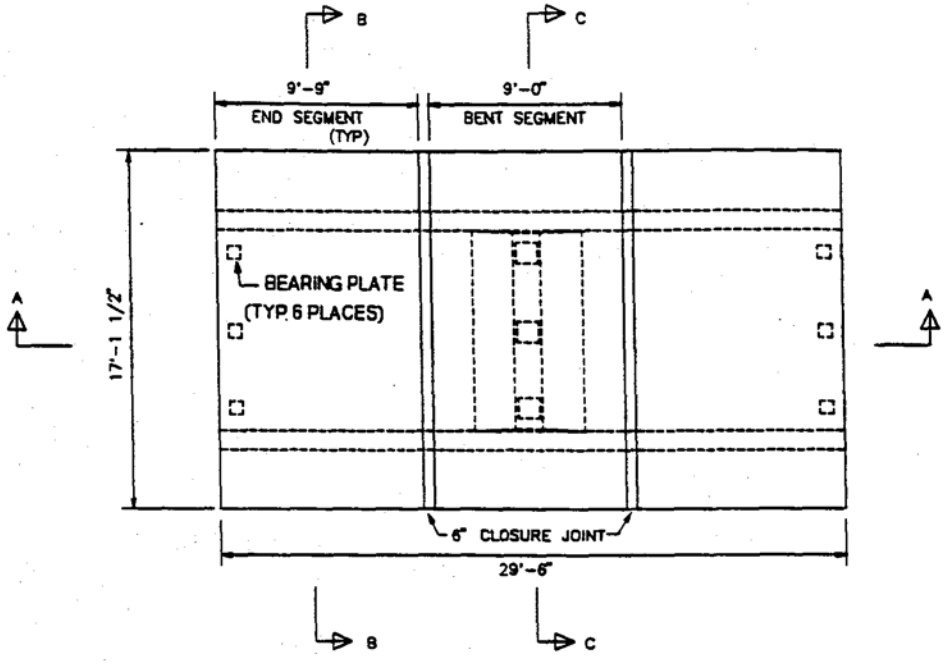

Figure 1.2 Model Plan View.

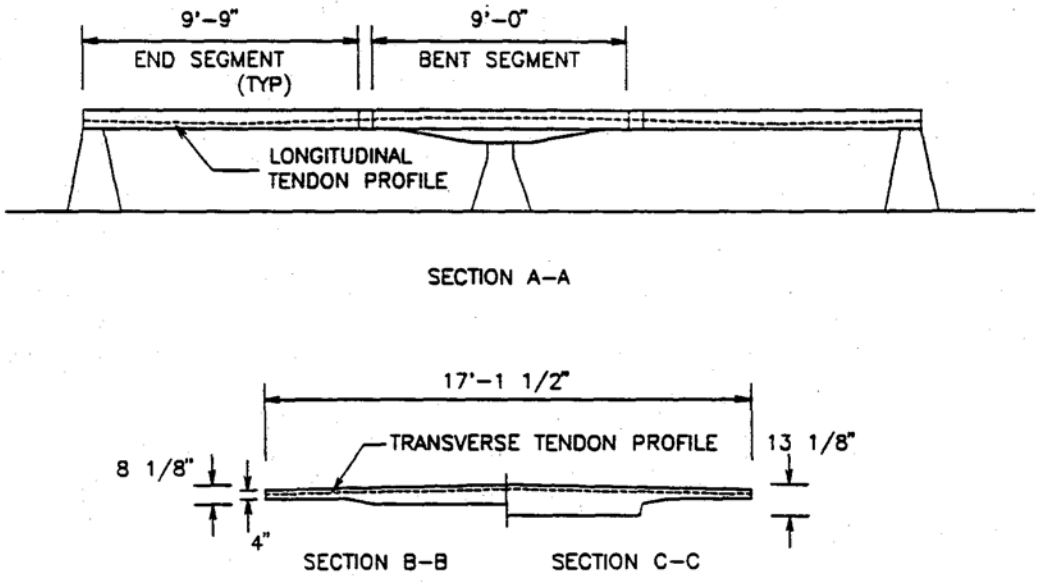

Figure 1.3 Model Elevation and Cross-Section.

1.4.4 Behavior Under Service Load

The model was tested for service load in both the positive and negative moment regions. The experimental data collected from these tests verified that the behavior of this system could be very closely predicted using a commercially available computer program [4]. Furthermore, the model remained in the linear elastic response range throughout this phase of the testing program and no cracking developed. Complete results for service load testing are presented in the final report [2] for Phase I of the testing program.

CHAPTER 2
DEVELOPMENT OF TESTING PROGRAM

2.1 Introduction

This chapter presents a discussion of the various load cases and the methods used to predict the response of the bridge system. Magnitude and location of loads are discussed for the fatigue load tests (service level fatigue and fatigue after cracking). The loading arrangement and predicted loads for the cracking and ultimate load tests are also presented.

2.2 Service Level Fatigue Load Tests

Fatigue loading was performed in two phases: service level fatigue load and fatigue loading after cracking. The service level fatigue load test was performed to evaluate the response of the bridge to. repetitive loading at a level which represented the maximum probable service level loading. The purpose of the second phase of fatigue loading was to determine if the bridge could withstand an even higher level of cyclic loading after it had been cracked. This section discusses the service level fatigue load tests. Section 2.4 discusses the fatigue testing performed after the bridge was cracked.

2.2.1 Load Configuration

Two load configurations were used for the service level fatigue load tests. The load configuration used for the first test produced the maximum negative bending moment over the middle support. The load configuration used for the second test produced the maximum positive bending moment at midspan. Figure 2.1 shows the load configuration for both tests. Note that each load case consists of only two lines of load. Although an AASHTO HS20 truck [3] has three axles, analyses showed that the front axle contributed very little to the results, and was therefore neglected.

In the negative moment load case, the axle loads straddled the middle support. The loading points were spaced 12'-2 1/2" apart with the middle support located directly between the two loading points.

In the positive moment load case both axles were placed on one span. To maximize the effect of the load, the loading points were set seven feet apart. This spacing corresponds to the minimum axle spacing required by AASHTO [3].

2.2.2 Determination of Service Level Fatigue Load

In order to determine how this bridge system would respond to fatigue loading, the model was subjected to a dynamic load which reproduced the maximum stresses and moments present in the seven-span bridge system. Although the bridge was designed for three lanes of traffic, the probability of three trucks crossing at the critical location at exactly the same instant for more than a few hundred cycles was considered to be

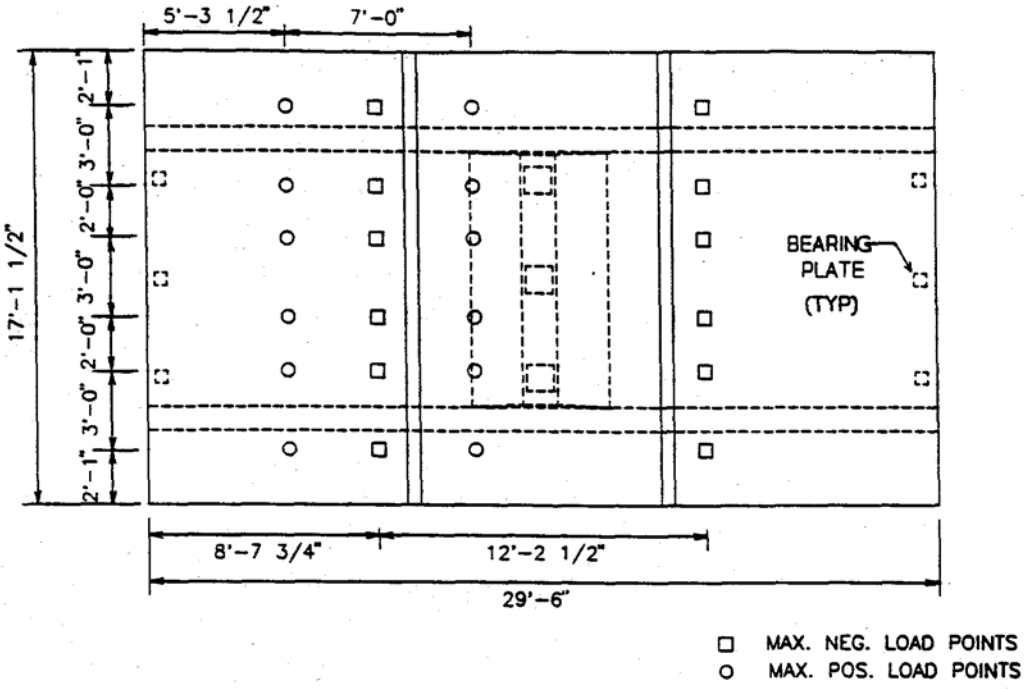

Figure 2.1 Loading Configurations for Negative and Positive Moment Service Level Fatigue Load.

minimal. For this reason, the maximum service level fatigue loading was considered to be two lanes of AASHTO HS20-44 truck loading. This condition assumes that two trucks are located at the worst possible position at the same time. This loading condition was repeated for a total of three million cycles which is much higher than would be expected during the lifetime of: the structure.

The magnitude of the load used for the maximum negative moment test was calculated to reproduce the largest negative moment occurring over any support in the seven span bridge. The maximum positive moment test was performed using a load which reproduced the largest positive moment occurring

anywhere in the seven-span bridge. In both cases, the load was essentially the same and was equal to a two lane truck loading on the model bridge. Based on these results, the target load for those tests was 41.6 kips. This load represents two trucks with four 16 kip wheel loads each, an impact factor of 1.3, and a model scale factor of one-fourth for load. A detailed explanation of the analysis of the seven-span and two-span bridges for two lanes of service load is presented by Mayer [5].

The model was subjected to two million cycles in the negative moment load case, and one million cycles in the positive moment load case. Upon completion of each load case the behavior of the bridge was examined by performing static tests equal to the three lane design load. As discussed previously [2], the three lane design load was 56.2 kips based on three trucks with four 16 kip wheel loads each, an impact factor of 1.3, a reduction factor of 0.9 for three lanes, and a model scale factor of one-fourth for load. Section 4.2 discusses the results of this test sequence.

2.3 Cracking Load Test

Following testing under the service level fatigue loading, the model was statically loaded to its cracking load. This test was performed to determine if the cracking strength of the bridge could be accurately predicted using traditional reinforced, prestressed concrete beam analysis. This section discusses the

configuration of the load points for this test and the methods used to calculate the cracking load.

2.3.1 Load Configuration

In order to optimize the loading capabilities of the laboratory, the loading configuration was revised for the cracking load test. The revised load configuration is shown in Figure 2.2. The load frame was designed to evenly distribute the total load to the four load points shown in Figure 2.2. This revised configuration was used for all subsequent tests (i.e., fatigue load after cracking and ultimate load).

The load configuration shown in Figure 2.2 produces positive moment under the load and negative moment in the unloaded span. These are the same types of moments produced by the positive moment test configuration shown in Figure 2.1. This distribution of moment was found to be the critical case for both cracking load and ultimate load. The negative moment over the support (i.e., a symmetrical load distribution as shown in Figure 2.1) was not critical due to the increased cross-section over the support.

Since the loading configuration was changed, it was necessary to establish the load equivalence between the systems. Using the three lane truck loading as a basis, it was determined that, a 33.0 kip load applied as shown in Figure 2.2 produced the same effects as a 56.2 kip load (i.e., three lanes of AASHTO trucks) applied in the positive moment test configuration shown in Figure 2.1. The equivalence of these loads was

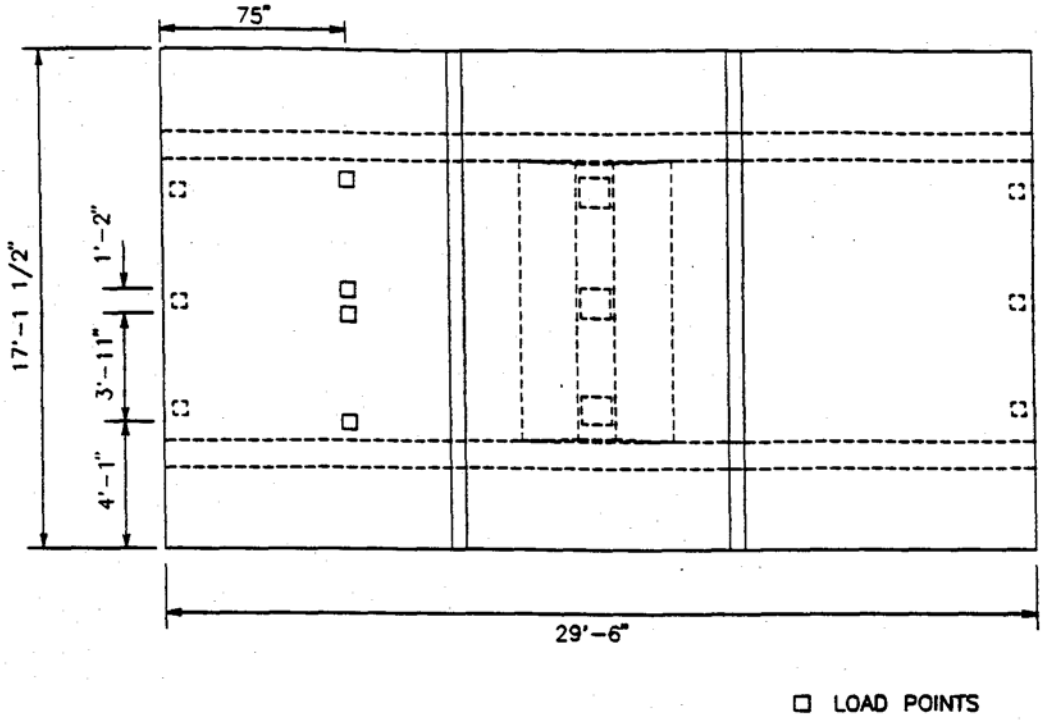

Figure 2.2 Configuration for Single Line of Load.

determined analytically by influence lines [2] and computer analysis. The results were verified experimentally by strain and deflection measurements. This means that a total load of 33.0 kips applied as shown in Figure 2.2 produces the same maximum moment, strain, and deflection as a total load of 56.2 kips applied in the positive moment load configuration shown in Figure 2.1. Therefore, a 1.70 multiplication factor can be used to determine the equivalent Figure 2.1 load for a load applied in the Figure 22 test configuration.

23.2 Predicted Cracking Load

The cracking load of the model was determined by elastic analysis of the prestressed bridge cross-section. The predicted location of the first crack was found to be near midspan due to the fact that the model's cross-section is smaller between supports than over the middle support. The live load necessary to cause cracking was calculated for two cases: cracking at the bottom fiber of the loaded span; and cracking at the top fiber of the unloaded span. Figure 23 shows the tension zones in which cracking was expected to occur. The material properties used for these calculations are discussed in Section 3.2.

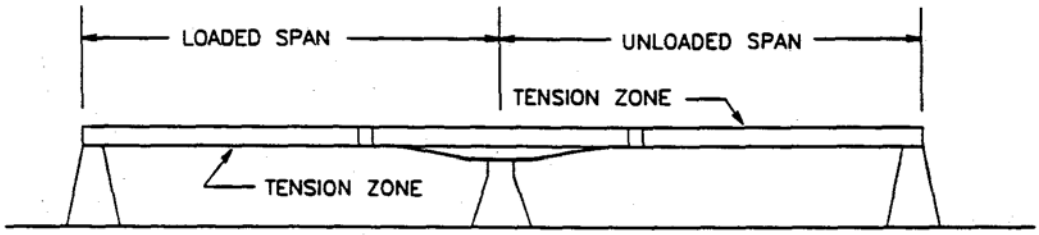

Figure 2.3 Tension Zones.

The cracking moments and ultimate moments were calculated using strain compatibility methods such as that as shown in Lin and Burns [6]. Figure 2.4 shows the cross-section of the bridge at the critical sections. The cross-section of the bridge shown in Fig. 2.4 occurred from 63" to 75" and from 279" to 291" . The area of mild reinforcement is designated as A_l, A_y and A_3. The area of prestressing steel is represented by A_{pg}. The areas of steel and the location of all steel areas are shown in Table 2.1. The effective prestress force was 904 kips [2].

The cracking moment in the loaded span, M_{cr}^{+}, was calculated as 264.2 kip-ft. In the unloaded span, the cracking moment, M_{cr}^{-} , was calculated as -632 kip-ft.

Assuming a single line load as shown in Figure 2.2, the required live load was calculated to be 77 kips for cracking at the bottom of the loaded span, and 68 kips for cracking at the top of the unloaded span. Although the calculated live load was smaller for cracking in the unloaded span, previous tests [2] have shown that measured strains and deflections are approximately 30% less than the predicted values in the unloaded span. As discussed previously [2] the reason for this difference is the

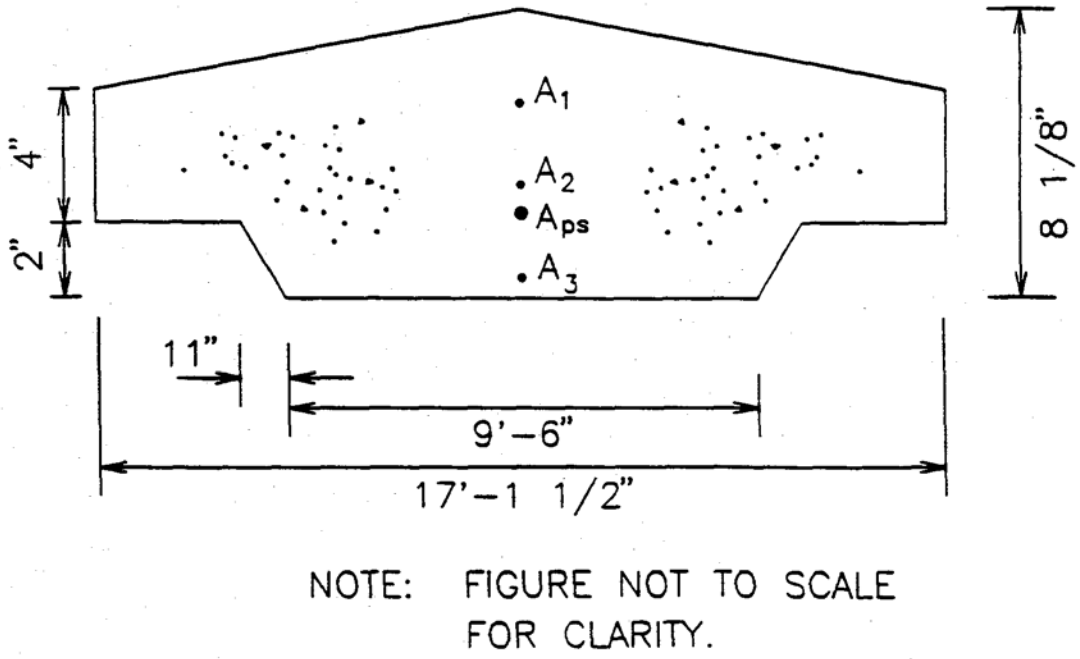

Figure 2.4 Cross-section of Model at 63"-75" and 279"-291" inches.

Table 2.1 Location and Area of Steel.

Reinforcement Designation	Area (in^2)	Distance from bottom, (in)
A_1	1.418	6.00
A_2	0.589	2.86
A_3	0.807	0.75
A_{ps}	5.508	2.25

rotational resistance provided by the center piers which was not accounted for in the analysis. Therefore, the critical case was predicted to be cracking in the loaded span at a load of 77 kips.

2.4 Fatigue Load Test After Cracking

After the cracking load test, the model was subjected to an increased fatigue load to investigate the behavior of the model under extreme loading conditions after cracking. This section discusses the methods used to establish this loading condition.

2.4.1 Load Configuration

Since the cracking and ultimate load tests were to be performed using a single line of load, the same load configuration was used for fatigue testing after cracking. However, to use this modified load configuration, the magnitude of the service load had to be adjusted.

2.4.2 Determination of Fatigue Load After Cracking

To insure that the adjusted load was greater than the largest load the bridge had been subjected to prior to the cracking test, the decision was made to use 150% of the three lane service live load. As discussed in Section 2.3.1, the equivalent three lane service load for this test configuration was 33.0 kips. Therefore, the load corresponding to 150% of the three lane service load was 49.5 kips.

This load was equivalent to 200% of the two lane service load, 64% of predicted cracking load, and using 177 kips for the ultimate capacity of the bridge (see Section 2.5), it was equivalent to 28% of the predicted ultimate load. This loading was repeated for two million cycles.

2.5 Ultimate Load Test

The final objective of this research project was to investigate the ultimate load capacity of the model. The purpose of this test was to determine the degree of accuracy with which the ultimate capacity of the bridge could be estimated using conventional methods. The methods used to calculate the load required to cause failure are discussed in this section.

2.5.1 Load Configuration

The load configuration used for cracking and the fatigue load test after cracking was also used for testing the model for ultimate load (see Figure 2.2).

Calculations indicated that negative moment in the unloaded span, and punching shear at the middle support were not critical. These results are discussed in Section 252.

2.5.2 Predicted Ultimate Load

The ultimate load was determined from the moment-curvature relationships for the bridge cross-section with the bridge modeled as a one-way beam continuous over three supports. The moment-curvature relationships for the loaded and unloaded spans were determined using conventional strain compatibility relationships for prestressed reinforced concrete. Lin and Burns [6] provide an example for this procedure which is summarized as follows. By assuming a value for strain at the top fiber of the loaded span, and at the bottom fiber for the unloaded span, the strain-compatibility relationships are used to determine the required moment and curvature to produce the assumed strain. Figure 25 is the moment-curvature diagram showing the results of these calculations. Note that the moment-curvature relationships for both the loaded and unloaded spans are shown in Figure 25 since they involve the same cross-section as shown in Figure 2.4.

The moments calculated by this method do not include dead load moment and secondary moments produced by prestressing. To determine the predicted live load, the combined effect of dead load and secondary moments must be included. The total moment at, for example, strain of 0.003, was calculated as532 kip-ft. The combined

dead load and secondary moment was found to be 41 kip-ft at -the critical location Figure 2.6 shows the dead load moment diagram, and Figure 2.7 shows the secondary moment diagram- Therefore, the live load required to produce a strain of 0.003 at the top fibers of the loaded span was calculated as

$$M_{LL} = M_{0.003} - M_{DL+sec} = 522 - 41 = 481 \text{ kip-ft}$$

The predicted live load at a strain of 0.003 was calculated by considering the bridge as a beam continuous over three supports and determining the live load which produced

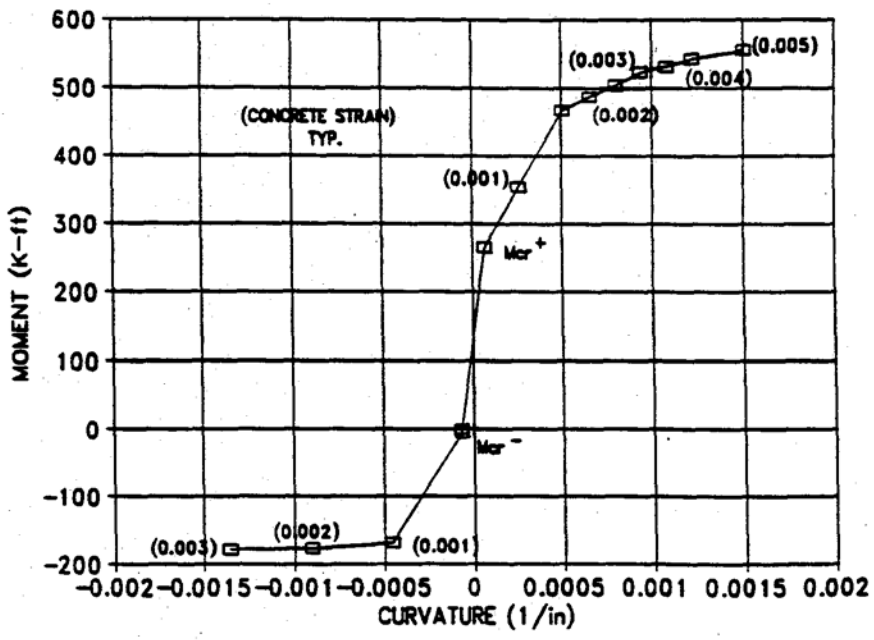

Figure 2.5 Moment Curvature Diagram.

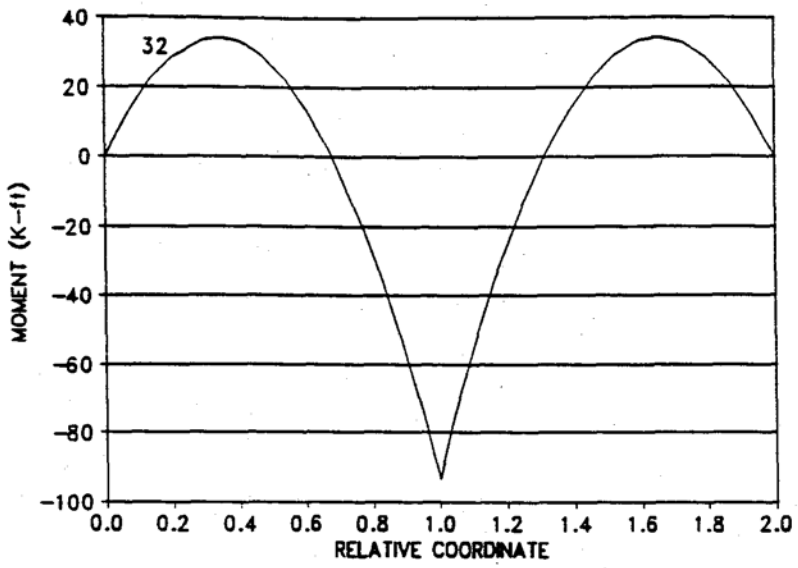

Figure 2.6 Dead Load Moment.

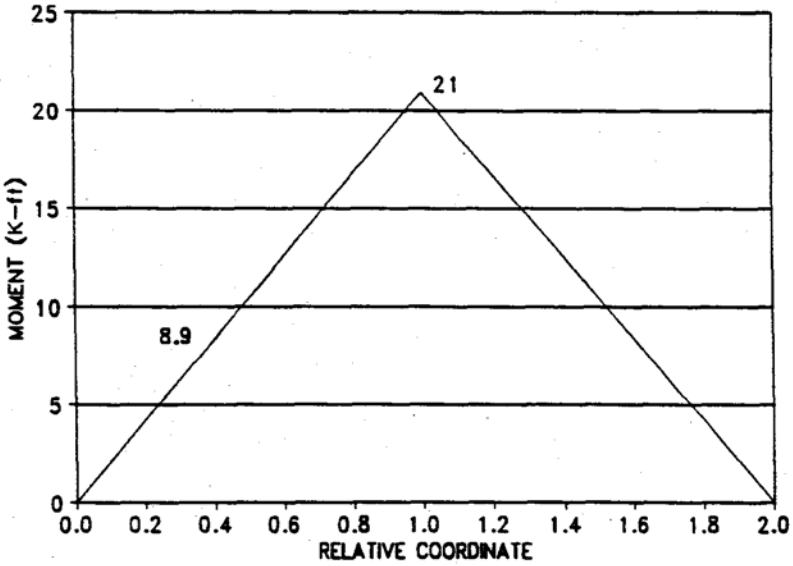

Figure 2.7 Secondary Moment.

a moment of 481 kip-ft under the load point (see Figure 22). For the case of a strain of 0.003 at the top fibers of the loaded span, the live load was calculated as 166 lips. Table 2.2 shows additional predicted loads at various strains.

Predicted load-deflection behavior was developed from the moment curvature relationships and the moment-curvature diagrams for the various live loads shown in Table 2.2. By replacing the moment at a given location by the curvature at that location, the conjugate beam method of calculating deflections was used to determine the anticipated deflections for a given load. Table 2.2 shows the predicted displacements for various strains and corresponding loads.

A similar procedure was used to determine the live load required to produce a strain of 0.003 at the bottom fibers of the unloaded span. This load was found to be 314 kips. Additionally, the required live load for punching shear failure at *the* middle support was calculated as approximately 900 kips.

Therefore, the controlling failure mode was positive moment at the critical section which was located under the load point shown in Figure 2.2.

2.6 Discussion of Predicted Values

Table 23 shows a summary of service live load, cracking load, ultimate load, and the ratios of cracking load and ultimate load to service live load. To accurately compare predicted loads, the values must be compatible with each other. Therefore, the service live load used in Table 2.3 is 33 kips based on the single line of load shown in Figure 22.

As mentioned previously, this load is equivalent to the three lane service load of 56.2 kips applied as shown in the positive moment test configuration shown in Figure 2.1.

To satisfy AASHTO requirements the moments due to dead load and live load with impact, multiplied by their appropriate scale factors, must be less than the factored ultimate moment. As shown in Figure 2.6, the dead load moment was 32 kip-ft. The moment due to live load plus impact was 95.4 kip-ft. The following calculations verify that this requirement was satisfied.

$$1.3 \times [\ 1.0\ M_{Deed} + 1.67\ M_{(Live + Impact)}\ ] \leq \emptyset M_n$$

$$1.3x[1.0x32 + 1.67x95.4] \leq 0.9x522$$

$$248.7 \text{ kip-ft} \leq 469.8 \text{ kip-ft}$$

AASHTO requirements also specify that the factored ultimate moment at the critical section must be at least 1.2 times the cracking moment. The following calculations show that this requirement was satisfied.

$$OM_B \geq 1.2M_{cr}$$

$$0.9 \times 522 \text{ kip-ft} \geq 1.2 \times 264.2$$

$$469.8 \text{ kip-ft} \geq 316.8 \text{ kip-ft}$$

Table 2.2 Predicted Live Load and Deflection for Various Top Surface Strains.

Top surface compressive strain	Predicted live load (kips)	Predicted deflection (in)
0.001	108	0.36
0.002	154	0.86
0.003	166	1.28
0.004	173	1.78
0.005	177	2.23

Table 2.3 Comparison of Predicted Live Loads.

Service load (kips) P_{SL}	Cracking load (kips) P_{CR}	Ultimate load (kips) P_{ULT}	P_{CR}/P_{SL}	P_{ULT}/P_{SL}	P_{ULT}/P_{CR}
33	77	166	2.3	5.0	2.2

CHAPTER 3
IMPLEMENTATION OF TESTING PROGRAM

3.1 Introduction

This chapter discusses material properties and equipment which was used for testing. All requirements for similitude between the model and existing system were met [2].

3.2 Material Properties

The following provides a summary of the materials used in the bridge. Detailed information is presented by Cook et al. [2].

3.2.1 Concrete

Cylinder tests were performed to determine the compressive strength of the concrete one year after the bridge was cast. The design strength of the mix, f, was 5500 psi at 28 days. The value for fC at the time of testing was found to be 6,590 psi. The value used for calculations was 6,600 psi.

The modulus of elasticity was calculated as

$$E_C = 57,\sqrt{6,600} = 4,631,000 \text{ psi}$$

and the modulus of rupture, f. was calculated as

$$f, = 7.5\ f\sim = 7.5\ 6{,}600 = 609\ \text{psi}.$$

3.2.2 Mild Reinforcing Steel

The mild reinforcing steel had a typical stress strain curve with a modulus of elasticity of 29,000,000 psi and a well defined yield point of 72,000 psi [2).

3.2.3 Prestressing Steel

All prestressing strands used were 0.5 inch diameter, 7-wire, low-relaxation strand. From the mill report supplied with the strand, the modulus of elasticity is 29,200,000 psi. The yield stress is 266,000 psi taken at 1% extension. The ultimate stress is 283,000 psi

3.3 Instrumentation

Linear variable differential transformers (LVDTs) were used to measure displacements. The 20 LVDTs used were Shaevitz model #GCD-121-1000 with a nominal linear range of ± 1 inch and a specified linearity of 0.25% of full range. Figure 3.1 shows the locations of the LVDTs.

Strains were measured using internal and surface strain gauges. The internal strain gauges were Micro-Measurements Division model #CEA XX- W250A 120. The

surface strain gauges were Micro-Measurements Division model #WA-06-20CBW-120.

Internal strain gauges were welded to short pieces of mild reinforcing steel and placed in the bridge slab. The surface strain gauges were epoxied to the slab after the slab had been sanded and cleaned with a light acid.

An HP-3497A analog to digital converter, data acquisition control unit was used to take the readings from the strain gauges and LVDTs. The digital converter then communicated the millivolt readings to a PC computer which used a program written in basic to transform the voltage readings into their corresponding strains and displacements. A hard copy of the output was printed, and also stored in a computer file with an ASCII format.

Strain gauges and LVDTs were placed on the model at locations which corresponded to nodal points in the mathematical model. By properly placing the instrumentation, a direct comparison could be made between analytical and measured results.

LVDT locations were kept constant for both fatigue load tests, cracking load and ultimate load tests. Most of the LVDTs were placed along the centerline to provide a longitudinal representation of the moders deflected shape. The two transverse lines of LVDTs were placed at the locations for maximum displacement.

Figure 3.1 shows the location of LVDTs. Strain gauge locations for the service level fatigue load tests are shown in Mayer [5]. Strain gauge locations for the all tests

following service level fatigue load tests are shown in Figures 32 through 3.4.

3.4 Loading Apparatus

3.4.1 Load Frame

The test frame used for the service fatigue load test is the same load frame used for service load testing and is shown in Cook et al. [2]. The load configuration for this test was two lines of load, each with 6 load points each for a total of 12 load points (see Section 2.2). To insure that each load point received an equal load, the frame was designed to be statically determinate by using a series of stacked beams, each having one load point and two reactions.

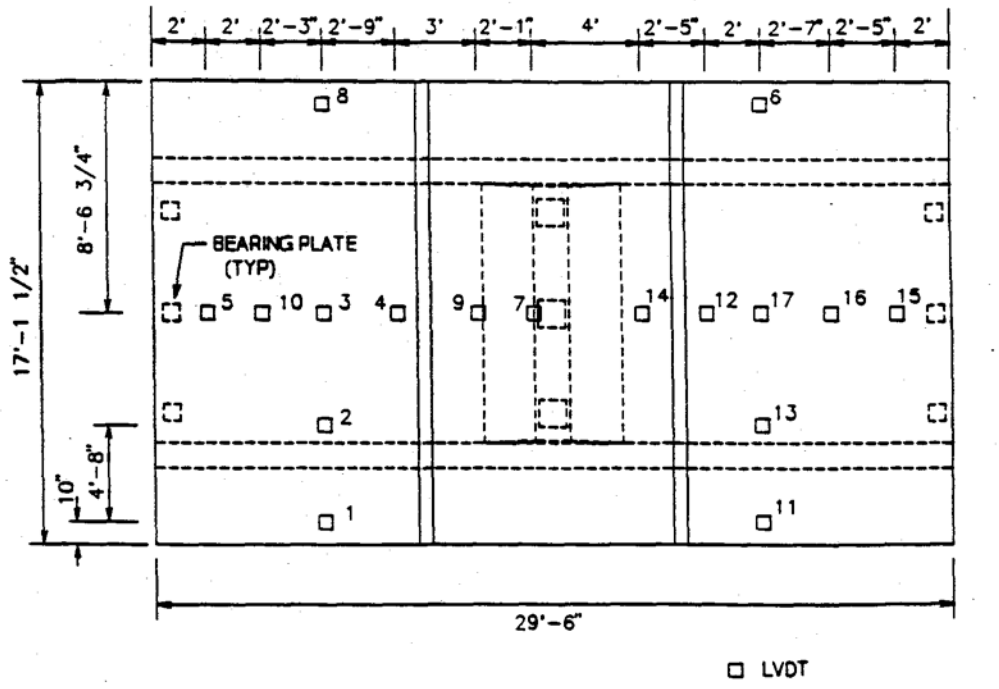

Figure 3.1 LVDT Location.

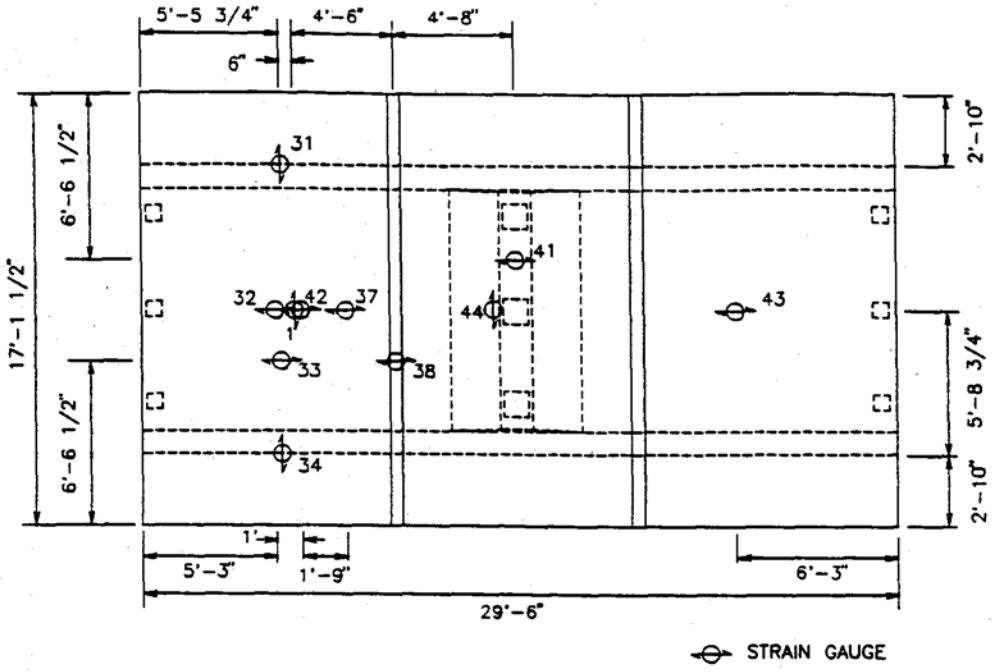

Figure 3.2 Top Strain Gauge Location.

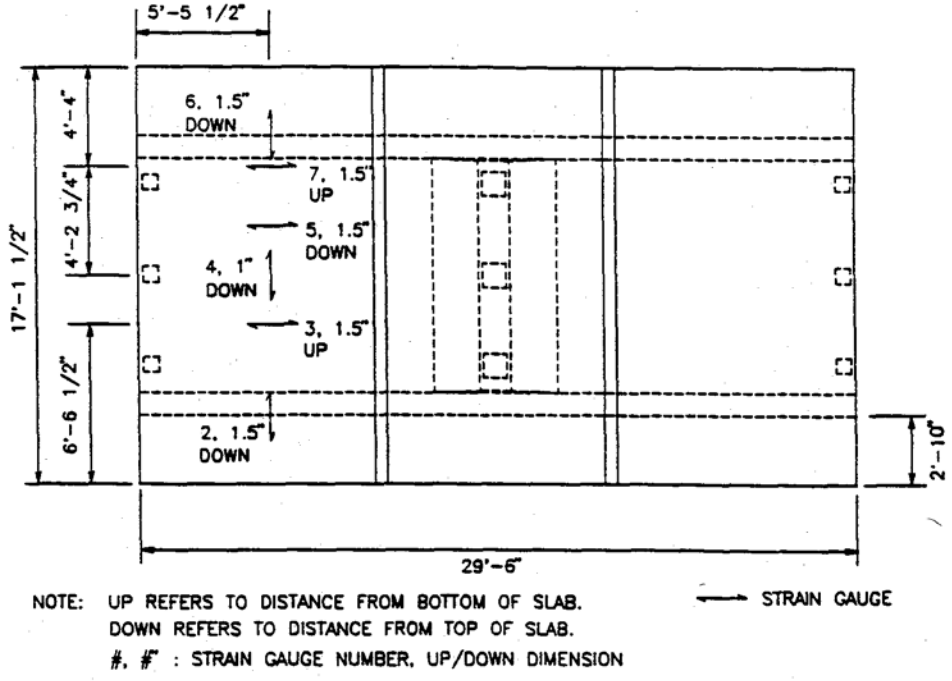

Figure 3.3 Interior Strain Gauge Location.

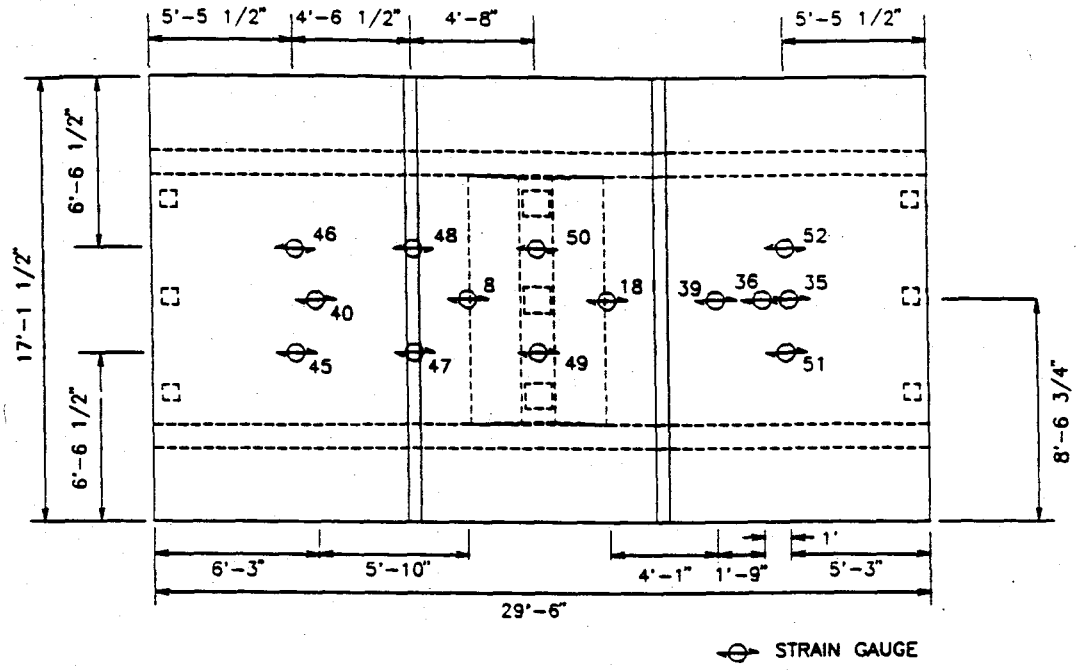

Figure 3.4 Bottom Strain Gauge Locations.

Neoprene bearing pads were used to simulate the contact area of a truck tire. The pads had a #60 durometer reading. Since the model was designed with a crown, steel plates were placed on the bearing pads to insure the same elevation at each load point.

Section 23.1 discusses the load configuration used for the cracking load test, the fatigue load test after cracking, and the ultimate load test. A schematic view of this load configuration is shown in Figure 3.5. To improve stability, braces were attached from the top of each beam to the dead load compensating blocks.

3.4.2 Loading Equintnent

An MTS system was utilized to control the load during fatigue tests. The load was applied in a sinusoidal pattern.The MM allowed for control of the magnitude of the load, the frequency of the load, and the range through which the load was applied. Additionally, the NM provided load control for periodic static loading during the fatigue tests.

During fatigue testing, the load was monitored with a 55 kip load cell. The load cell was calibrated using the laboratory's 400 kip Universal Testing Machine. The load cell was attached to a Nopak Class 3 hydraulic cylinder jack with a 5" bore, model XDD.

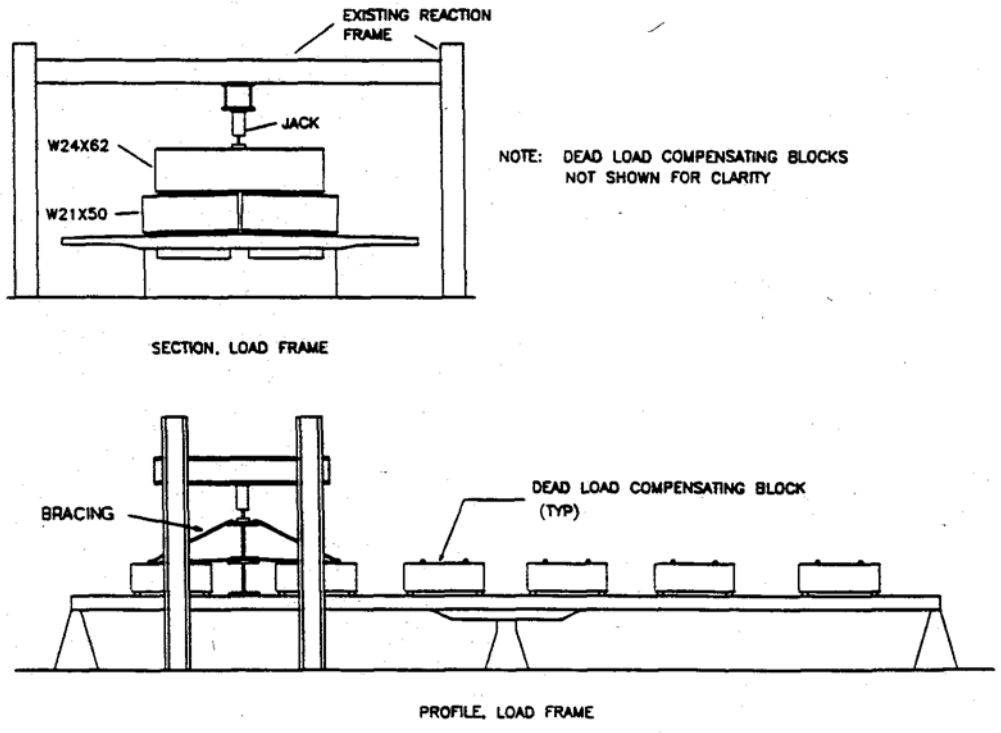

Figure 3.5 Schematic Views of Load Frame.

Since cracking and ultimate loading tests required static loading, a hydraulic, pump was used instead of the NITS. The hydraulic pump used was an Interpak, model #P-464, 10,000 psi capacity.

A much larger load was required for cracking and ultimate load testing than was needed for the fatigue tests, a higher capacity load cell was used The load cell was a Houston Scientific International, Inc., center hole load cell, Model #3500-200 Precision. The capacity of the load cell was 200 kips with a 0.10% of full scale nonlinearity. As with the 55 Idp load cell, the 200 Idp load cell was calibrated with the laboratory's Universal Testing Machine.

CHAPTER 4
DISCUSSION AND COMPARISON OF RESULTS

4.1 Introduction

In this chapter, experimental results obtained from the four load cases (Service Level Fatigue Load, Cracking Load, Fatigue Load After Cracking, and Ultimate Load) are presented and discussed.

Unless noted, all experimental results represent only the load case under consideration. For example, the deflections shown for the cracking load test are the deflections that occurred during that load case only, not the total deflections that occurred since construction of the model. For the figures in this report, positive strain is tensile. Locations for all instrumentation are shown in Figures 3.1 through 3.4.

4.2 Fatigue Load Test

As discussed in Sections 2.2 and 2.4, two types of fatigue load tests were performed. The first type of fatigue load test was performed for the maximum service level fatigue loading expected on the bridge. The load used for this test was two lanes of AASHTO HS20-44 trucks. The service level fatigue load tests were performed with the loading configuration shown in Figure 2.1. After the service level fatigue

load tests were performed, the loading configuration was changed to the single line loading shown in Figure 22. The bridge was then loaded monotonically until cracking occurred (see Section 4.3). After the bridge was cracked, another two million cycles of load were applied in the test configuration shown in Figure 2.2. The load used in this test was equivalent to 150% of the three lane design load (i.e., three lanes of AASHTO HS20-44 trucks).

4.2.1 Results of Service Level Fatigue Load Tests

The service level fatigue load tests were performed in two loading configurations. The first load configuration tested for maximum negative moment over two million cycles, and the second for maximum positive moment for an additional one million cycles' (see Section 22). Figure 4.1 shows the actual loading history in terms of the maximum service level fatigue loading of two lanes of AASHTO trucks (41.6 kips total load).

4.2.1.1 Maximum negative moment test

Figure 4.2 shows the load-deflection curve at the longitudinal centerline of the bridge under the load that was recorded in a static test to full three lane service load (56.2 lips) after two million cycles. The linearity of the experimental results demonstrates that the bridge remained elastic and that no cracks were formed.

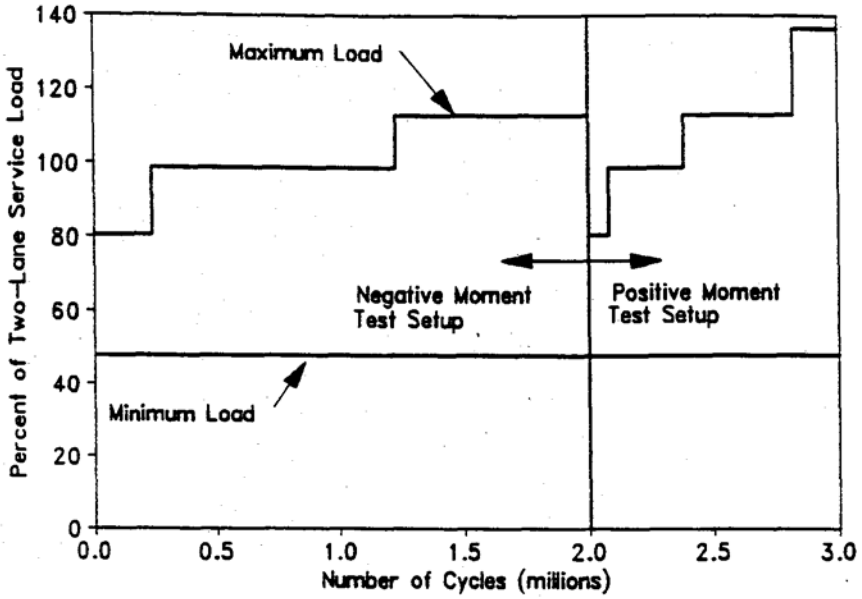

Figure 4.1 Load History for Service Level Fatigue Tests

Figure 4.3 shows typical values for relative stiffness of the bridge system which were calculated throughout the fatigue load testing. The relative stiffness was determined from static load tests performed approximately every 100,000 cycles. The relative stiffness represents the slope of the load-deflection curve for the LVDT under the load at the bridge longitudinal centerline. As shown in Figure 4.3, the relative stiffness remained essentially constant during the two million load cycles of the maximum negative moment test.

4.2.1.2 Maximum positive moment test

Figure 4.4 shows the load-deflection curve at the same location for the maximum positive moment load case. As n the negative moment load case, the response remained linear elastic. Figure 4.5 shows that after three million cycles,

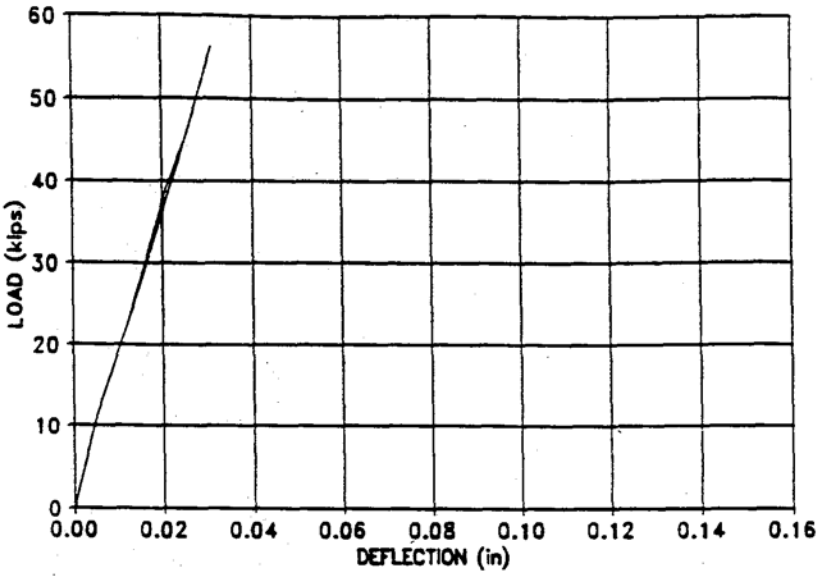

Figure 4.2 Load vs. Deflection, LVDT 3, Service Level Fatigue Load Test, Negative Moment Load Case.

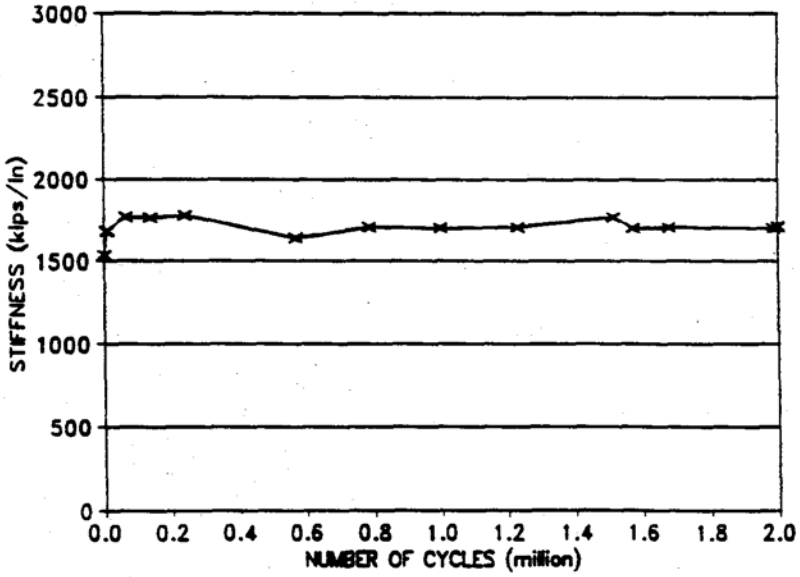

Figure 4.3 Stiffness vs. Number of Cycles, LVDT 3, Service Level Fatigue Load Test, Negative Moment Load Case.

there was no degradation of relative stiffness. The difference in relative stiffness between this test and the previous test was caused by the difference in load configurations.

4.2.2 Results of Fatigue Load Test After Cracking

As discussed in Section 2.3, the fatigue load test after cracking was performed at a load equivalent to 150% of the three lane service load for two million cycles. The maximum load applied for this test was 49.5 kips and the minimum load was 20 kips. Approximately every 100,000 cycles a static test was performed to a load equivalent to 150% of the three lane service load (49.5 kips).

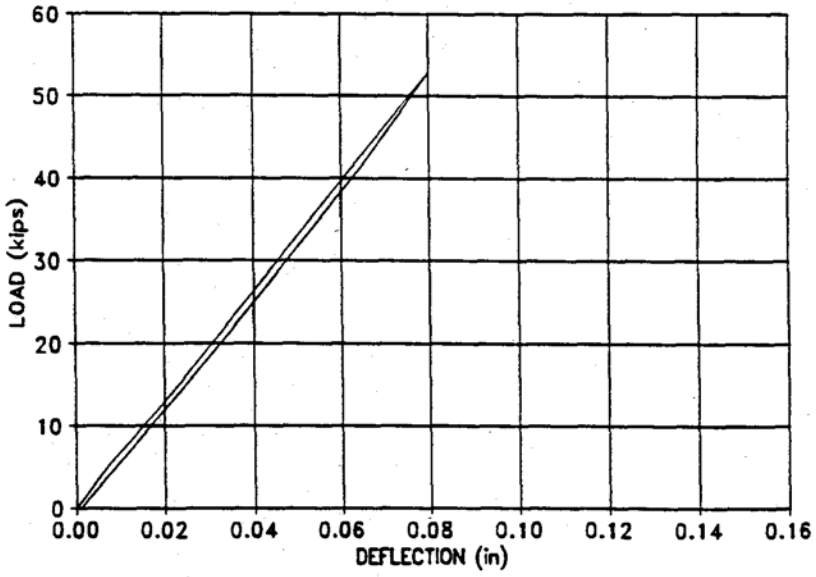

Figure 4.4 Load vs. Deflection, LVDT 3, Service Level Fatigue Load Test, Positive Moment Load Case.

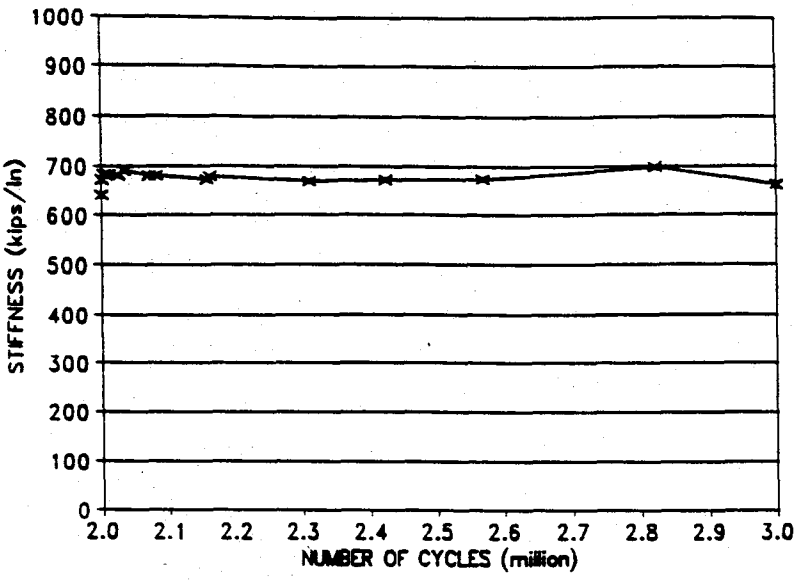

Figure 4.5 Stiffness vs. Number of Cycles, LVDT 3, Service Level Fatigue Load Test, Positive Moment Load Case.

The load-displacement and load-strain measurements from these tests were used to determine if any degradation had occurred in the bridge.

Figure 4.6 shows the load-displacement measurements directly under the load at the centerline of the bridge for the static test performed after two million cycles of 150% three lane service load. Figure 4.7 shows the strain at the top and bottom of the bridge deck at the longitudinal centerline of bridge under the load for the same test. Both Figure 4.6 and Figure 4.7 show that the response of the bridge remained linear after a total of five million cycles of fatigue load.

Figure 4.8 shows the relative stiffness of the bridge over the last two million cycles of load. As mentioned previously, the relative stiffness represents the slope of the load-deflection curve for each static test measured at the LVDT

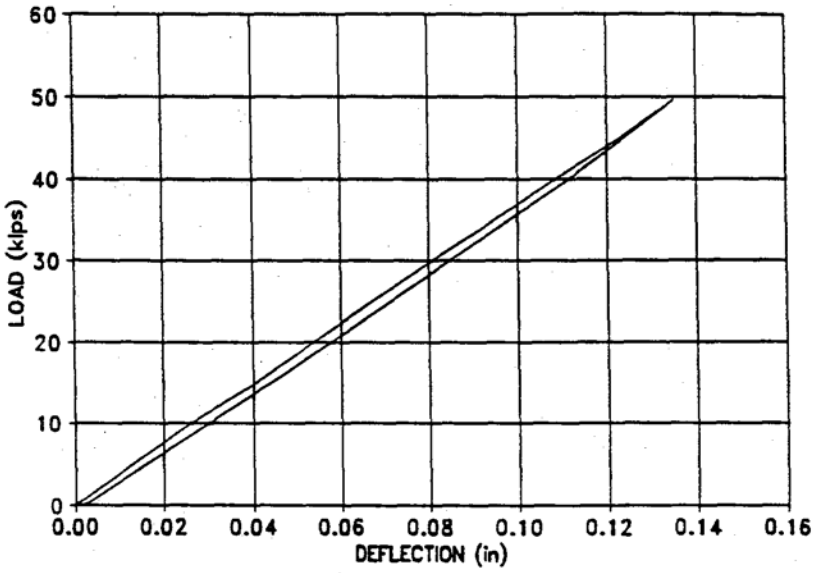

Figure 4.6 Load vs. Deflection, LVDT 3, Fatigue Load Test After Cracking.

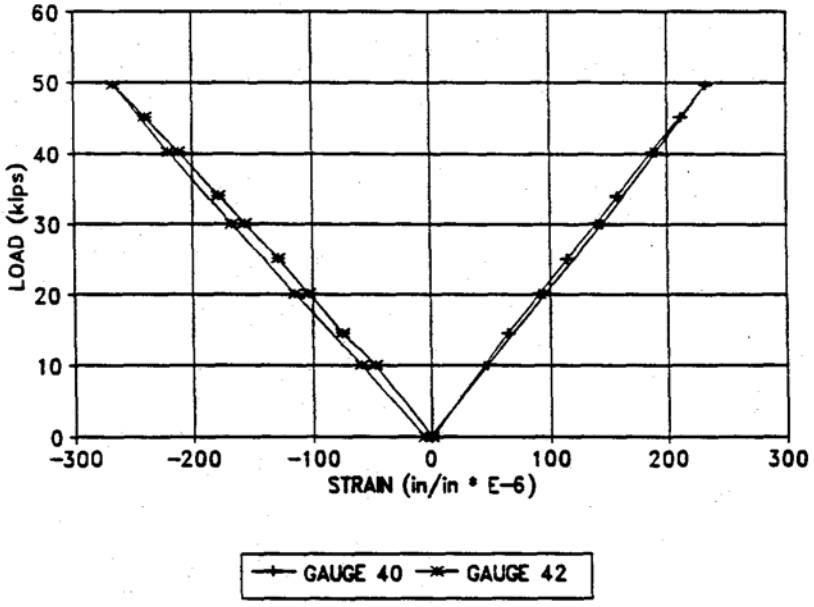

Figure 4.7 Load vs. Strain, Gauge 40 (Bottom) and Gauge 42 (Top), Fatigue Load Test After Cracking.

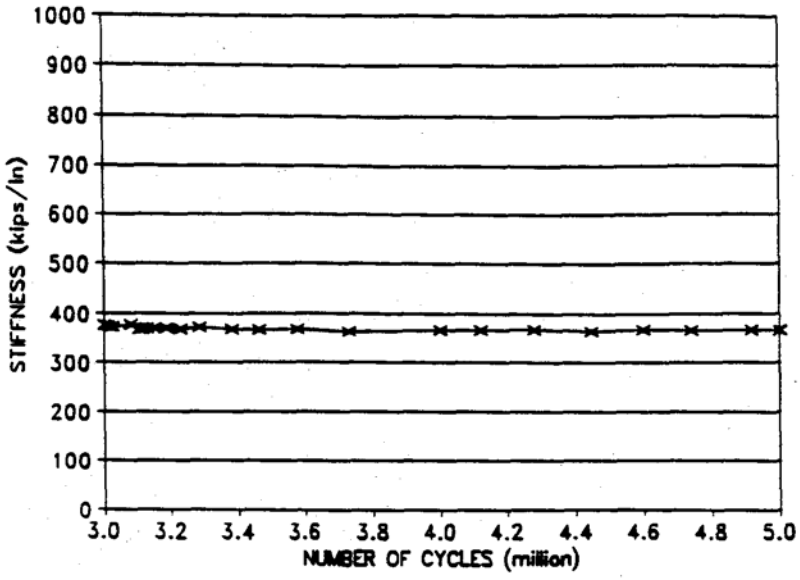

Figure 4.8 Stiffness vs. Number of Cycles, LVDT 3, Fatigue Load Test After Cracking.

directly below the load at the centerline of the bridge. Figure 4.8 indicates that no degradation of stiffness occurred during the fatigue load test after cracking.

4.2.3 Summary of Fatigue Load Tests

No degradation of stiffness or structural integrity were noted during any of the fatigue load tests. The system response remained linear elastic throughout the fatigue load testing program. This is not surprising since the load applied in these tests was below the cracking load of the prestressed bridge system. As with most prestressed, post-tensioned systems with grouted tendons, reasonable fatigue loading does not affect the integrity of the system. In order to obtain early fatigue failure, the bridge would need to be subjected to fatigue loads above cracking. In the case of this particular system, this would amount to a

loading above 50% of the ultimate load or 270% of the three lane design service load. Since these load levels will never be experienced in the actual bridge, it is reasonable to assume that fatigue loading is not a problem for the new bridge system.

4.3 Cracking Load Test

Upon completion of the service level fatigue load tests, the cracking load test was performed. This was accomplished by increasing the load until cracking occurred, and the measured deflections and strains in the model were no longer linear.

4.3.1 Results of Cracking Load Test

Figures 4.9 through 4.11 show the results from the cracking load test. This test was conducted after the service level fatigue load test.

Figure 4.9 illustrates the longitudinal deflection profile of the bridge at different loads. Note that the deflection at 100 lips is greater than two times the deflection at 50 kips. This indicates that the bridge had cracked since the deflection did not increase linearly with the load.

Figure 4.10 is the load-deflection curve for the cracking load test measured under the load at the longitudinal centerline of the bridge. The cracking load was the point at which the load-deflection curve became nonlinear (90 lips).

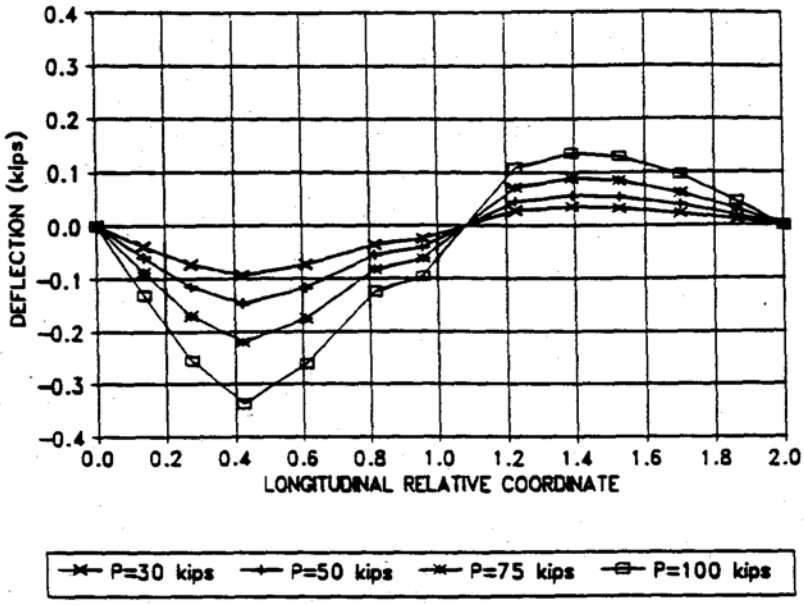

Figure 4.9 Longitudinal Deflection, Cracking Load Test.

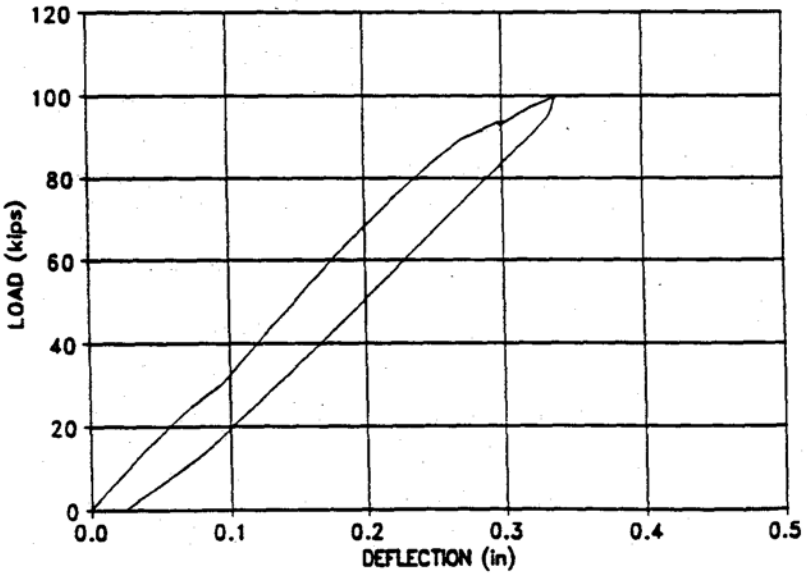

Figure 4.10 Load vs. Deflection, LVDT 3, Cracking Load Test.

As expected, the first crack appeared in the loaded span under the load and not in the unloaded span. The crack formed under the load on the bottom surface of the deck. It extended transversely from approximately 4' from one side of the bridge to 4' from the other side, which corresponded to the thickened section of the bridge. After formation of the first crack, small cracks opened. These cracks originated at the first crack and ran essentially parallel to it, approximately 4" away and towards the center support. No cracks were observed which extended the total width of the bridge. The experimental cracking load was found to be 90 kips, which was approximately 15% greater than the predicted cracking load (see Section 2.3).

Figure 4.11 shows the strain at the bottom and top surface of the bridge on the longitudinal centerline directly below the load. Note that the bottom surface strain decreased after 90 kips. This was due to the fact that once a crack opened on the bottom surface, the neutral axis began to move upwards, and the steel carried more strain. After the bridge cracked, the strain at the top surface of the bridge became nonlinear, and the rate of change of compressive strain at the top surface increased.

4.3.2 Summary of Cracking Load Test

In summary, the behavior of the bridge could be predicted very closely using conventional prestressed, reinforced concrete beam theory. As shown in Figures 4.17 and 4.18 (see Section 4.4), the experimental deflections and strains

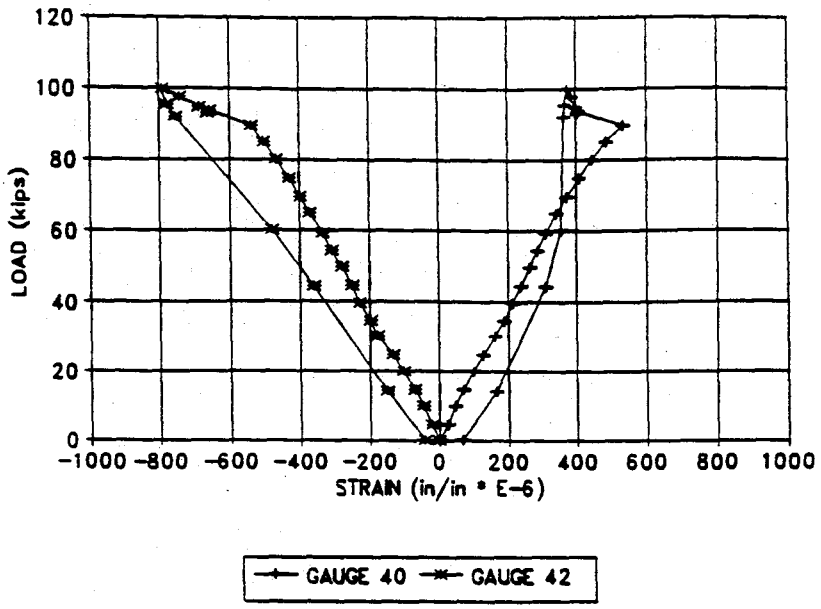

Figure 4.11 Load vs. Strain, Gauge 40 (Bottom) and Gauge 42 (Top), Cracking Load Test.

up to cracking load were very close to the predicted values. The ratio of experimental to predicted cracking load was 1.22. In terms of both experimental and predicted results, the cracking load was about 2.5 times the design service load.

4.4 Ultimate Load Test

Upon completion of the fatigue load after cracking test, the ultimate load test was performed. This was accomplished by increasing the load until the measured deflections and strains indicated that the bridge had exceeded its ultimate load capacity.

4.4.1 Results of Ultimate Load Test

Figure 4.12 shows the cracks which had formed on the bottom surface of the bridge during the ultimate load test. Figure 4.13 shows the crushing zone in the loaded span and the cracks in the unloaded span which had formed on the. top surface. Figures 4.14 through 4.18 represent typical data collected during the ultimate load test.

This test was conducted in two parts due to an equipment failure. During testing, a loud noise was heard after a load of 173 kips had been reached. A sudden drop was experienced for' both the load and the deflections. After the sudden drop, the bridge was unloaded and inspected. Since the ram was not leaking, and the bridge did not appear to have failed, the decision was made to reapply the load. The test was then run successfully up to a load of 187 kips, at which point a flexural compression failure occurred in the top surface of the bridge under the load. A post-test inspection indicated that a seal had been broken in the ram but had apparently reseated itself for the final loading.

In this section, "ultimate 1" corresponds to the first test to a load of 173 kips; and, "ultimate 2" corresponds to the final test which began after the bridge had been unloaded.

Figure 4.14 shows the longitudinal deflection profile for the entire ultimate load test. Table 4.1 shows the actual magnitude of the loads used in Figure 4.14. The data for deflection at 187 kips was obtained from the "ultimate 2" test. All other load cases in this graph were from "ultimate 1 " Note that the deflection at the ultimate

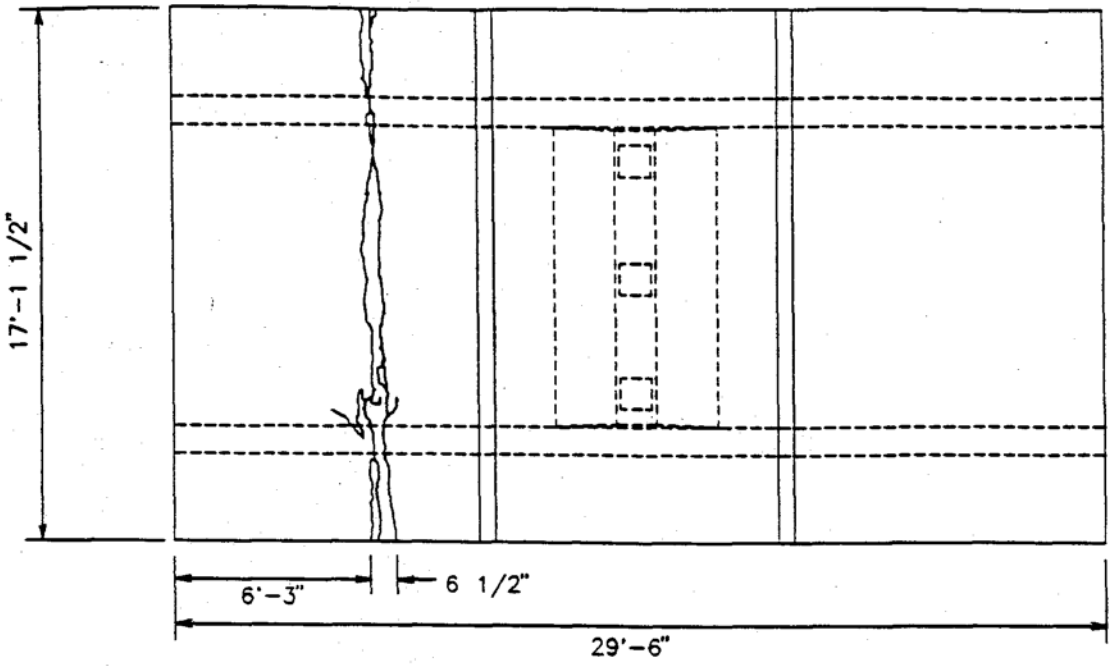

Figure 4.12 Bottom Surface, Ultimate Load Test.

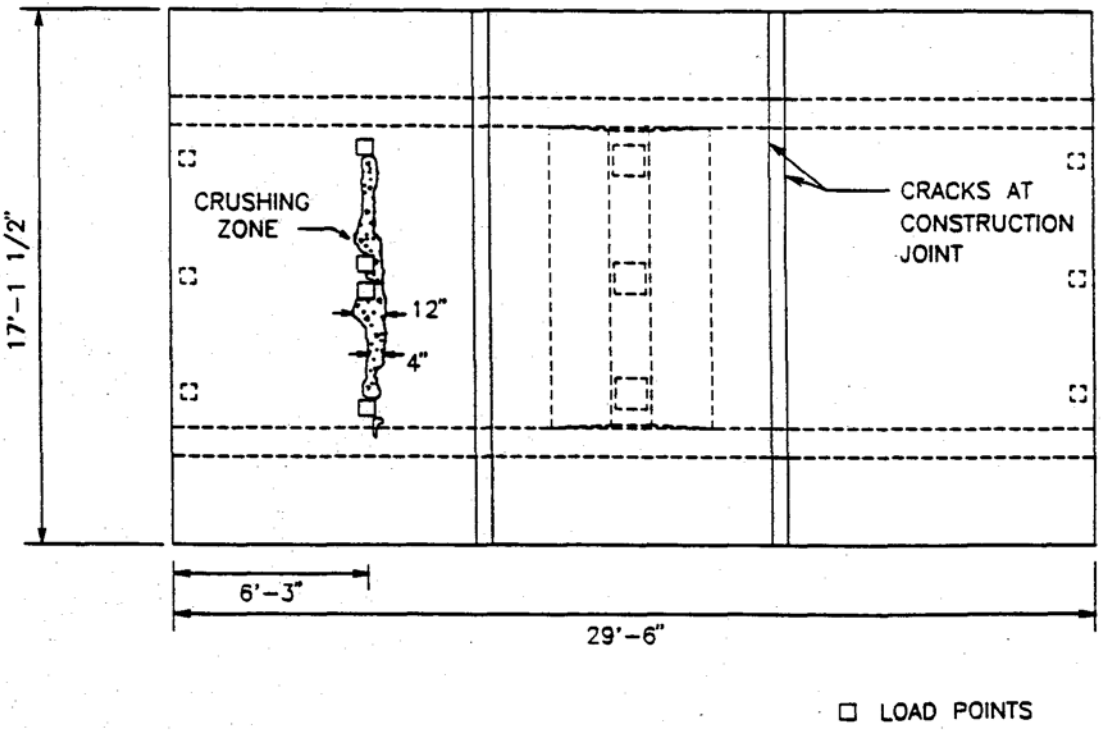

Figure 4.13 Top Surface, Ultimate Load Test.

load was over three times the deflection at 75% of the ultimate load. 'This indicates that the bridge had failed and could no longer successfully resist the load.

Also of interest is the shape of the deflection profile shown in Figure 4.14. The curve shows that a plastic hinge formed under the load and that the deflection was discontinuous at this point. As indicated in Figure 4.14, nonlinear displacements also developed in the unloaded span at some load between 75% and 100% P_{ult}. A post-test inspection indicated that a crack had formed at both sides of the 6" closure pour. The fact that both the loaded and unloaded spans exhibited nonlinear displacements at ultimate load indicates that the design of the bridge system is well balanced for both positive moment in the loaded span and negative moment in the unloaded span.

Load-strain curves for both the top and bottom surface directly under the load are shown in Figure 4.15. This figure includes the results from both the "ultimate 1" and "ultimate 2" tests. After a load of 183 kips was reached, the concrete at the location

Table 4.1 Critical Loads for Ultimate Load Test.

Load designation	Magnitude of Load (kips)
$P_{service}$	33
P_{crack}	90
$P_{75\% ult}$	139
P_{ult}	187

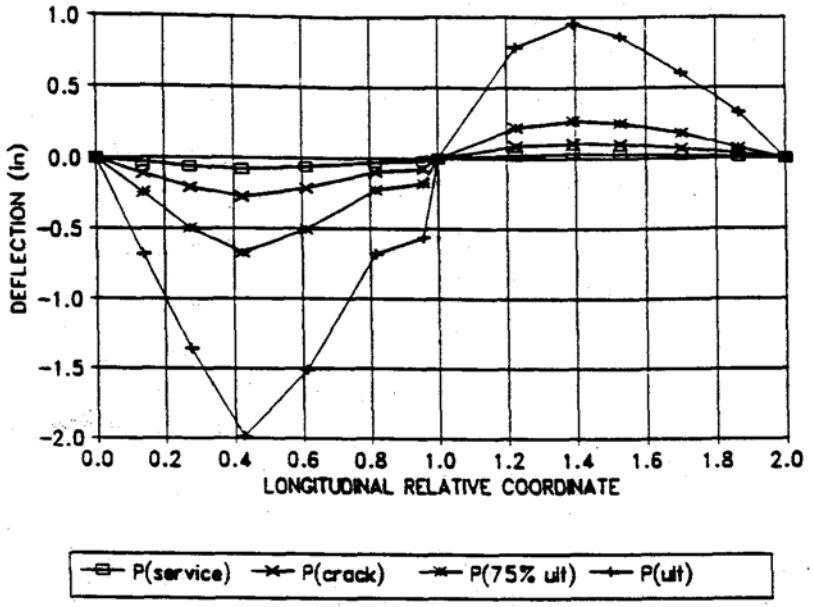

Figure 4.14 Longitudinal Deflection, Ultimate Load Test.

of the top strain gauge was crashed, and rendered the gauge unusable for readings during unloading. Figure 4.15 shows that the cracks had reopened at a load of 601dps. This is indicated by the point where the strain at the bottom surface became essentially constant.

Figure 4.16 shows the load-deflection curve measured directly under the load at the centerline of the bridge for both the "ultimate 1" and "ultimate 2" tests Figures 4.16 indicates that the deflection returned to nearly initial conditions upon unloading. This indicates that although the bridge had been loaded to its ultimate capacity, it retained some capacity to carry load.

Figures 4.17 and 4.18 show the load-strain and load-deflection curves for the ultimate load test measured at the centerline of the bridge under the load.

The results of the "ultimate 1" and "ultimate 2" tests were combined to generate a single load-strain curve (Figure 4.17) and load-deflection curve (Figure 4.18). The single curves were generated by connecting the point on "ultimate 1" corresponding to the maximum "ultimate 1" load of 173 kips to the point on "ultimate 2" corresponding to a load of 180 kips.

Figure 4.17 shows the experimental load-strain curve and the predicted load-strain curve. This figure demonstrates how closely the test results matched the predicted results.

The modified load-deflection curves shown in Figure 4.18 include both experimental and predicted values. Comparing the linear portion of the

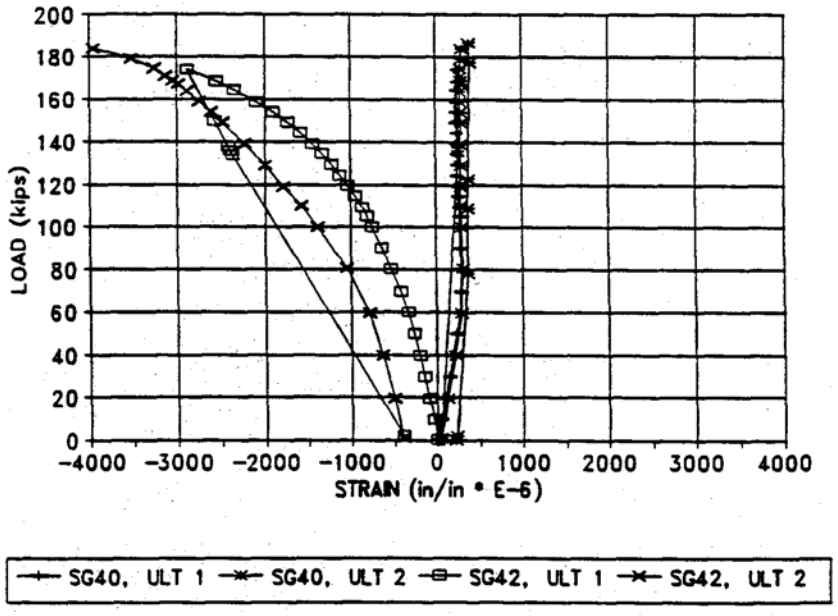

Figure 4.15 Load vs. Strain, Gauge 40 (Bottom) and Gauge 42 (Top), Ultimate Load Test.

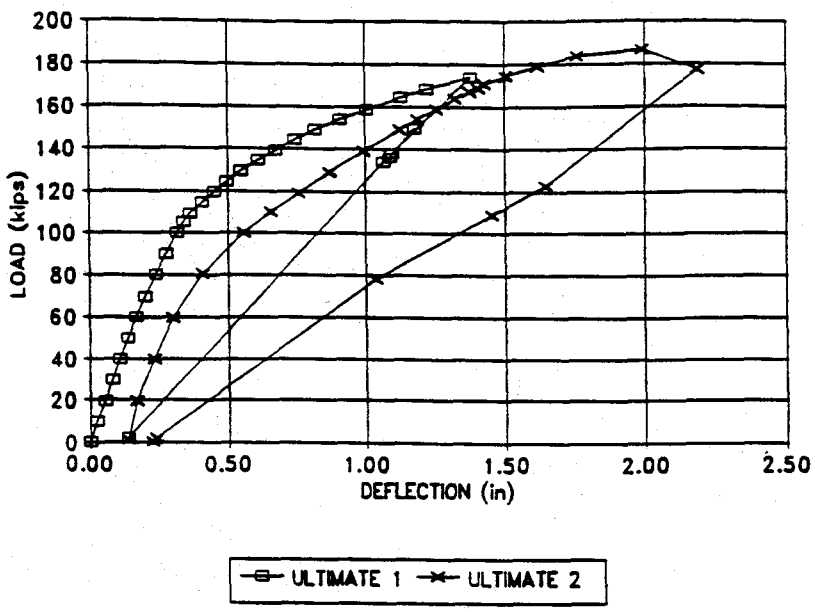

Figure 4.16 Load vs. Deflection, LVDT 3, Ultimate Load Test.

experimental curve to the load-deflection curve from the cracking load test shows that the bridge deflected' at the same rate as before cracking; and very close to the predicted value.

Figure 4.18 also shows the point at which the bridge failed. The bridge was loaded to 187 kips, at which point the load-deflection curve began to flatten. After this point was reached the bridge continued to deflect although the load was decreasing.

Upon completion of the ultimate load test, core drillings were taken at two locations of interest. The first cores were taken at the closure pour in the loaded span. This was done to check if the loud noise experienced during testing was caused by a sudden shear failure at the closure pour. Inspection of the core verified that a shear failure

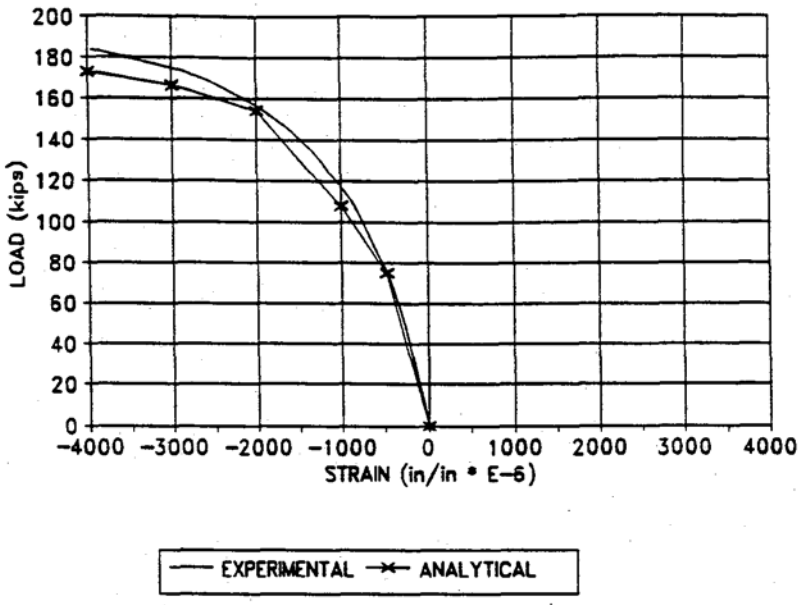

Figure 4.17 Modified Load vs. Strain, Gauge 42 (Top), Ultimate Load Test.

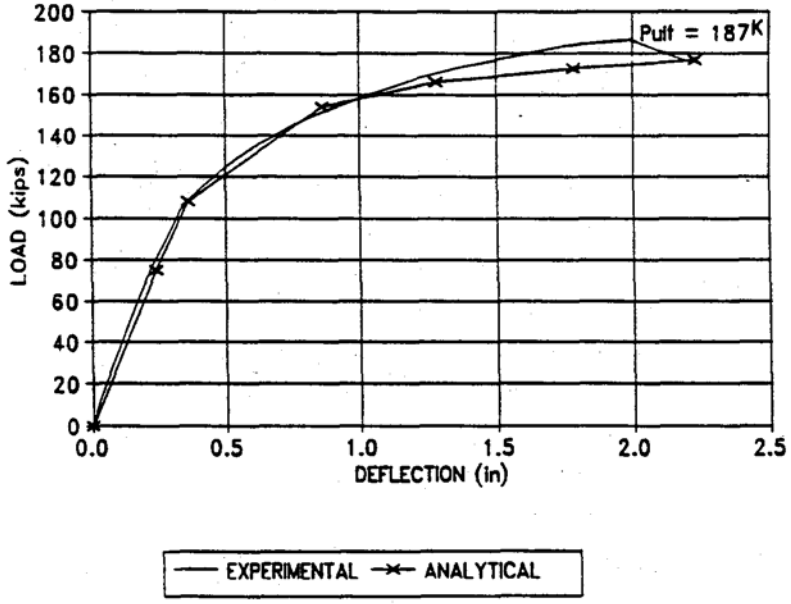

Figure 4.18 Modified Load vs. Deflection, LVDT 3, Ultimate Load Test.

did not occur. The next core was taken in the loaded span, directly over the largest crack on the bottom surface. This core showed that the loud: noise could not be attributed to delamination of the concrete at the level of the prestressing tendons. As previously discussed, the loud noise was finally attributed to a broken seal in the hydraulic ram.

4.4.2 Summary of Ultimate Load Test

In summary, the behavior of the bridge from cracking to failure could be accurately predicted using conventional prestressed, reinforced concrete beam theory. As shown in Figures 4.17 and 4.18, the experimental deflections and strains for the ultimate load test were very close to the predicted values. The ratio of experimental to predicted ultimate load was 1.06. The actual ultimate load was about 53 times the design service load.

CHAPTER 5
SUMMARY AND CONCLUSIONS

5.1 Summary

A half-scale model of a precast, post-tensioned, flat-slab bridge system was built and tested in the Structures Laboratory at the University of Florida. The model was evaluated for service load, fatigue load, cracking load, and ultimate load. The results of service load tests are provided in Ref. [2]. Results of the fatigue load, cracking load, and ultimate load tests are presented in this report.

Two load configurations were used for the service level fatigue load tests. The load configuration used for the first test produced the maximum negative bending moment over the middle support. The load: configuration used for the second test produced the maximum positive bending moment at midspan

The magnitude of the load used for the maximum negative moment test was calculated to reproduce the largest negative moment occurring over any support in the seven-span bridge prototype. The maximum positive moment test was performed using a load which reproduced the largest positive moment occurring anywhere in the seven-span bridge. In both cases, the load was essentially the same and was equal to a two lane truck loading on the model bridge.

The model was subjected to two million cycles in the negative moment load case, and one million cycles in the positive moment load case. Upon completion of each load case the behavior of the bridge was examined by performing static tests equal to the three lane design load.

Following testing under the service level fatigue loading, the model was statically loaded to its cracking load. This test was performed to determine if the cracking strength of the bridge could be accurately predicted using traditional reinforced, prestressed concrete beam analysis. The cracking load of the model was determined by elastic analysis of the prestressed bridge cross-section. The cracking moments were calculated using strain-compatibility methods.

After the cracking load test, the model was subjected to an increased fatigue load to investigate the behavior of the model` under extreme loading conditions after cracking. To insure that the increased fatigue load was greater than the largest load the bridge had been subjected to prior to the cracking test, the decision was made to use 150% of three lane service live load.

The final objective of this research project was to investigate the ultimate load capacity of the model. The purpose of this test was to determine the degree of accuracy with which the ultimate ¯capacity of the bridge could be estimated using conventional methods.

The ultimate load was determined from the moment-curvature relationships for the bridge cross-section with the bridge modeled as a one-way beam continuous over three supports. The moment-curvature relationships for the loaded and unloaded spans

were determined using conventional strain compatibility relationships for prestressed concrete sections. Predicted load-strain and load-deflection diagrams were developed from the moment-curvature relationships.

5.2 Conclusions

The results of the analytical and experimental evaluation of the posttensioned flat-slab bridge system for service, fatigue, and ultimate loads indicated the following:

1) Test results from previous work [2] showed that the behavior of the bridge at service loads could be accurately predicted using a finite element model.

2) The results of fatigue load tests for three million cycles of two-lane service load and an additional two million cycles of 150% of the three-lane service load performed after cracking indicated that the bridge remained in the linear-elastic range. No degradation of stiffness was observed over the five million cycles of fatigue load.

3) Test results for the ultimate load test indicated that the behavior of the system beyond cracking load (i.e., the elastic range) could be adequately predicted using a one-way beam model and conventional prestressed concrete beam theory.

In conclusion, the bridge system behaved as predicted for all load cases. With the apparent cost savings, short erection time, and the multi-span continuity

of this system, it should certainly be considered as a viable alternative for trestletype bridge applications.

APPENDIX A
FATIGUE LOAD TEST

The following figures show the data collected for the fatigue load tests. Figures A.1 and A.2 represent the negative moment load case for service level fatigue load. Figures A.3 and A.4 represent the positive moment load case for service level fatigue load. The. test results for the fatigue load test after cracking are shown in Figures A.5 through A.7. All figures represent the data collected for the static loading for three lanes of AASHTO HS20-44 truck that was performed at the end of the corresponding test.

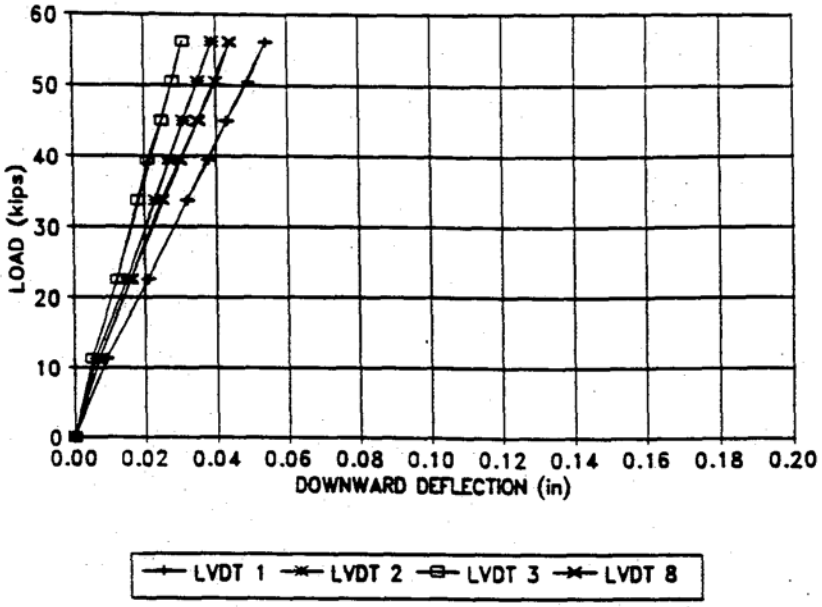

Figure A.1 Negative Moment Load Case for Service Level Fatigue Load Test, Load vs. Deflection, LVDTs 1, 2, 3, & 8.

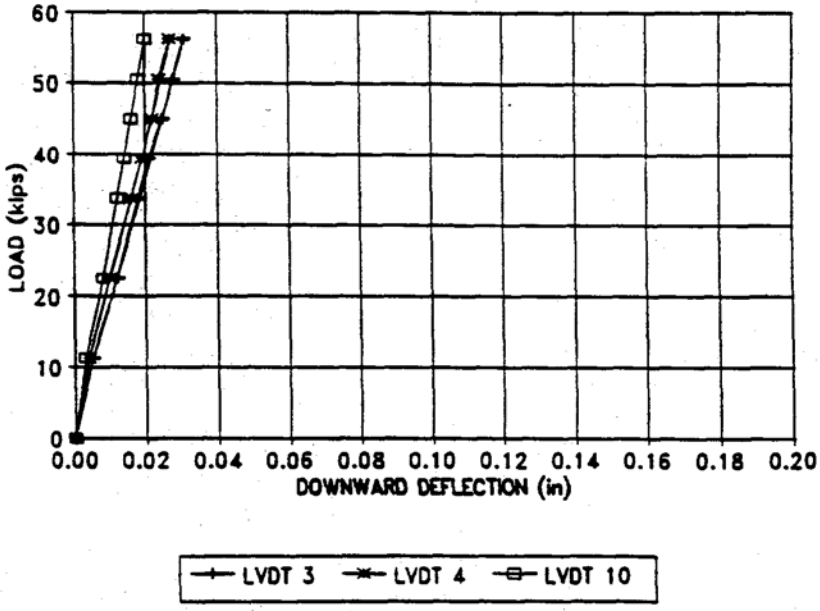

Figure A.2 Negative Moment Load Case for Service Level Fatigue Load Test, Load vs. Deflection, LVDTs 3, 4, & 10.

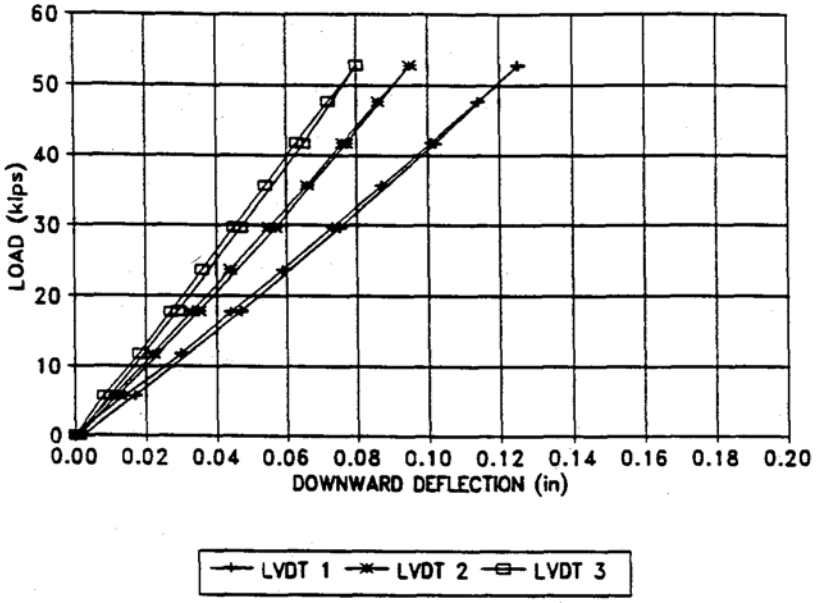

Figure A.3 Positive Moment Load Case for Service Level Fatigue Load Test, Load vs. Deflection, LVDTs 1, 2, & 3.

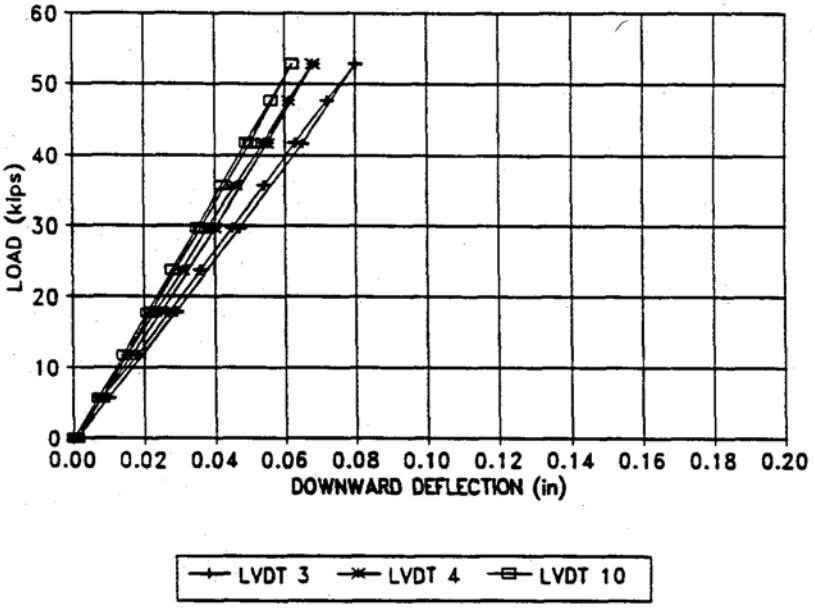

Figure A.4 Positive Moment Load Case for Service Level Fatigue Load Test, Load vs. Deflection, LVDTs 3, 4, & 10.

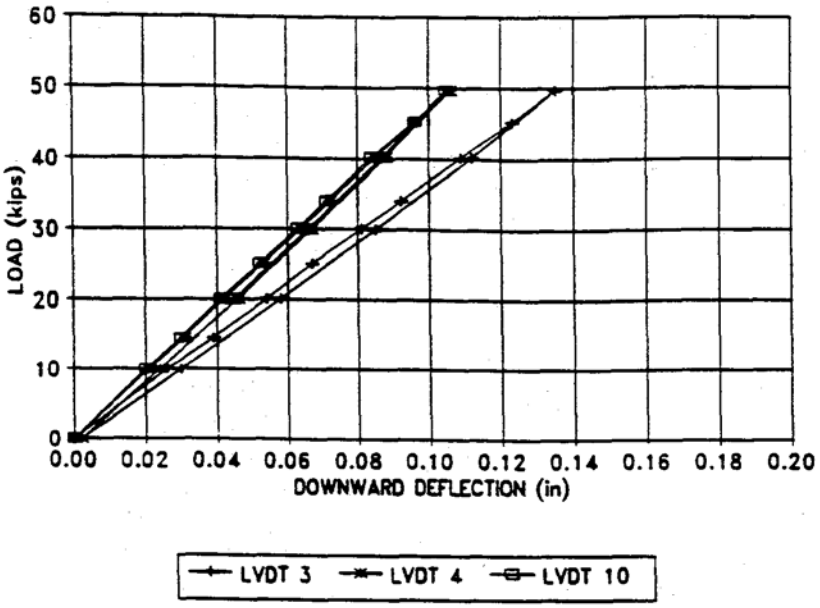

Figure A.5 Fatigue Load After Cracking, Load vs. Deflection, LVDTs 3, 4, & 10.

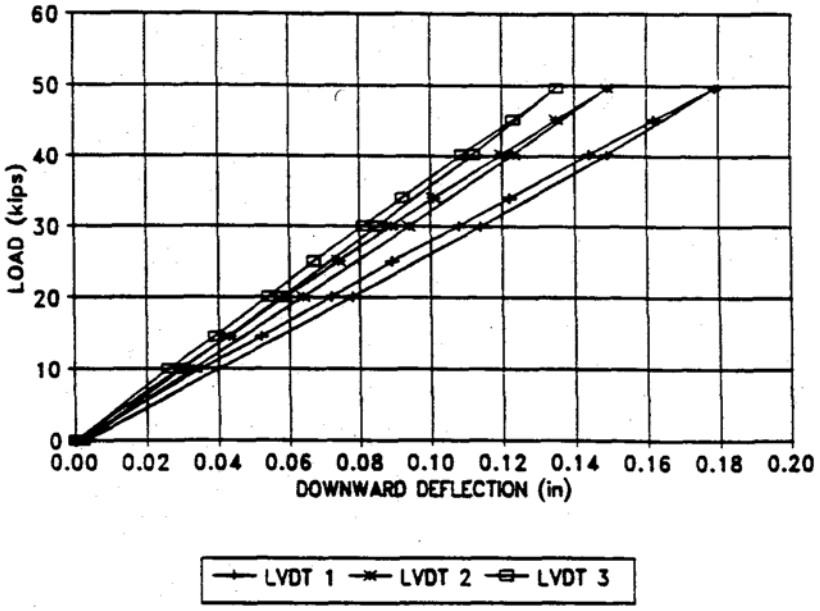

Figure A.6 Fatigue Load After Cracking, Load vs. Deflection, LVDTs 1, 2, & 3.

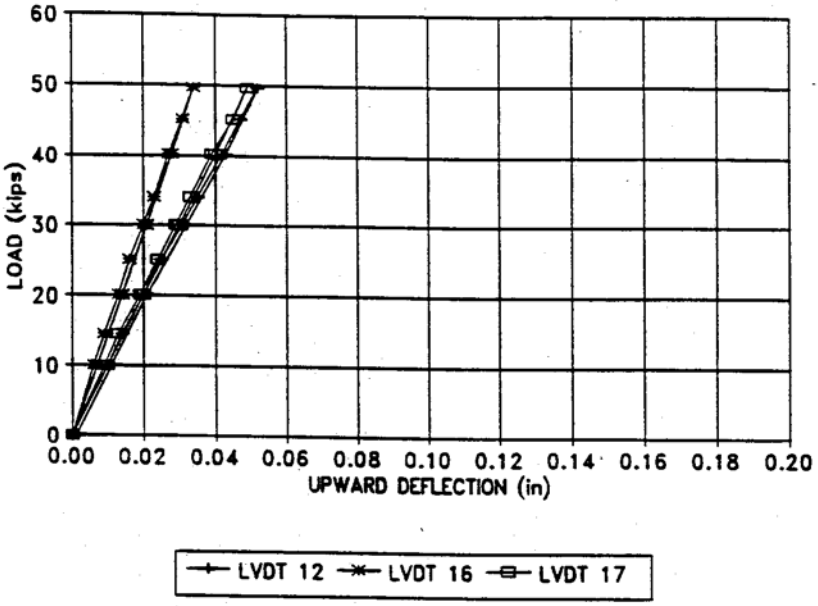

Figure A.7 Fatigue Load After Cracking, Load vs. Deflection, LVDTs 12, 16, & 17.

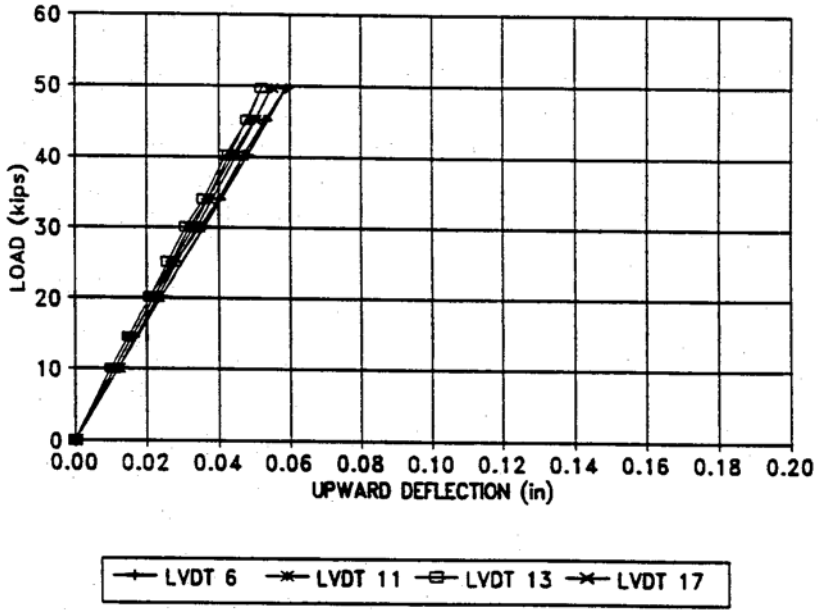

Figure A.8 Fatigue Load After Cracking, Load vs. Deflection, LVDTs 6, 11, 13 & 17 .

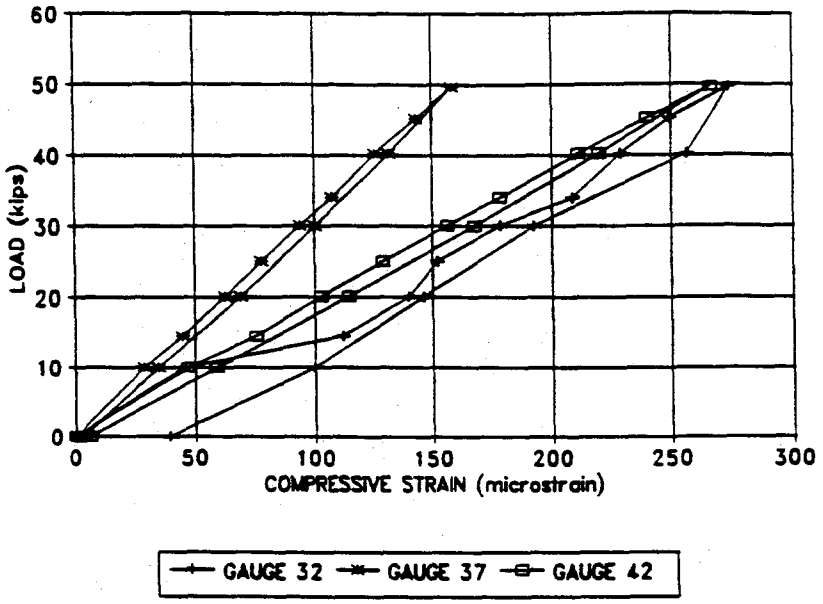

Figure A.9 Fatigue Load After Cracking, Load vs. Strain, Gauges 32, 37, & 42 .

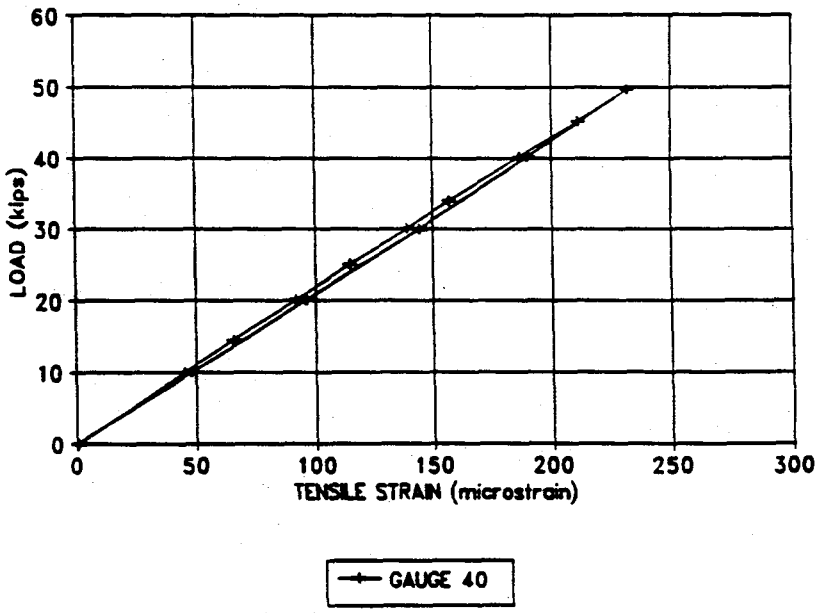

Figure A.10 Fatigue Load After Cracking, Load vs. Strain, Gauge 40.

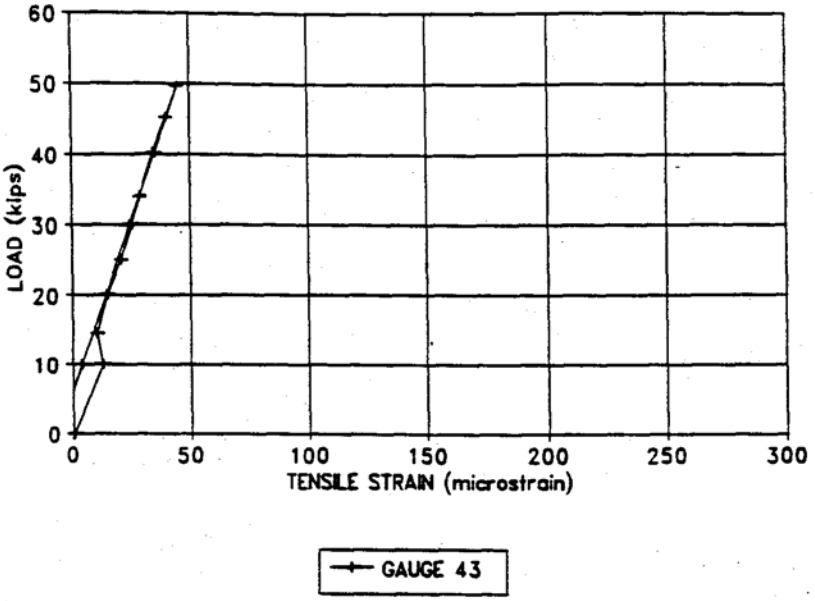

Figure A.11 Fatigue Load After Cracking, Load vs. Strain, Gauge 43.

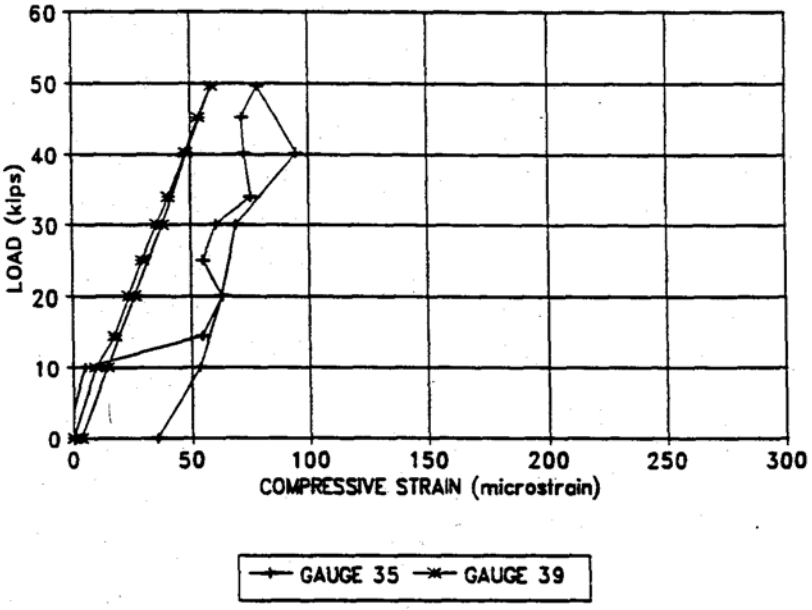

Figure A.12 Fatigue Load After Cracking, Load vs. Strain, Gauges 35 & 39.

APPENDIX B
CRACKING LOAD TEST

The following figures show the data collected for the cracking load test. The LVDT data is arranged first with the strain gauge data following.

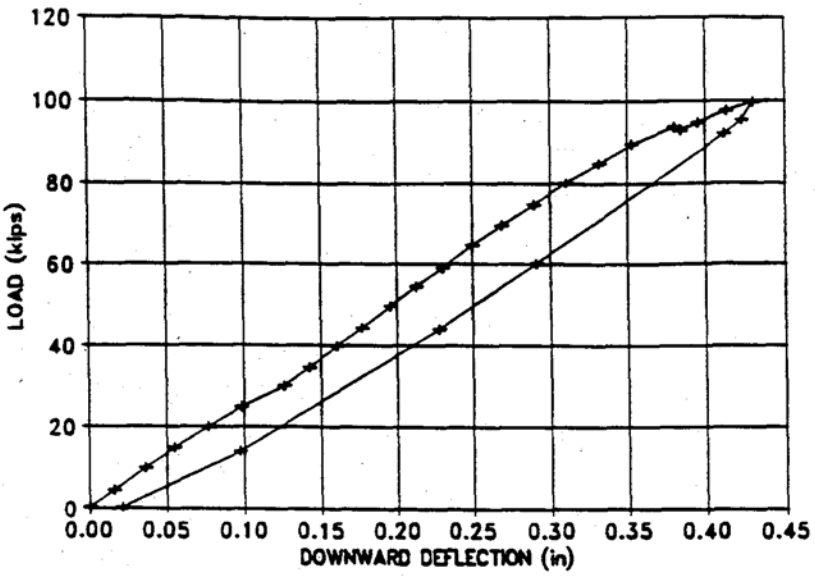

Figure B.1 Cracking Load Test, Load vs. Deflection, LVDT 1.

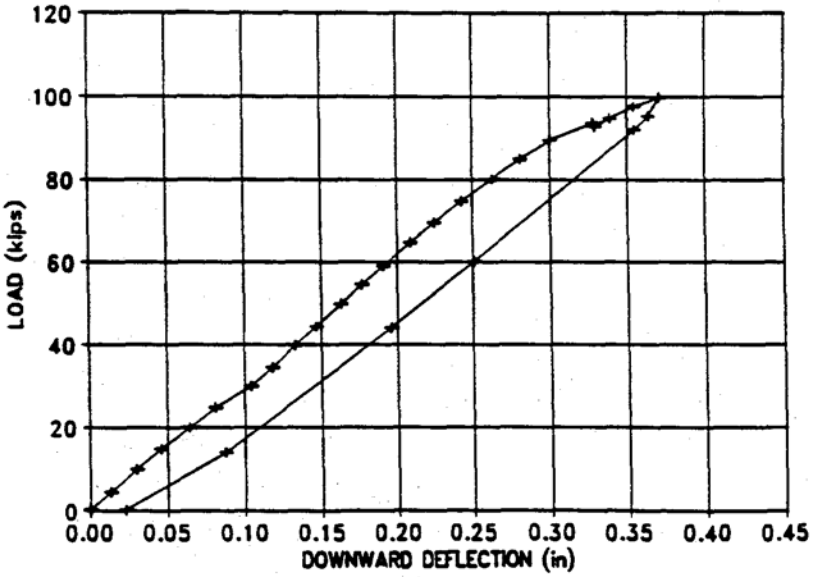

Figure B.2 Cracking Load Test, Load vs. Deflection, LVDT 2.

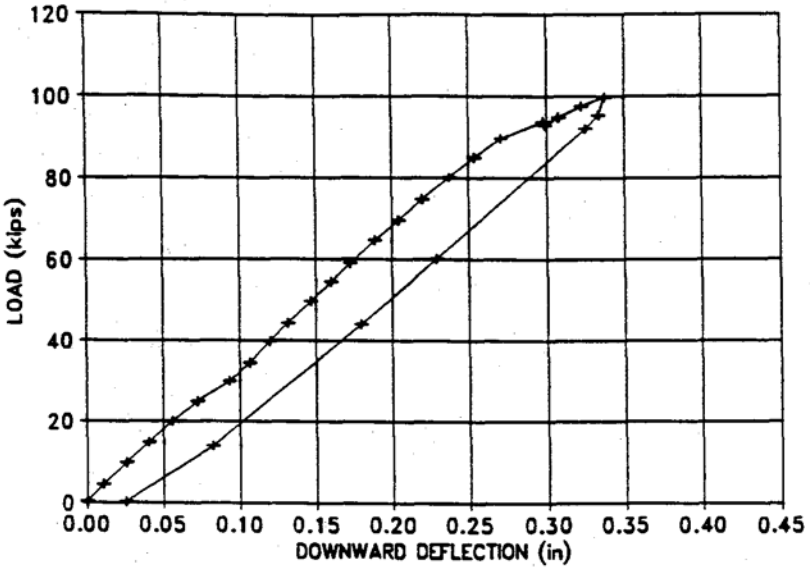

Figure B.3 Cracking Load Test, Load vs. Deflection, LVDT 3.

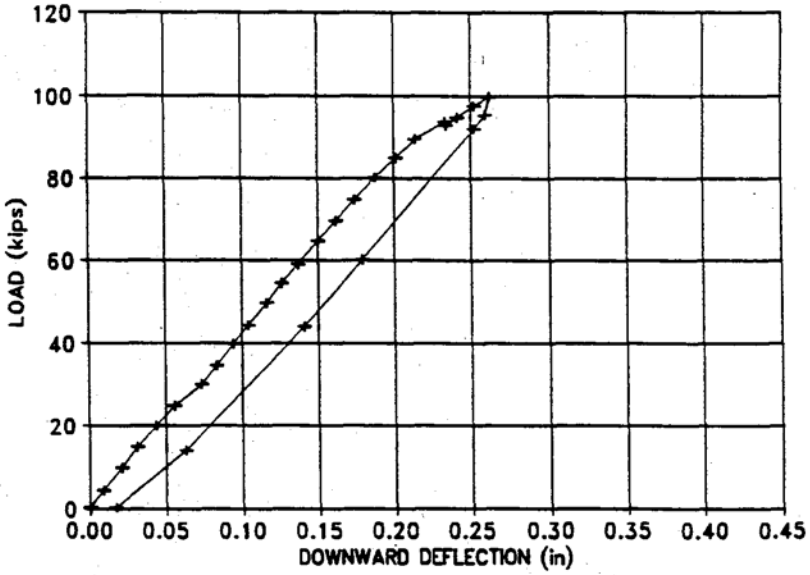

Figure B.4 Cracking Load Test, Load vs. Deflection, LVDT 4.

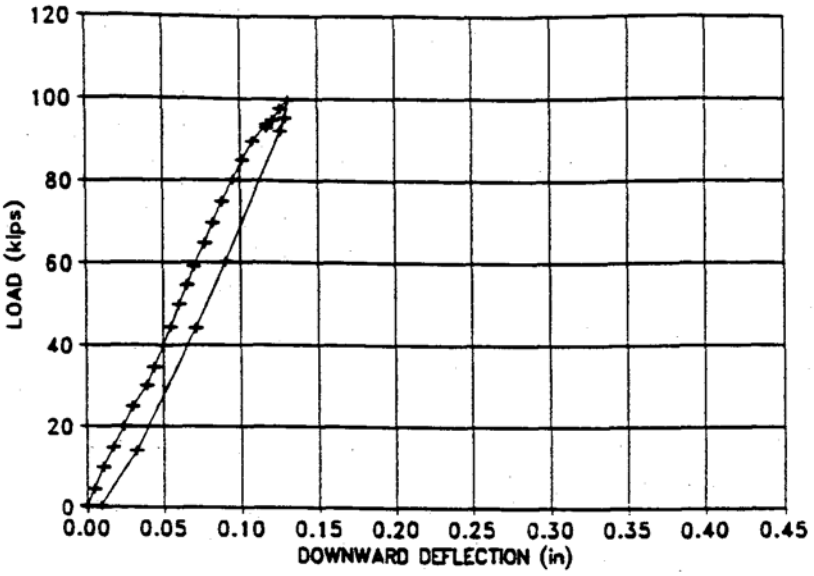

Figure B.5 Cracking Load Test, Load vs. Deflection, LVDT 5.

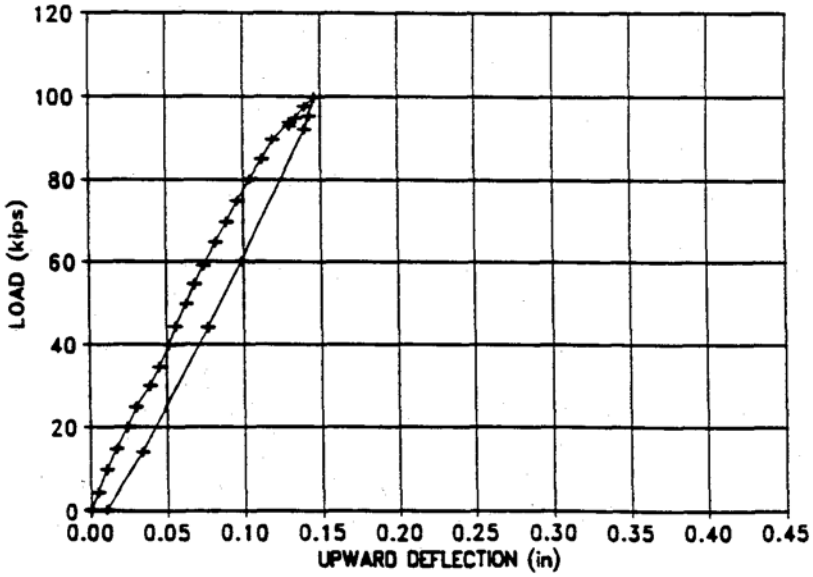

Figure B.6 Cracking Load Test, Load vs. Deflection, LVDT 6.

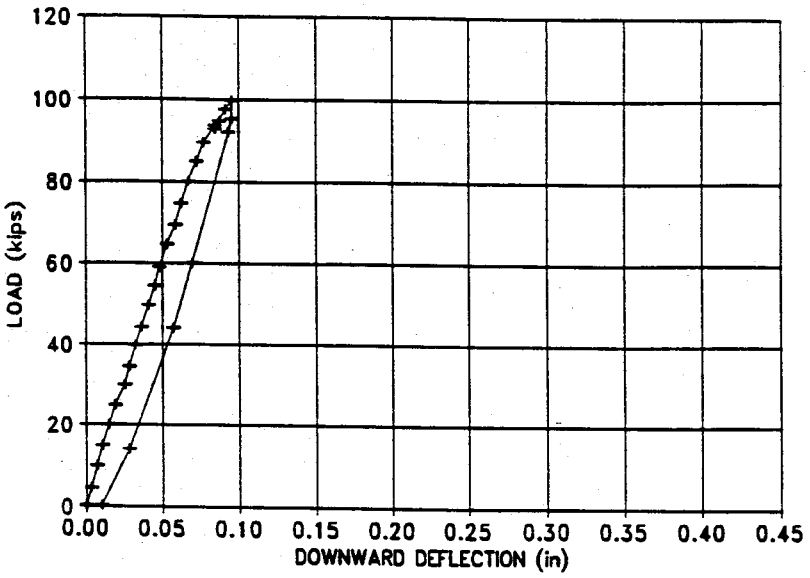

Figure B.7 Cracking Load Test, Load vs. Deflection, LVDT 7.

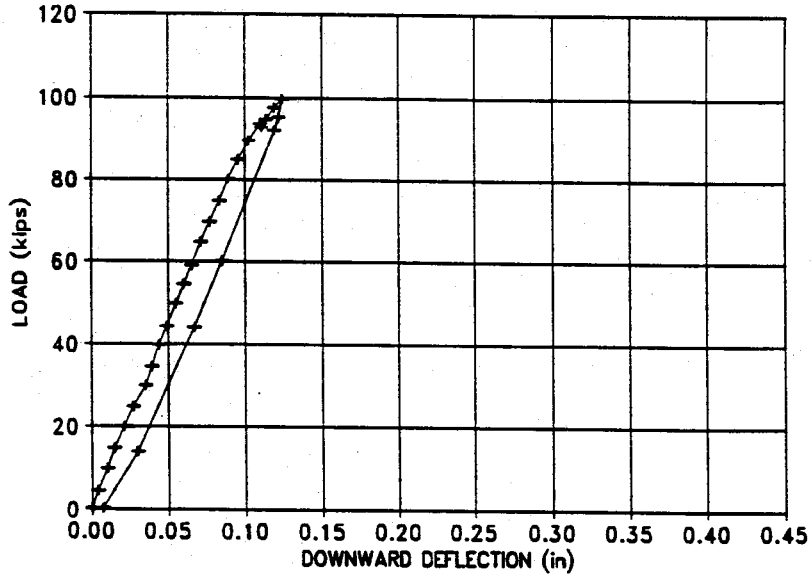

Figure B.8 Cracking Load Test, Load vs. Deflection, LVDT 9.

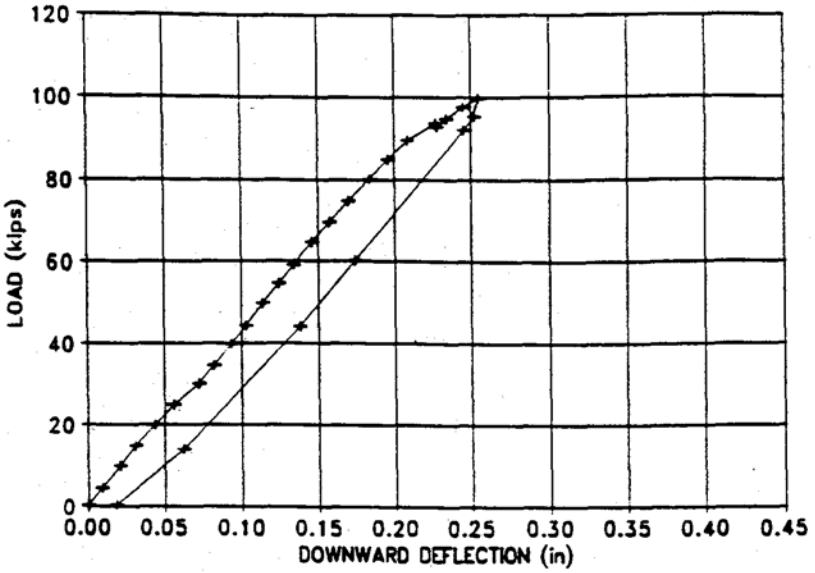

Figure B.9 Cracking Load Test, Load vs. Deflection, LVDT 10.

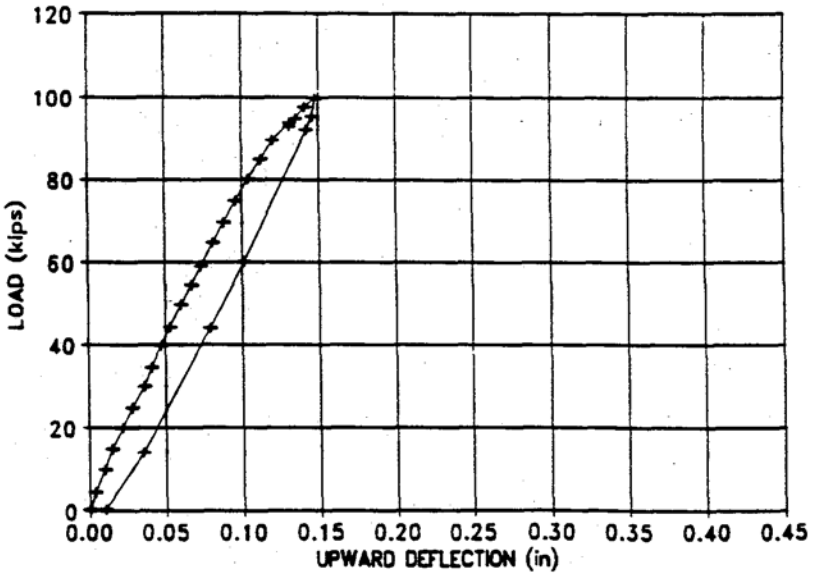

Figure B.10 Cracking Load Test, Load vs. Deflection, LVDT 11.

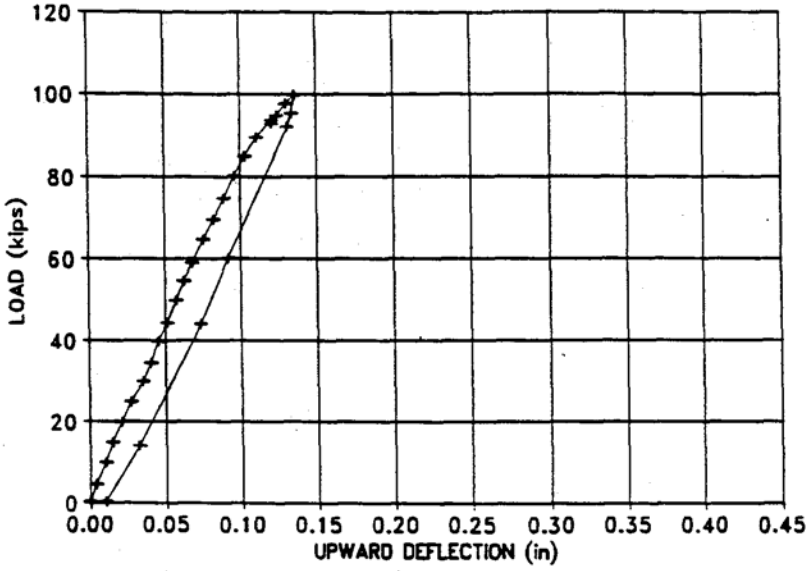

Figure B.11 Cracking Load Test, Load vs. Deflection, LVDT 12.

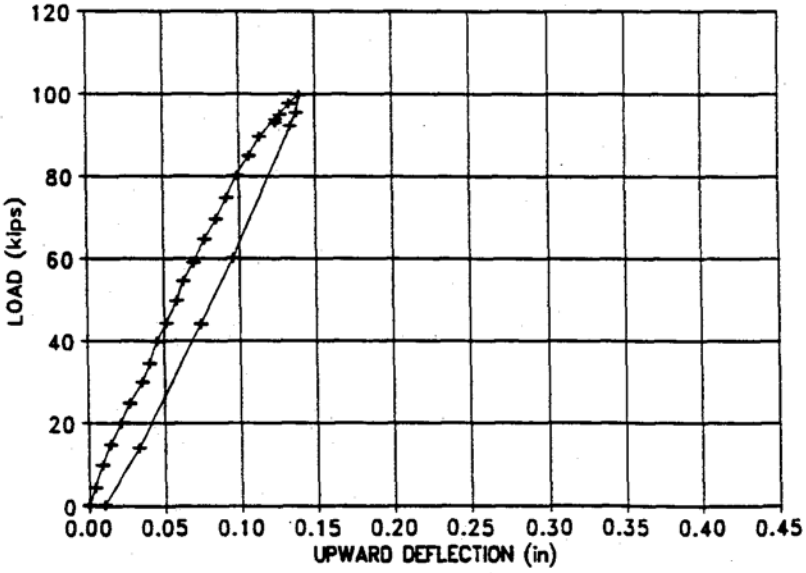

Figure B.12 Cracking Load Test, Load vs. Deflection, LVDT 13.

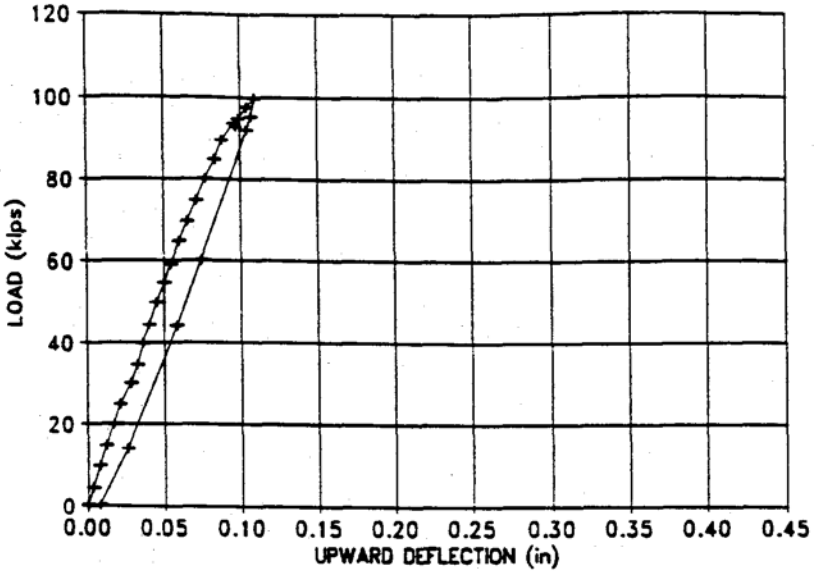

Figure B.13 Cracking Load Test, Load vs. Deflection, LVDT 14.

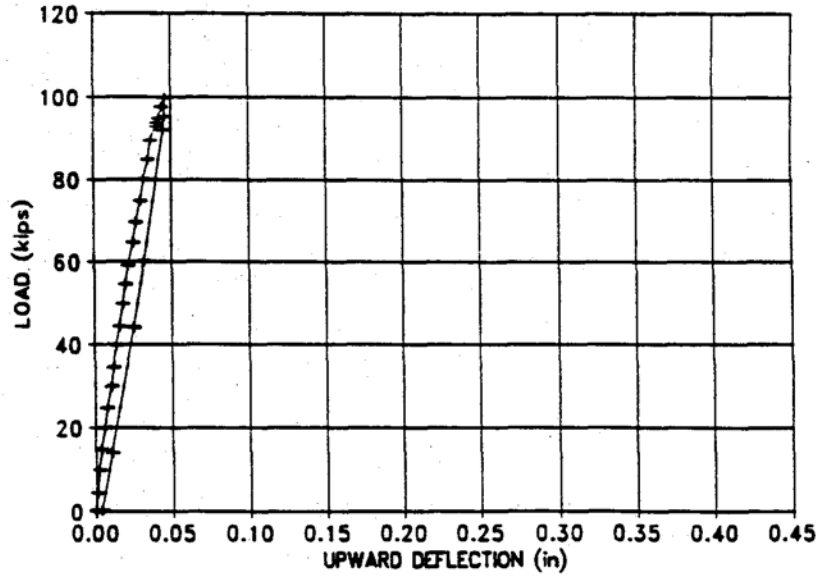

Figure B.14 Cracking Load Test, Load vs. Deflection, LVDT 15.

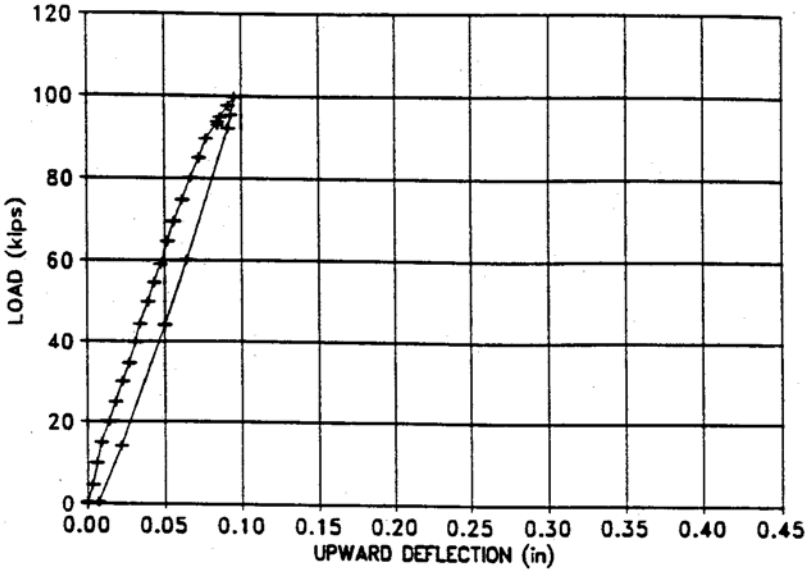

Figure B.15 Cracking Load Test, Load vs. Deflection, LVDT 16.

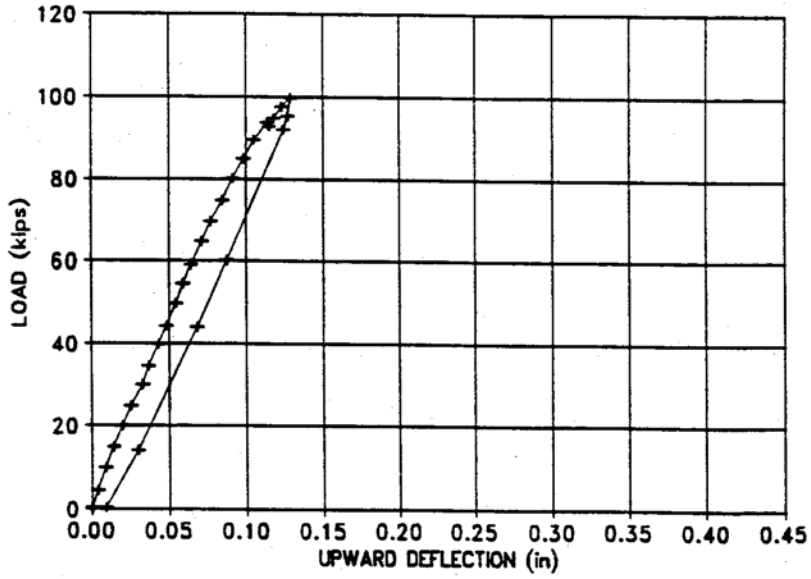

Figure B.16 Cracking Load Test, Load vs. Deflection, LVDT 17.

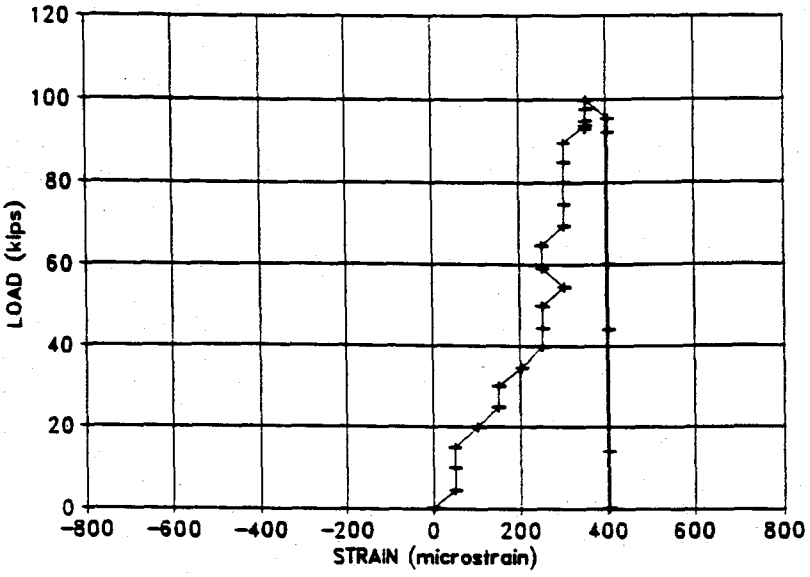

Figure B.17 Cracking Load Test, Load vs. Strain, Gauge 1.

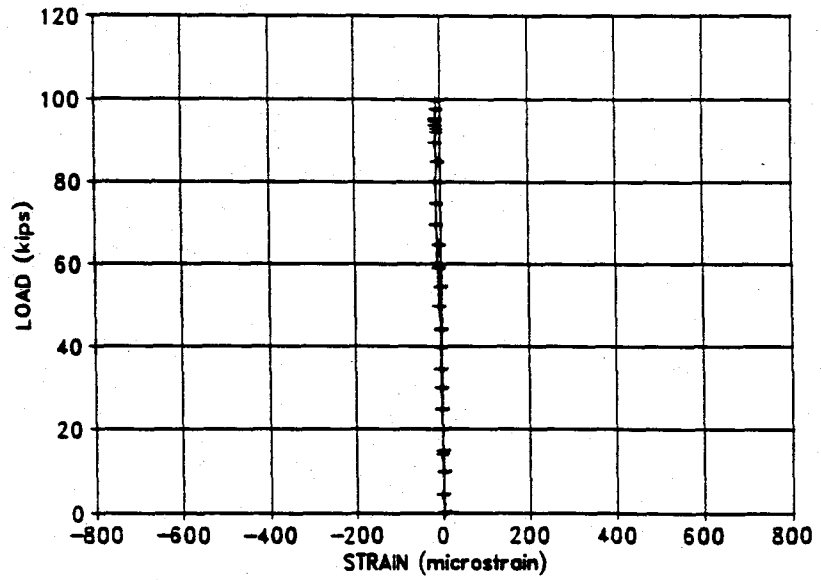

Figure B.18 Cracking Load Test, Load vs. Strain, Gauge 2.

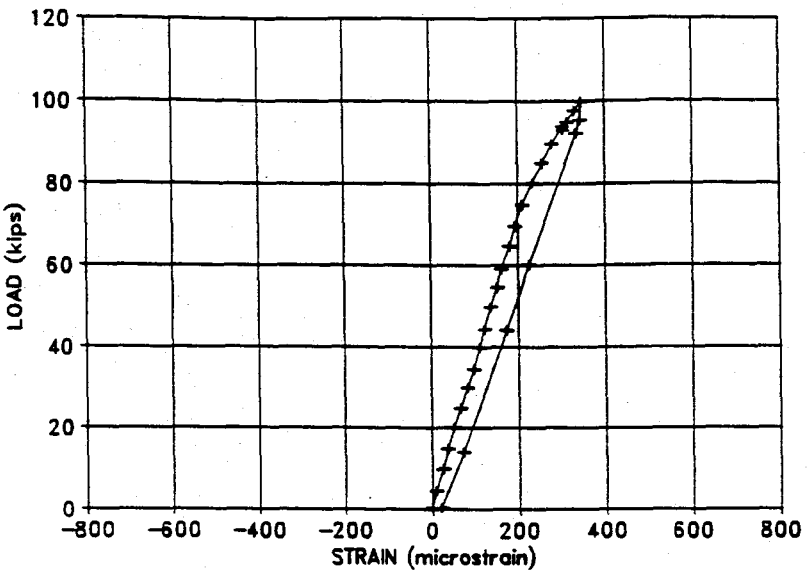

Figure B.19 Cracking Load Test, Load vs. Strain, Gauge 3.

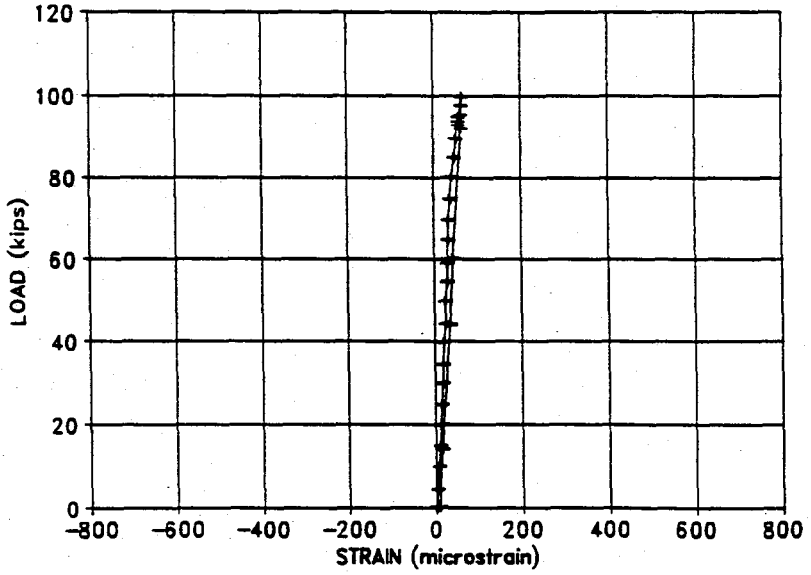

Figure B.20 Cracking Load Test, Load vs. Strain, Gauge 4.

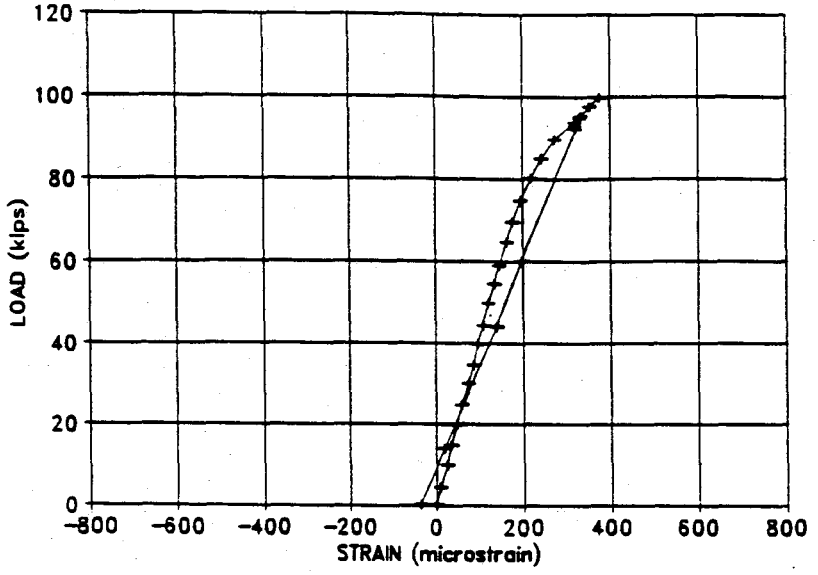

Figure B.21 Cracking Load Test, Load vs. Strain, Gauge 5.

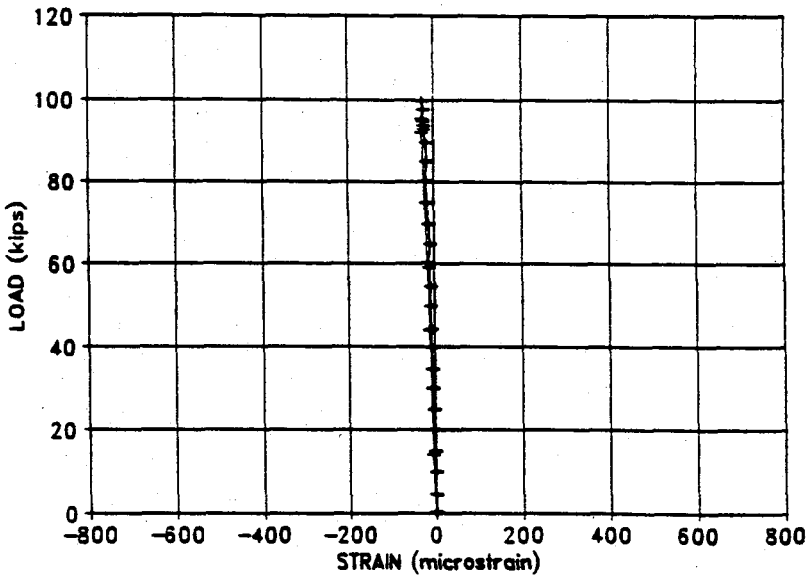

Figure B.22 Cracking Load Test, Load vs. Strain, Gauge 6.

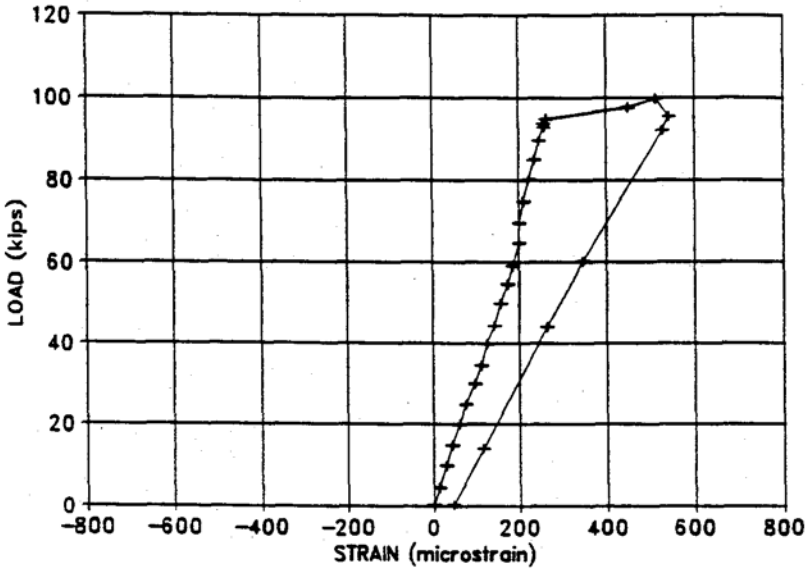

Figure B.23 Cracking Load Test, Load vs. Strain, Gauge 7.

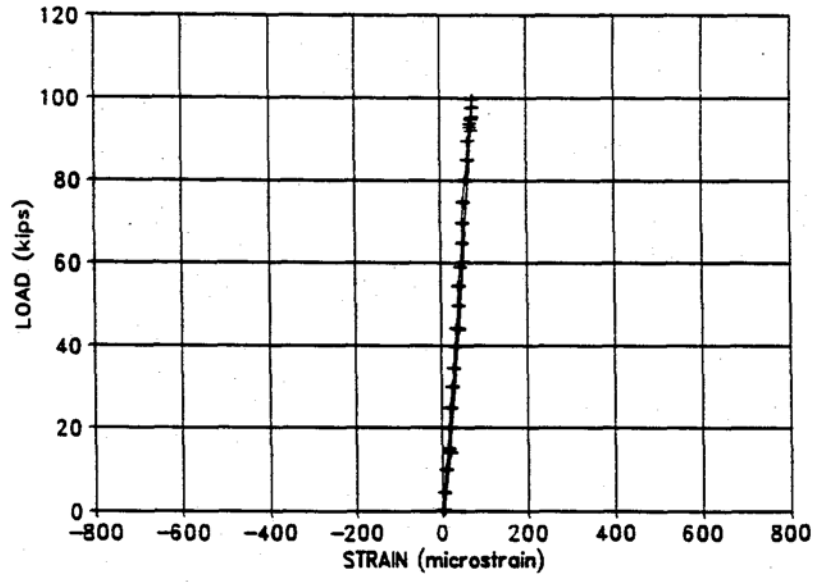

Figure B.24 Cracking Load Test, Load vs. Strain, Gauge 8.

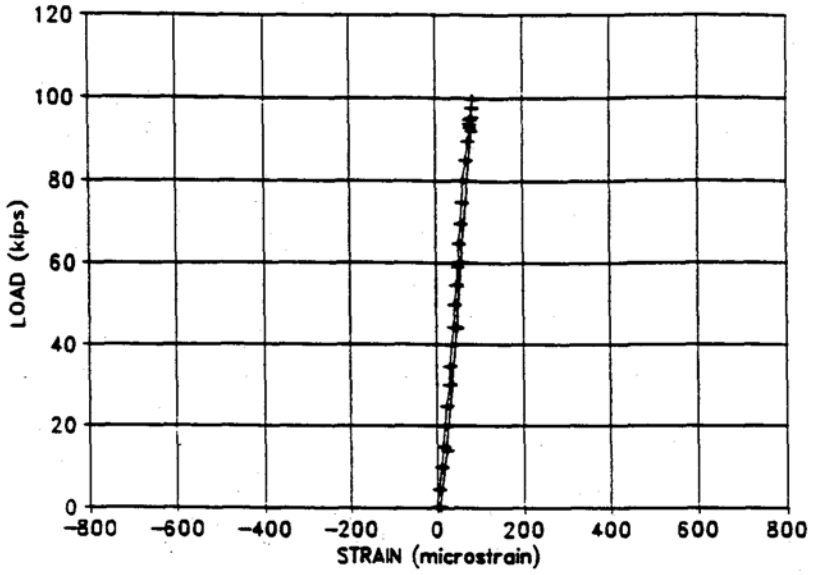

Figure B.25 Cracking Load Test, Load vs. Strain, Gauge 9.

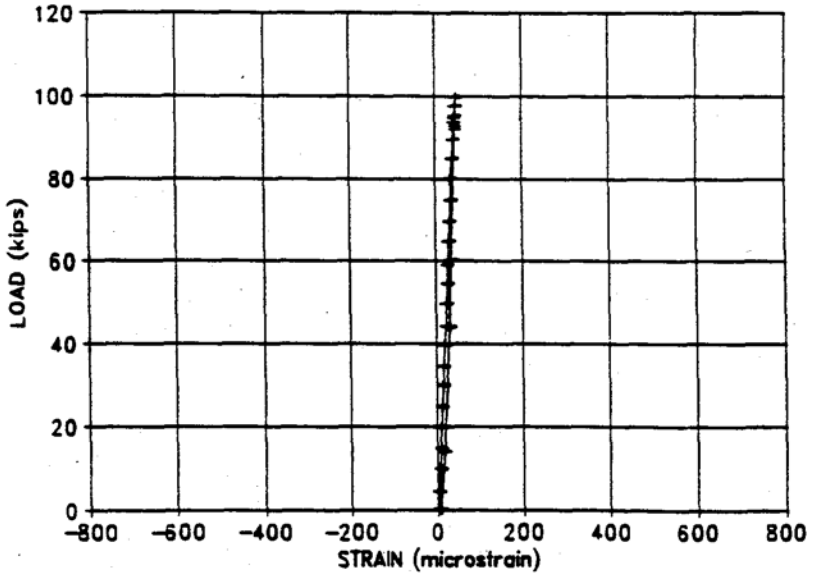

Figure B.26 Cracking Load Test, Load vs. Strain, Gauge 18.

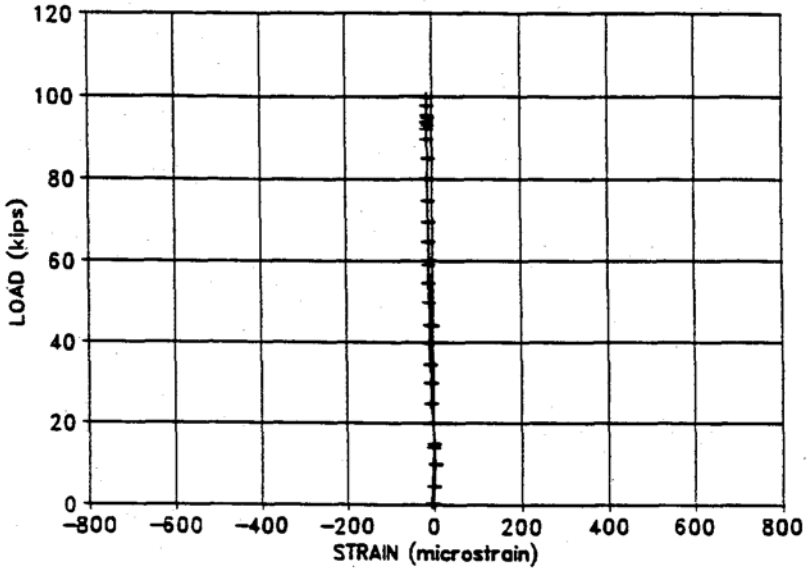

Figure B.27 Cracking Load Test, Load vs. Strain, Gauge 31.

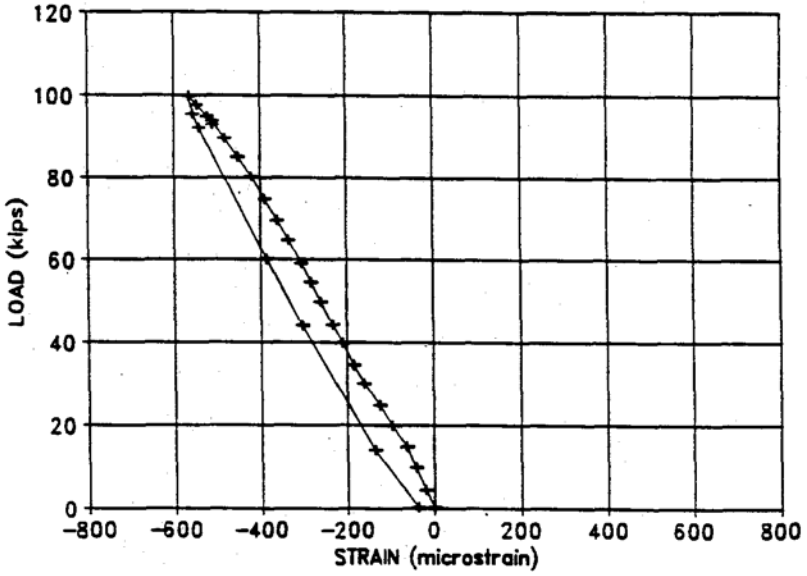

Figure B.28 Cracking Load Test, Load vs. Strain, Gauge 32.

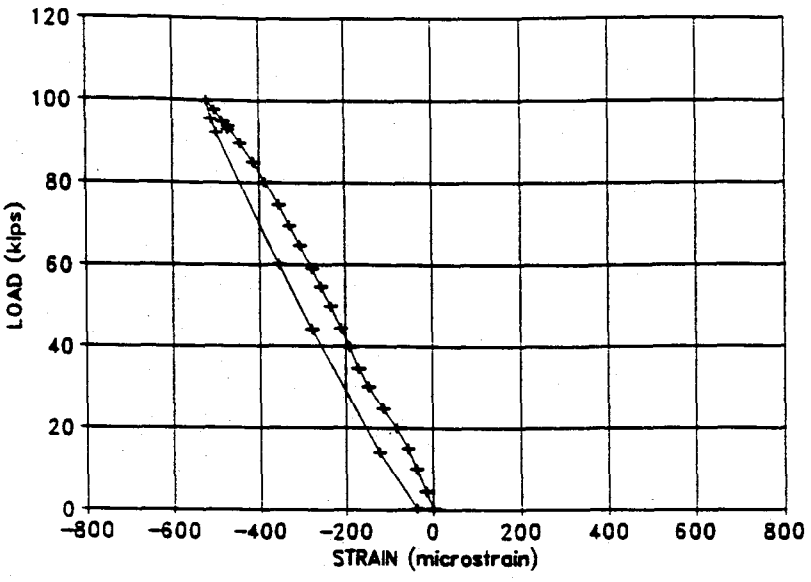

Figure B.29 Cracking Load Test, Load vs. Strain, Gauge 33.

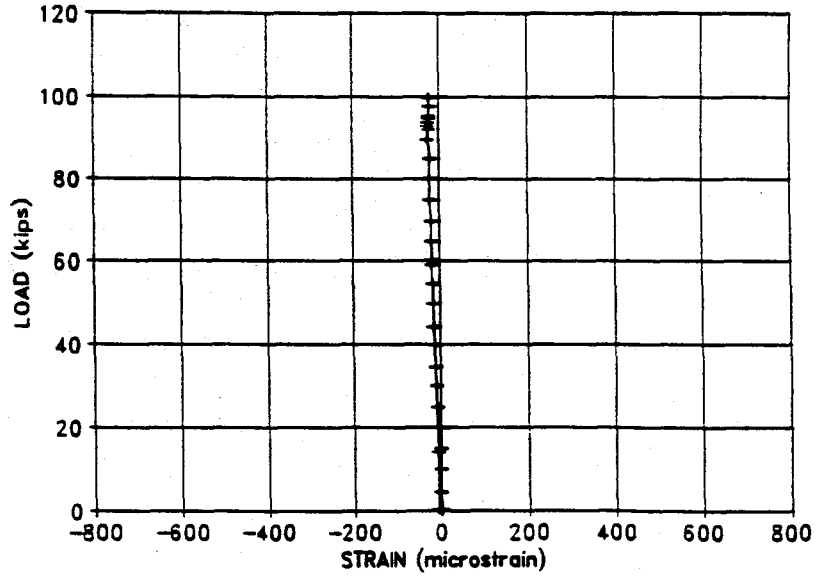

Figure B.30 Cracking Load Test, Load vs. Strain, Gauge 34.

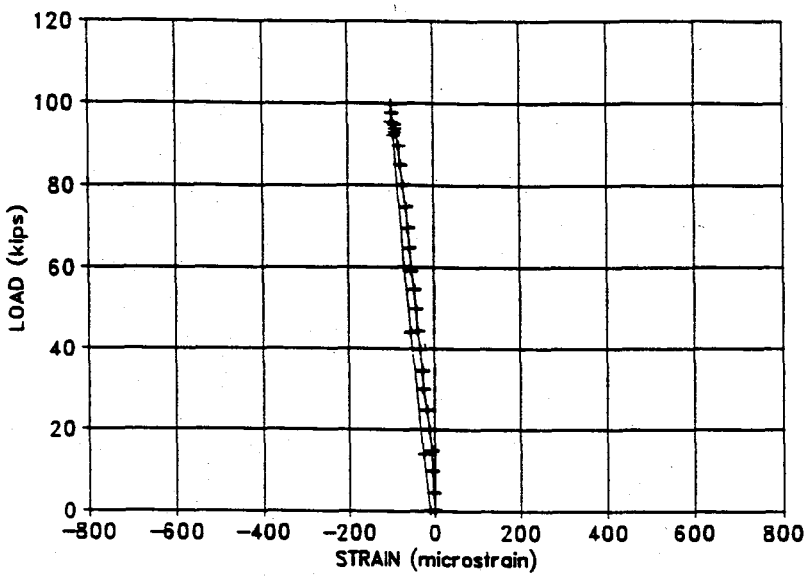

Figure B.31 Cracking Load Test, Load vs. Strain, Gauge 35.

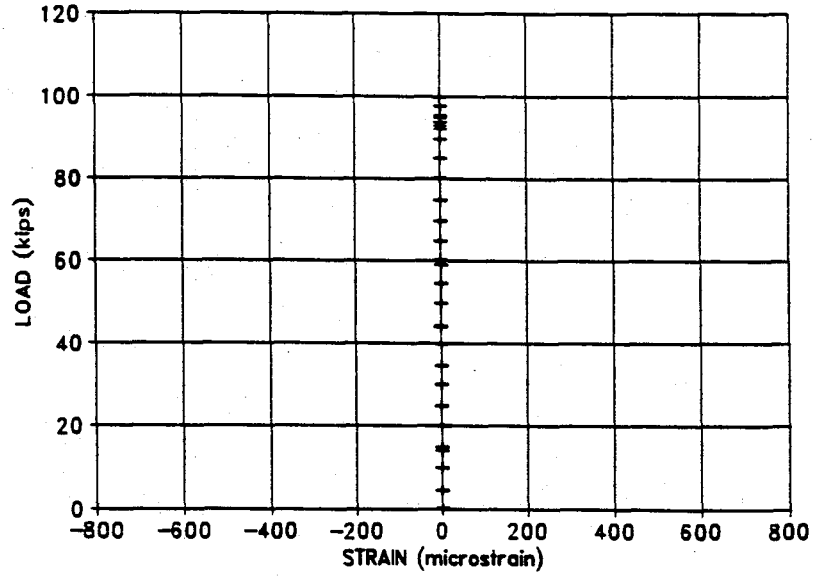

Figure B.32 Cracking Load Test, Load vs. Strain, Gauge 36.

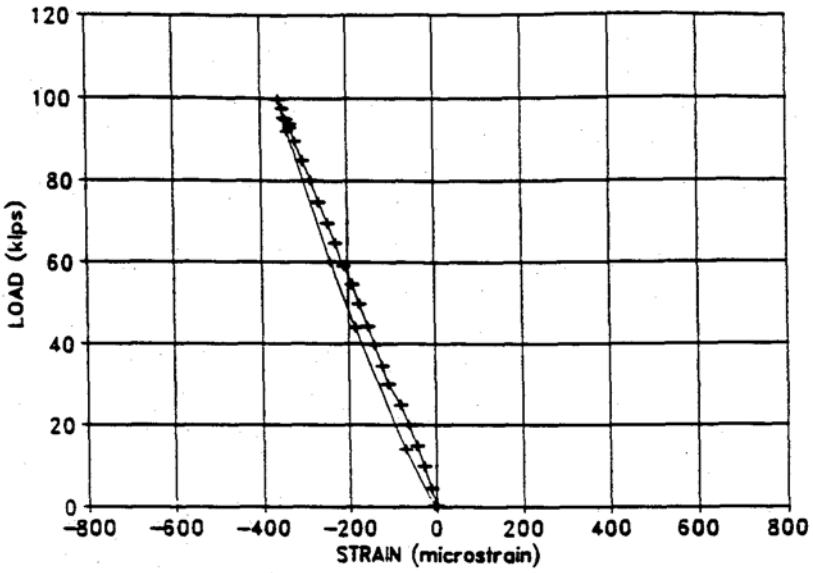

Figure B.33 Cracking Load Test, Load vs. Strain, Gauge 37.

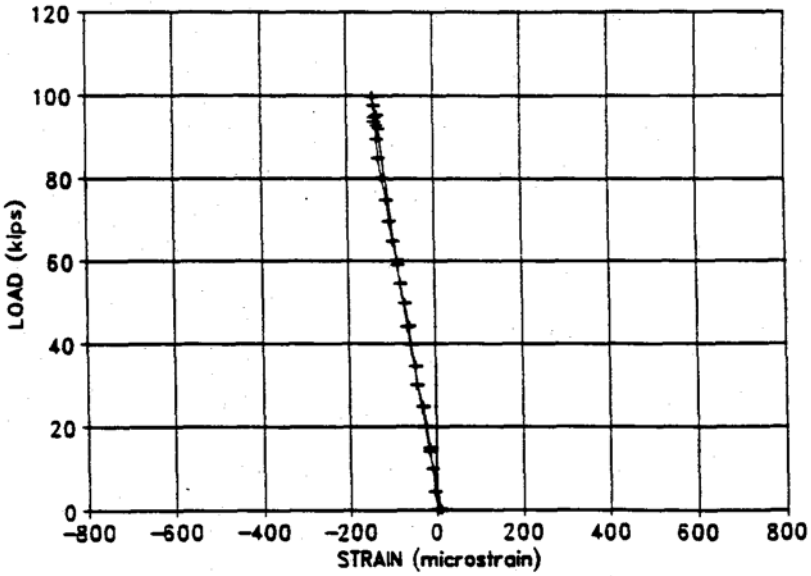

Figure B.34 Cracking Load Test, Load vs. Strain, Gauge 38.

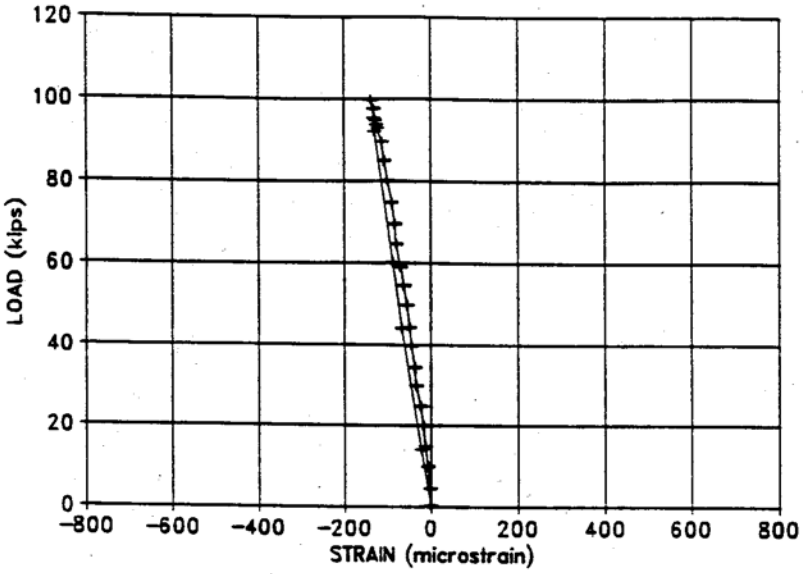

Figure B.35 Cracking Load Test, Load vs. Strain, Gauge 39.

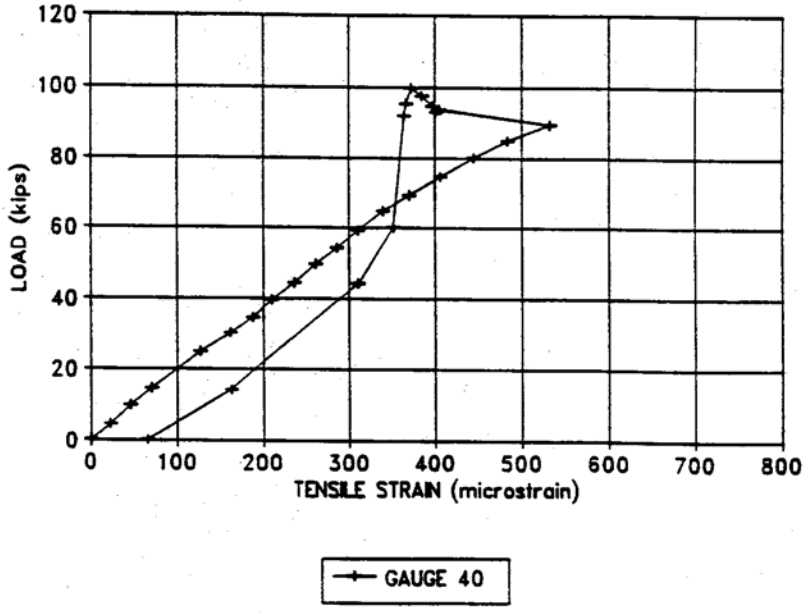

Figure B.36 Cracking Load Test, Load vs. Strain, Gauge 40.

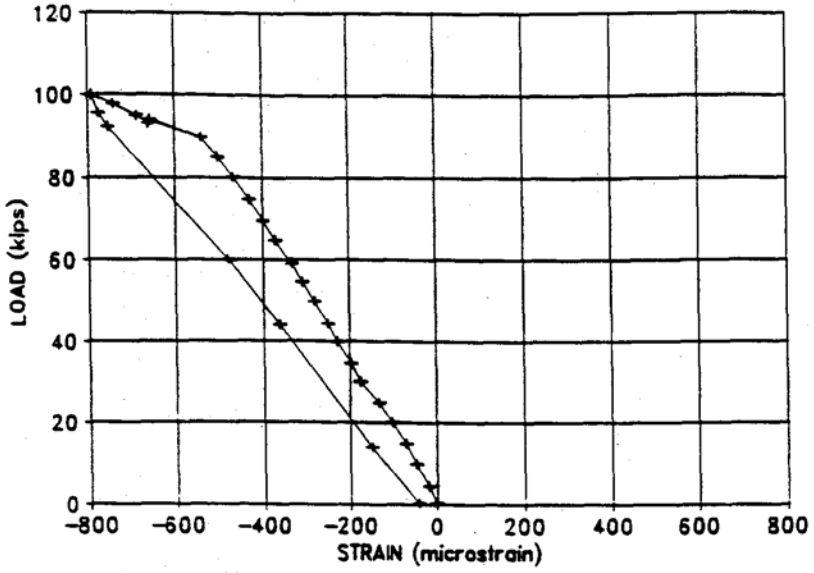

Figure B.37 Cracking Load Test, Load vs. Strain, Gauge 42.

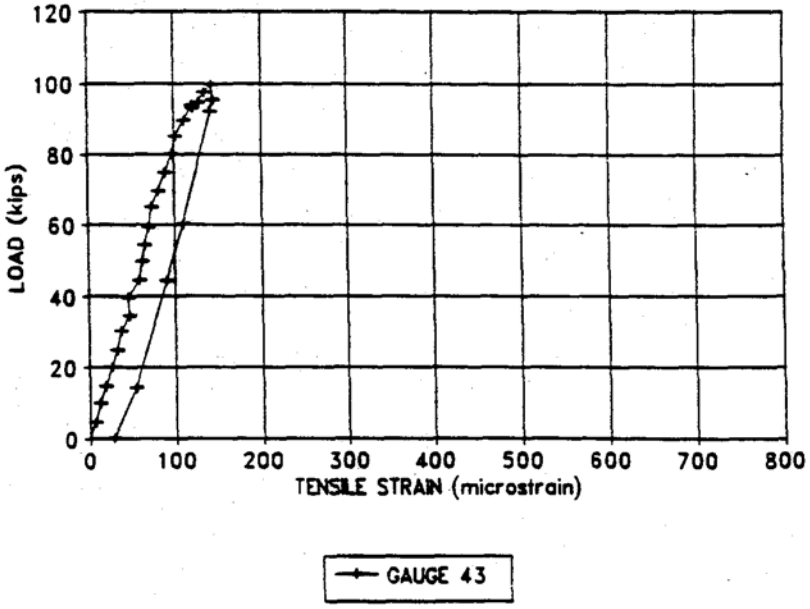

Figure B.38 Cracking Load Test, Load vs. Strain, Gauge 43.

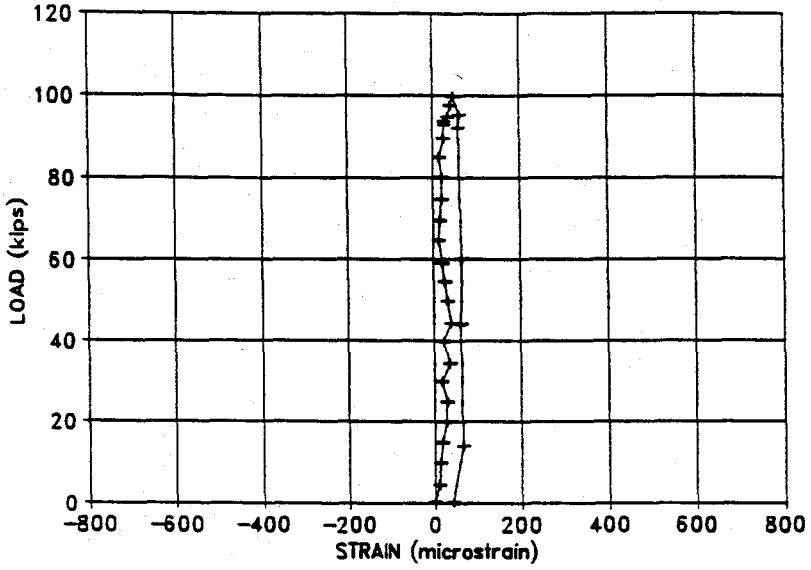

Figure B.39 Cracking Load Test, Load vs. Strain, Gauge 44.

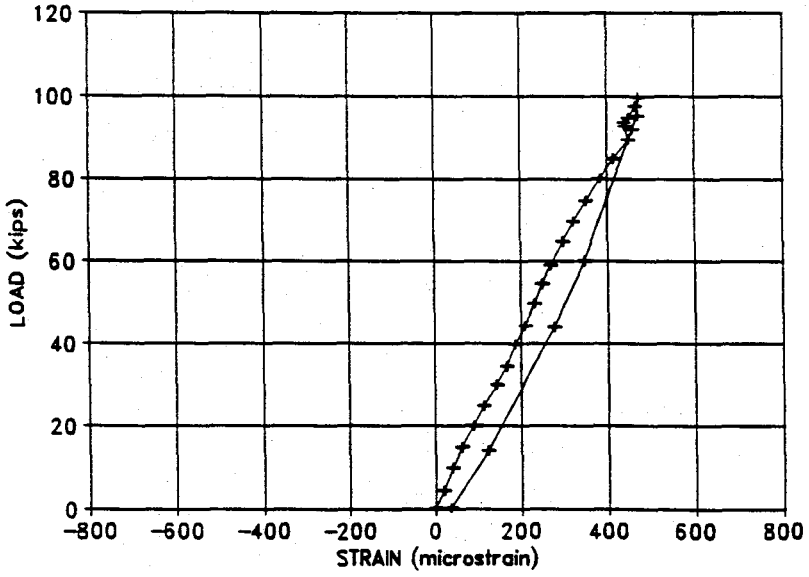

Figure B.40 Cracking Load Test, Load vs. Strain, Gauge 45.

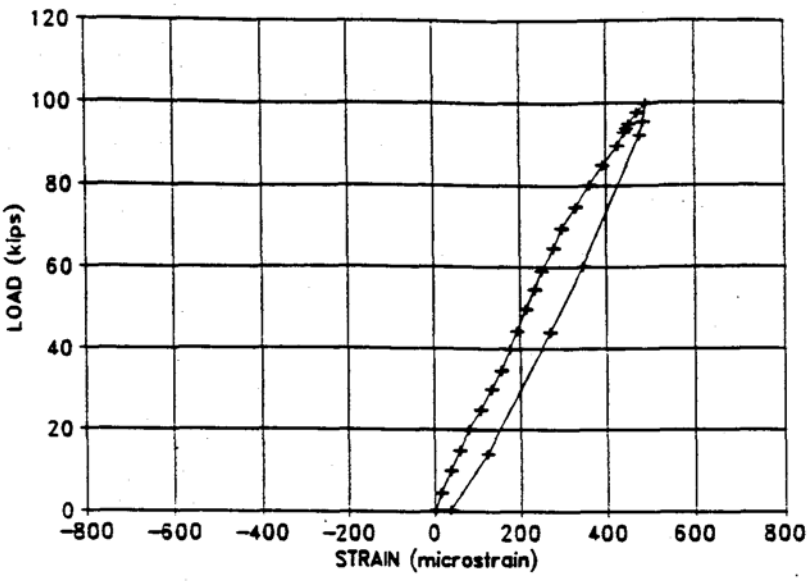

Figure B.41 Cracking Load Test, Load vs. Strain, Gauge 46.

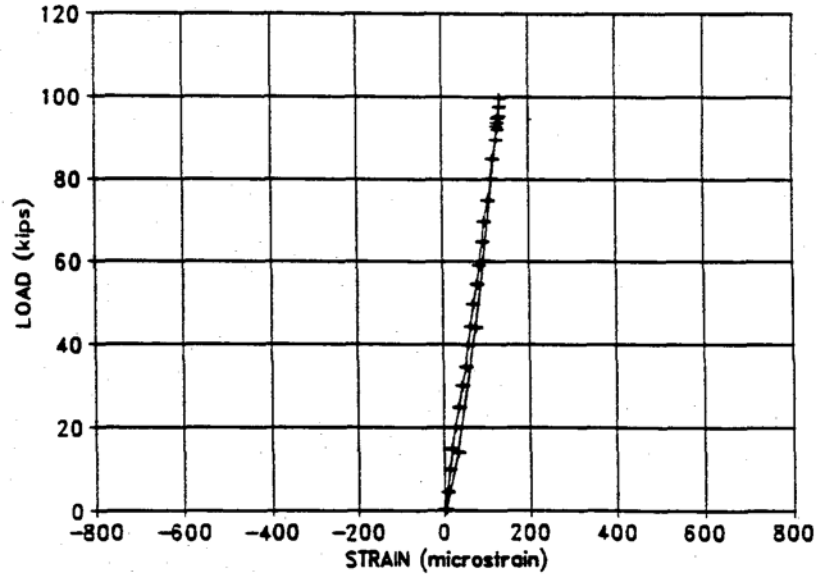

Figure B.42 Cracking Load Test, Load vs. Strain, Gauge 47.

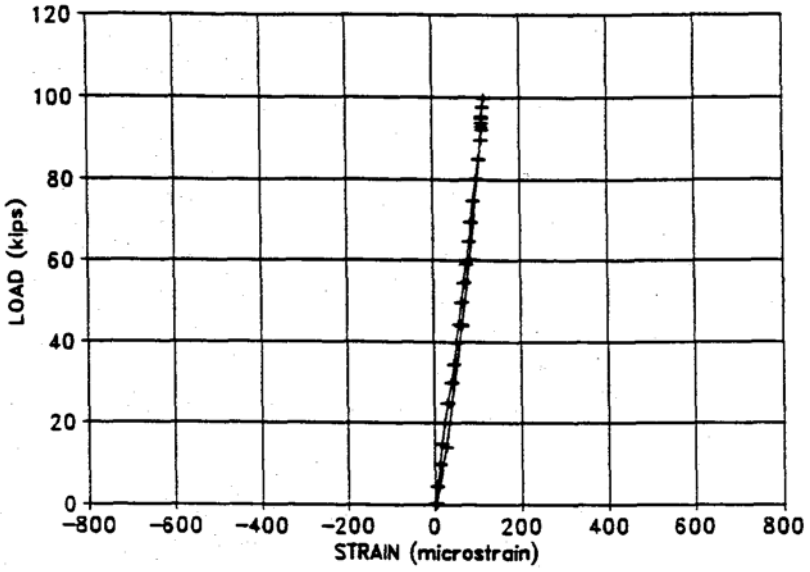

Figure B.43 Cracking Load Test, Load vs. Strain, Gauge 48.

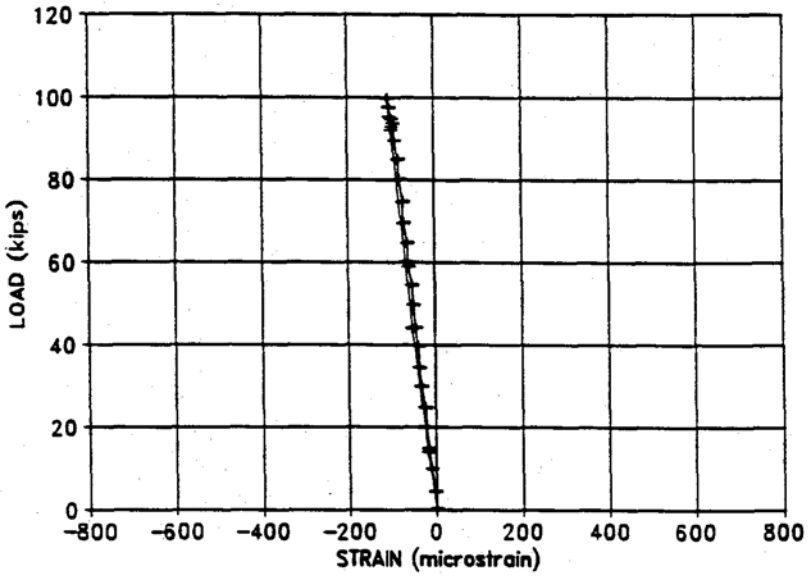

Figure B.44 Cracking Load Test, Load vs. Strain, Gauge 49.

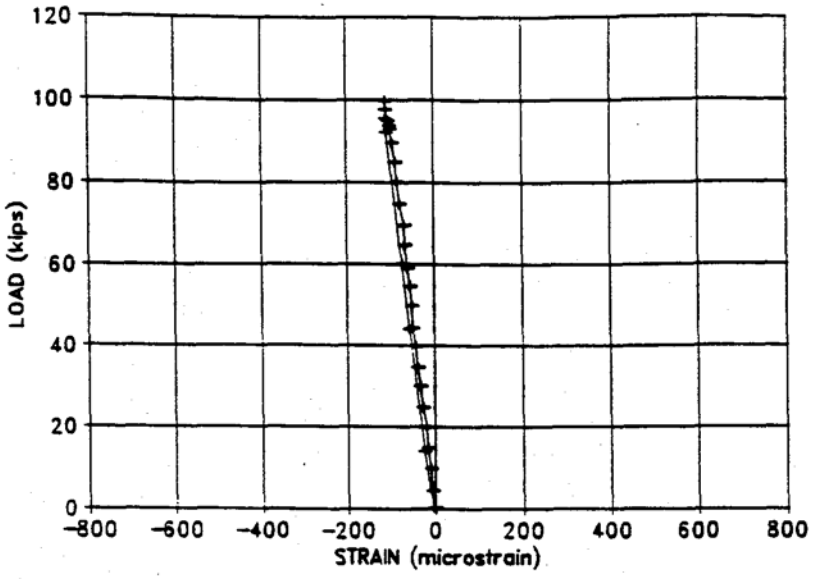

Figure B.45 Cracking Load Test, Load vs. Strain, Gauge 50.

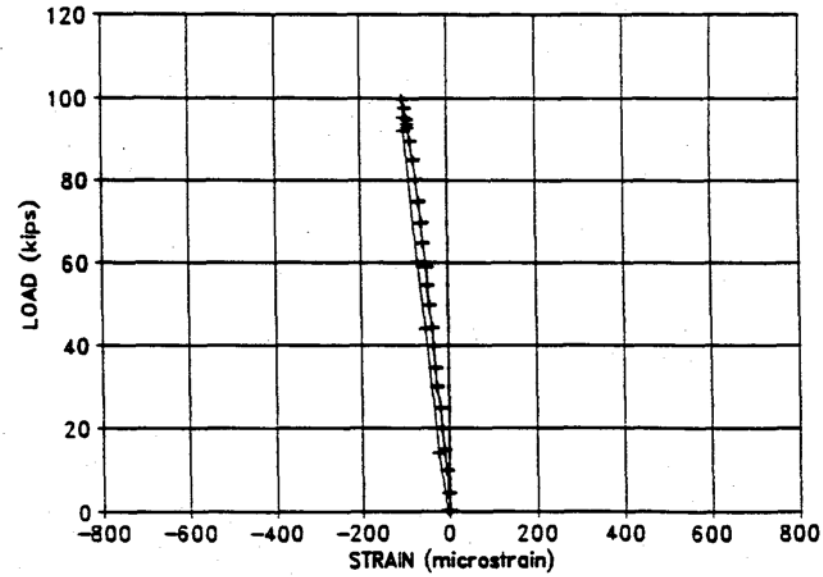

Figure B.46 Cracking Load Test, Load vs. Strain, Gauge 51.

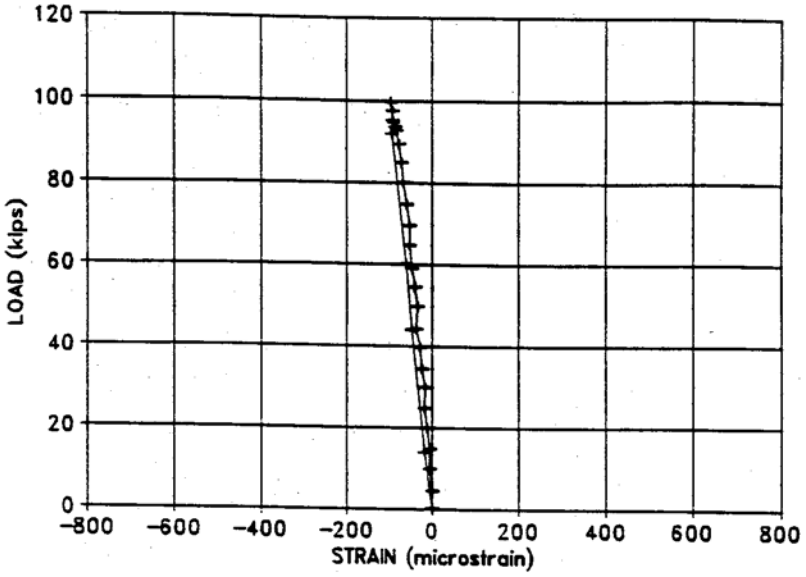

Figure B.47 Cracking Load Test, Load vs. Strain, Gauge 52.

APPENDIX C
ULTIMATE LOAD TEST

The following figures show the data collected for the ultimate load test. The LVDT data is arranged first with the strain gauge data following.

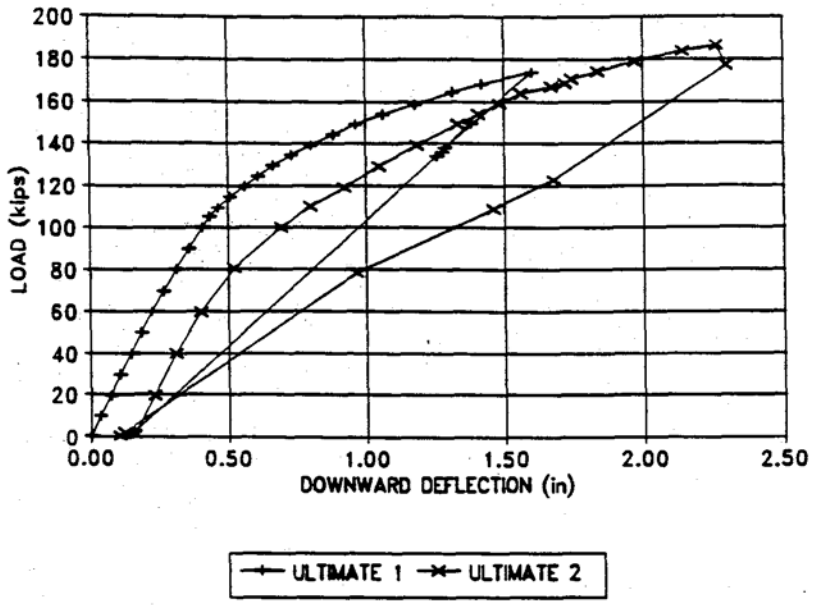

Figure C.1 Ultimate Load Test, Load vs. Deflection, LVDT 1.

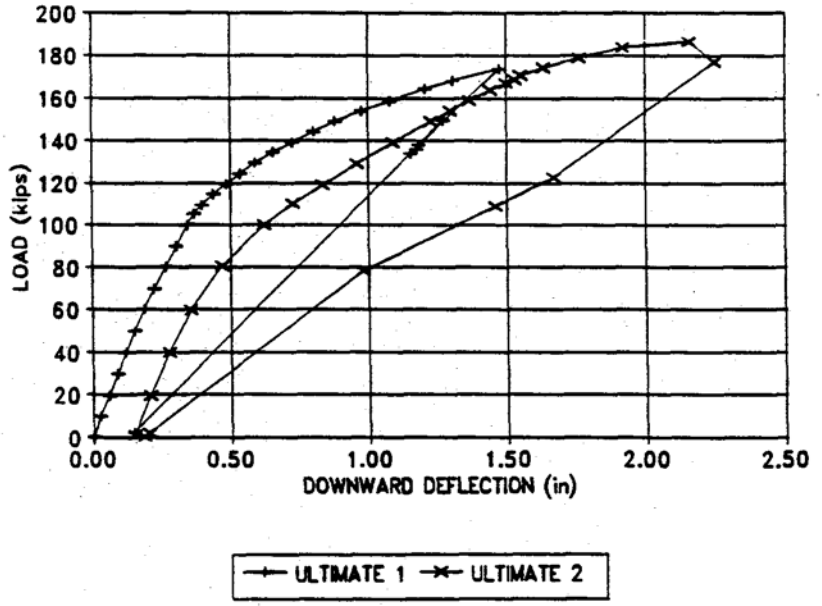

Figure C.2 Ultimate Load Test, Load vs. Deflection, LVDT 2.

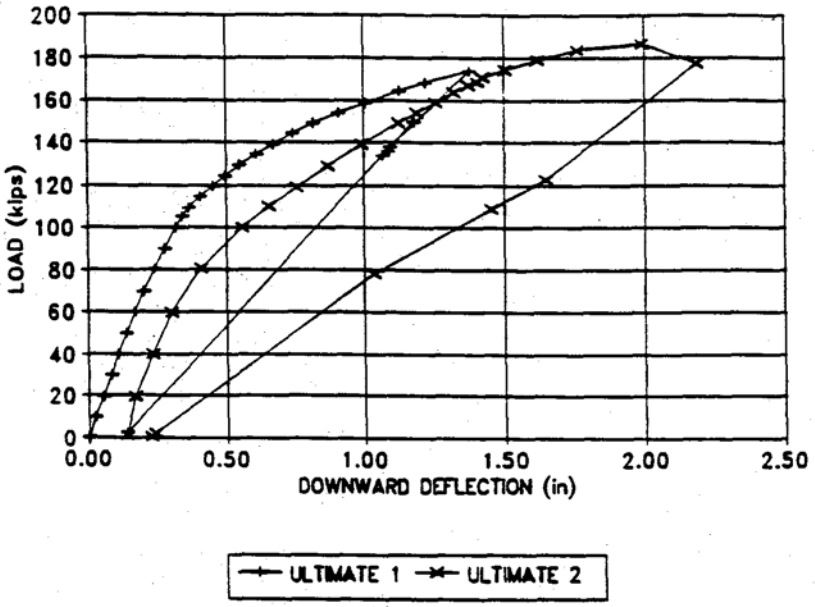

Figure C.3 Ultimate Load Test, Load vs. Deflection, LVDT 3.

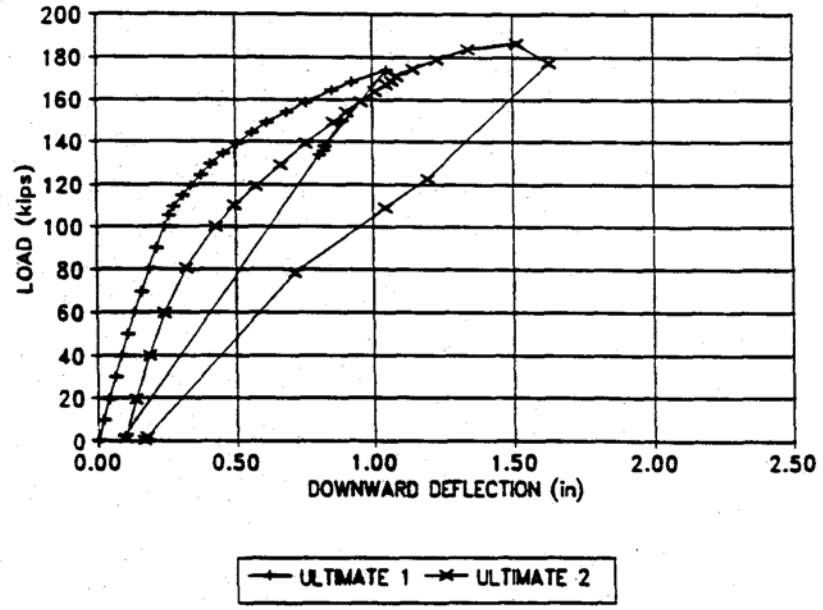

Figure C.4 Ultimate Load Test, Load vs. Deflection, LVDT 4.

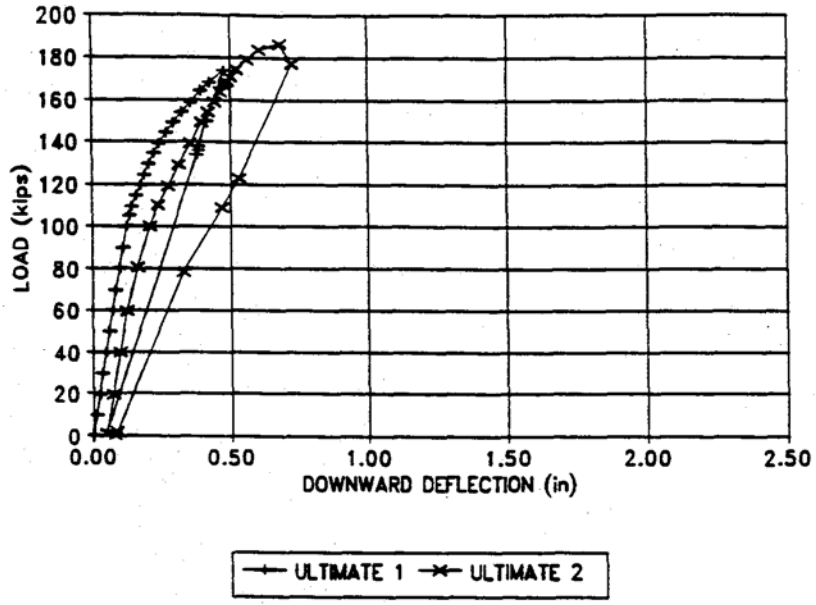

Figure C.5 Ultimate Load Test, Load vs. Deflection, LVDT 5.

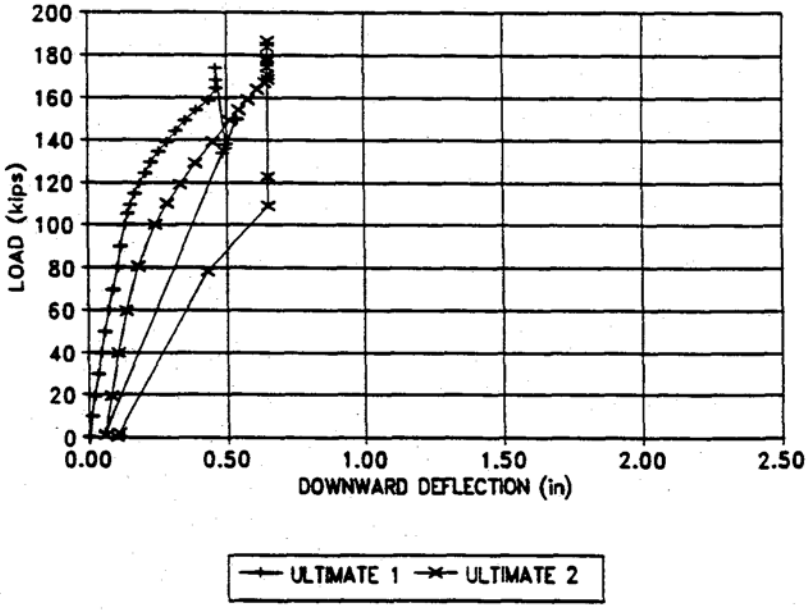

Figure C.6 Ultimate Load Test, Load vs. Deflection, LVDT 6.

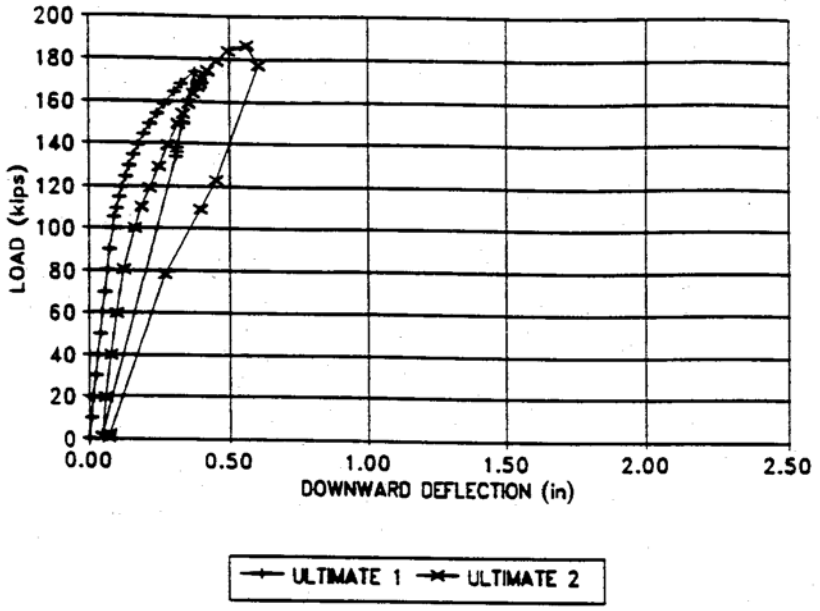

Figure C.7 Ultimate Load Test, Load vs. Deflection, LVDT 7.

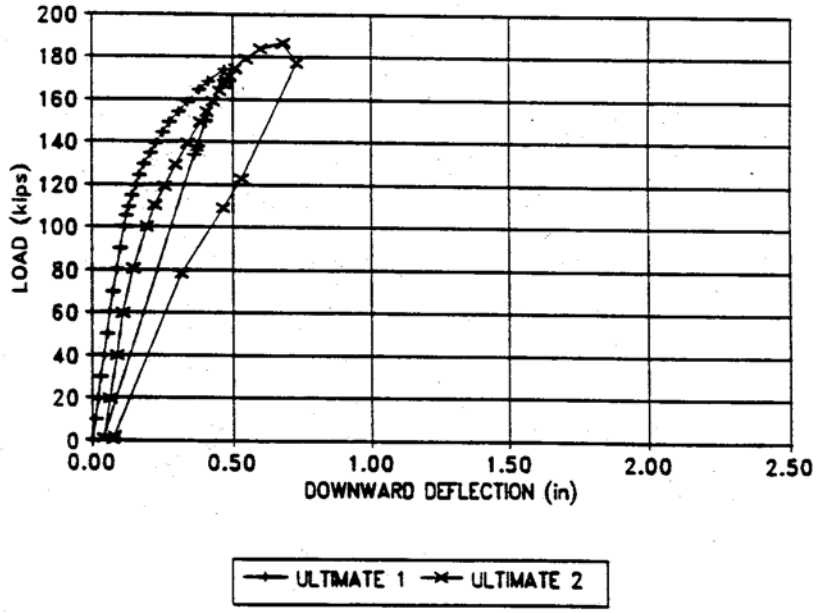

Figure C.8 Ultimate Load Test, Load vs. Deflection, LVDT 9.

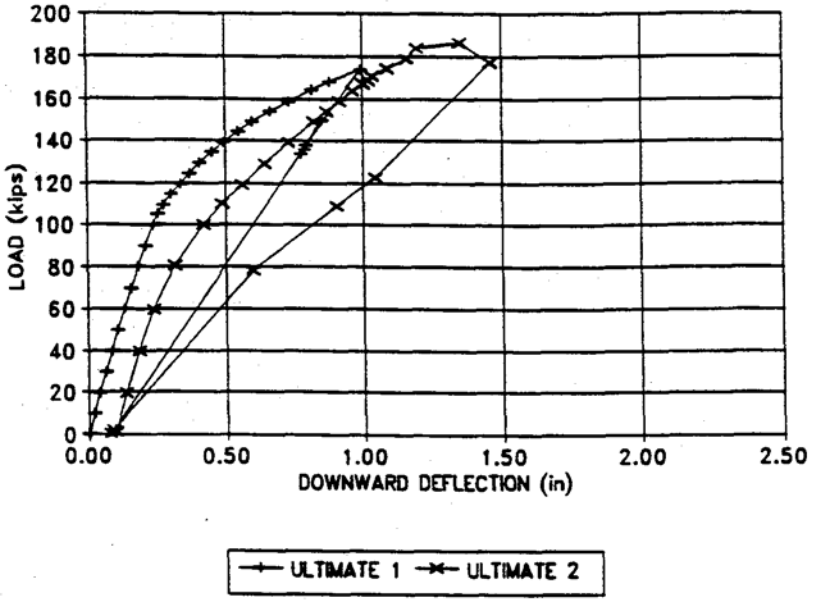

Figure C.9 Ultimate Load Test, Load vs. Deflection, LVDT 10.

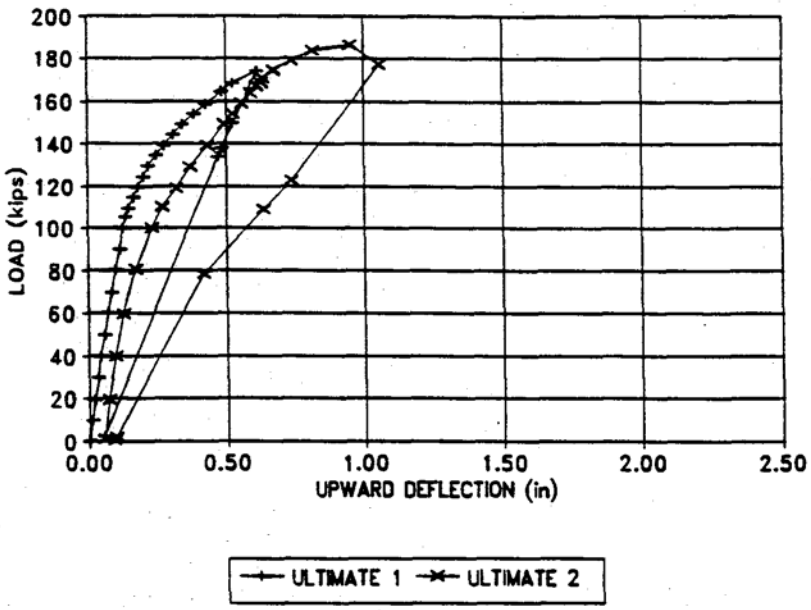

Figure C.10 Ultimate Load Test, Load vs. Deflection, LVDT 11.

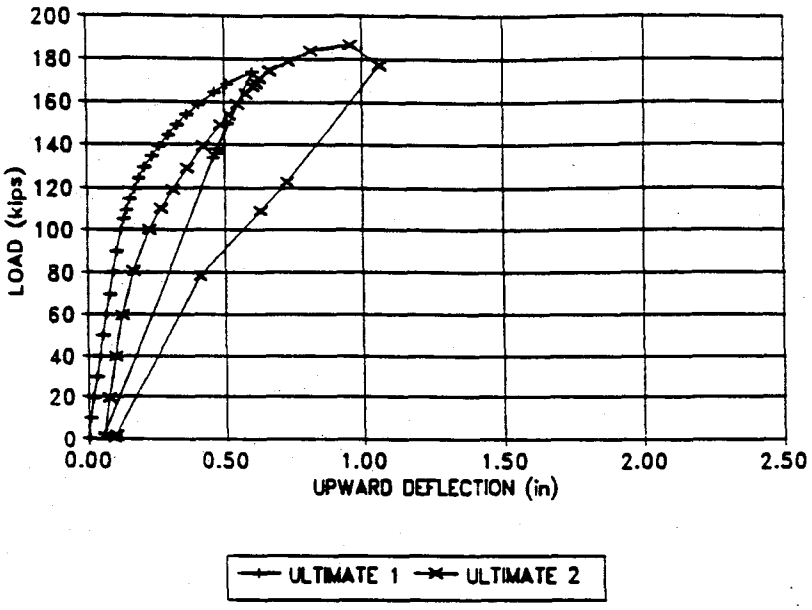

Figure C.11 Ultimate Load Test, Load vs. Deflection, LVDT 12.

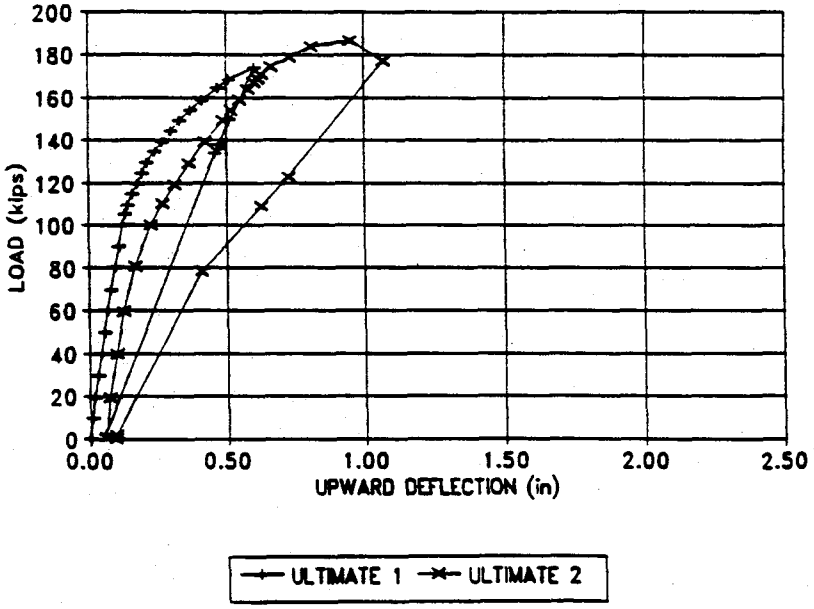

Figure C.12 Ultimate Load Test, Load vs. Deflection, LVDT 13.

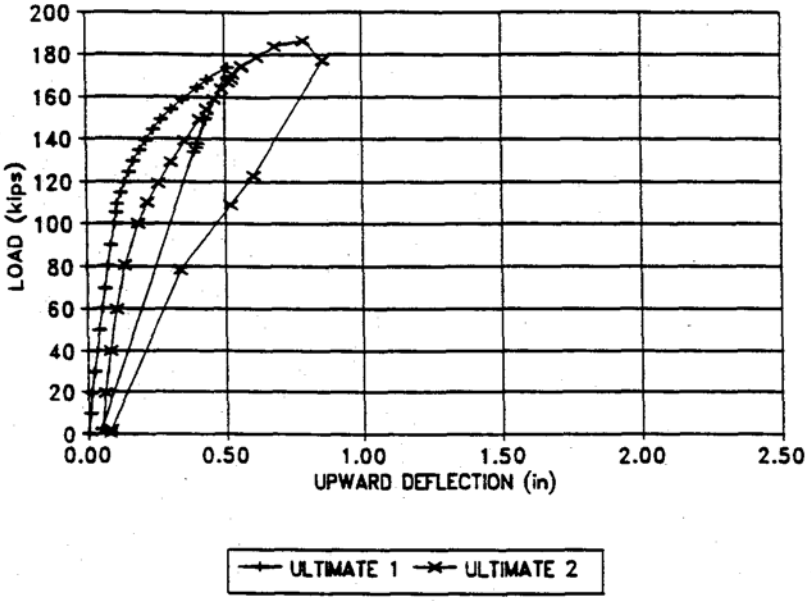

Figure C.13 Ultimate Load Test, Load vs. Deflection, LVDT 14.

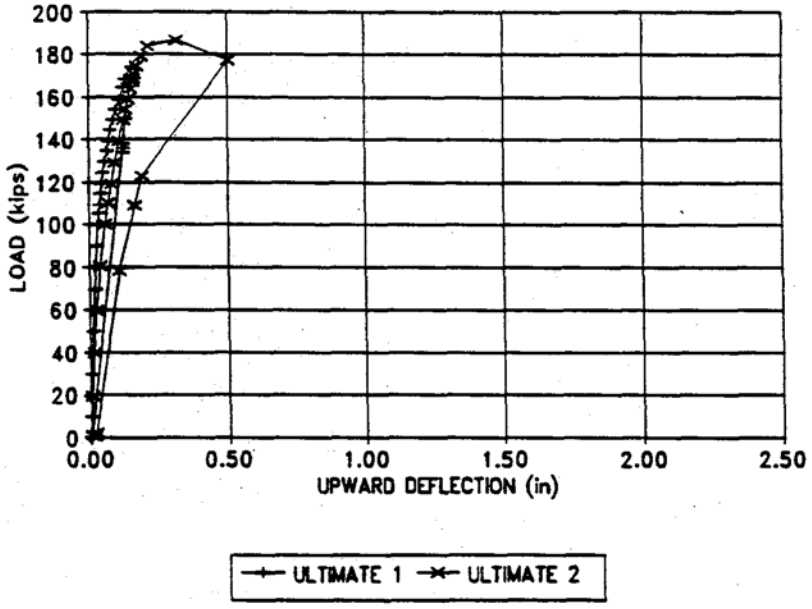

Figure C.14 Ultimate Load Test, Load vs. Deflection, LVDT 15.

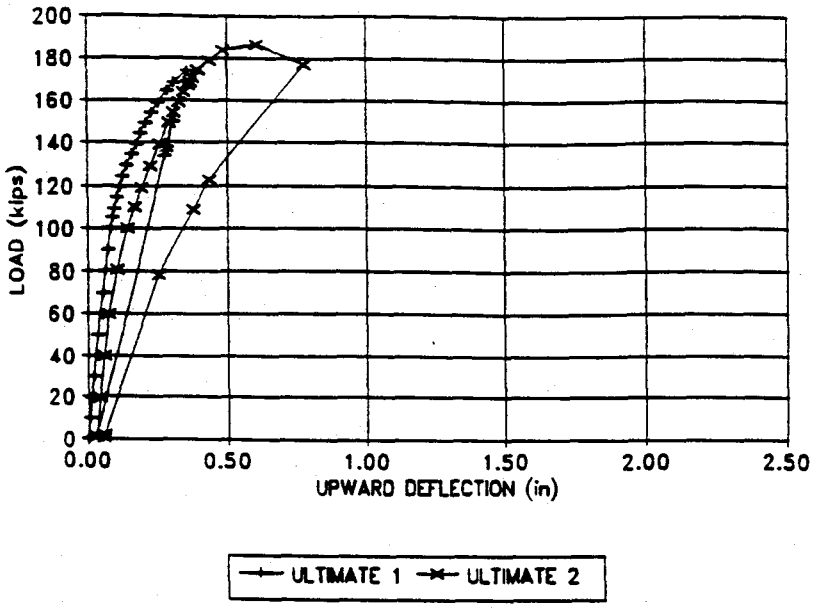

Figure C.15 Ultimate Load Test, Load vs. Deflection, LVDT 16.

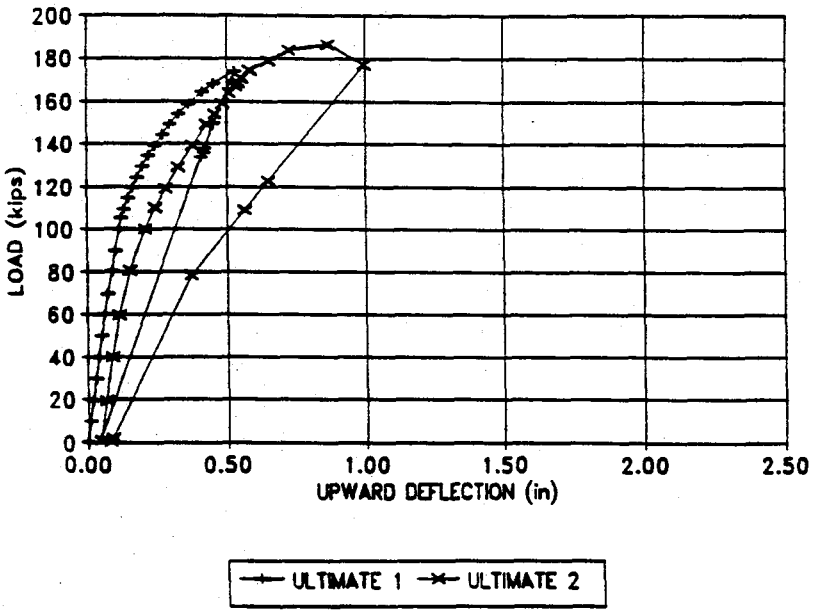

Figure C.16 Ultimate Load Test, Load vs. Deflection, LVDT 17.

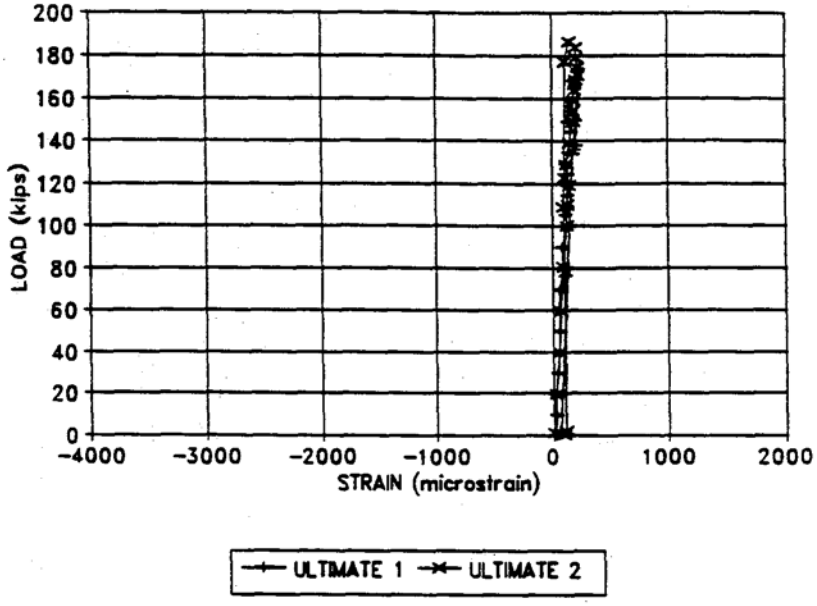

Figure C.17 Ultimate Load Test, Load vs. Strain, Gauge 1.

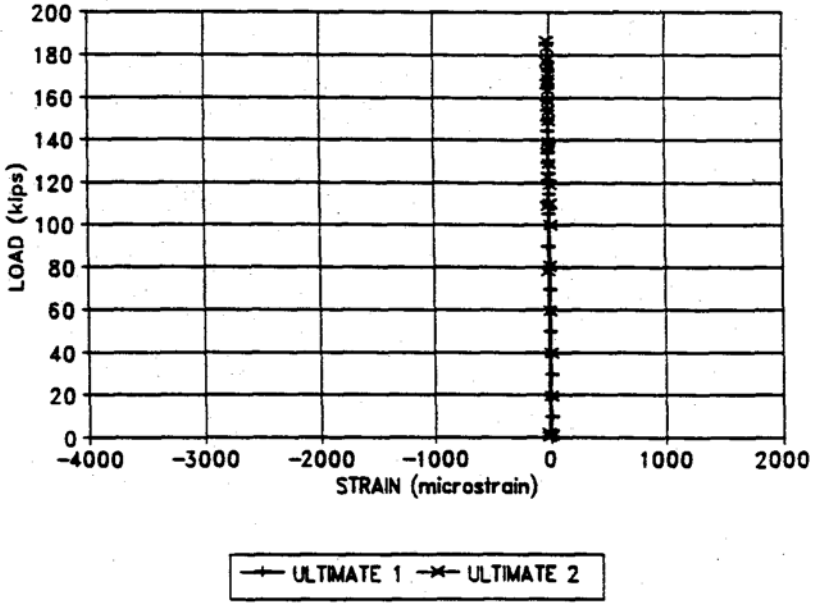

Figure C.18 Ultimate Load Test, Load vs. Strain, Gauge 2.

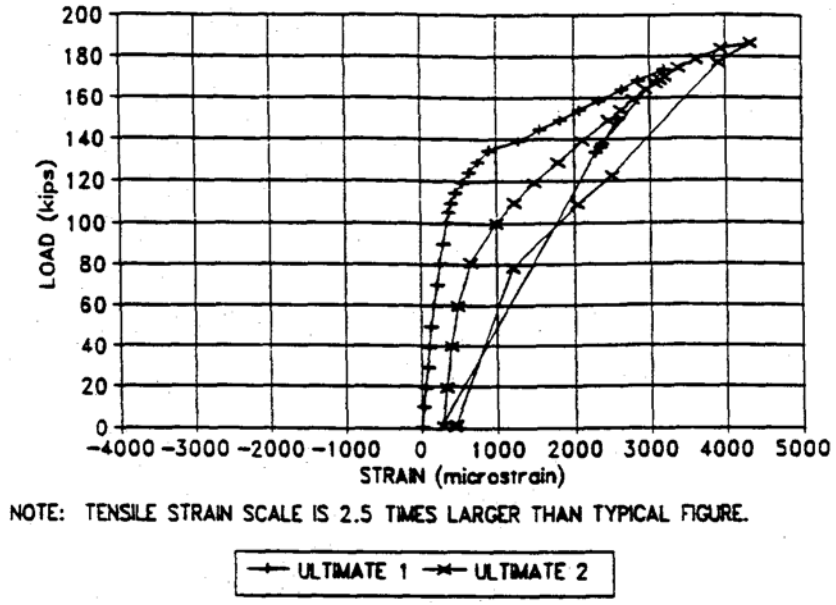

Figure C.19 Ultimate Load Test, Load vs. Strain, Gauge 3.

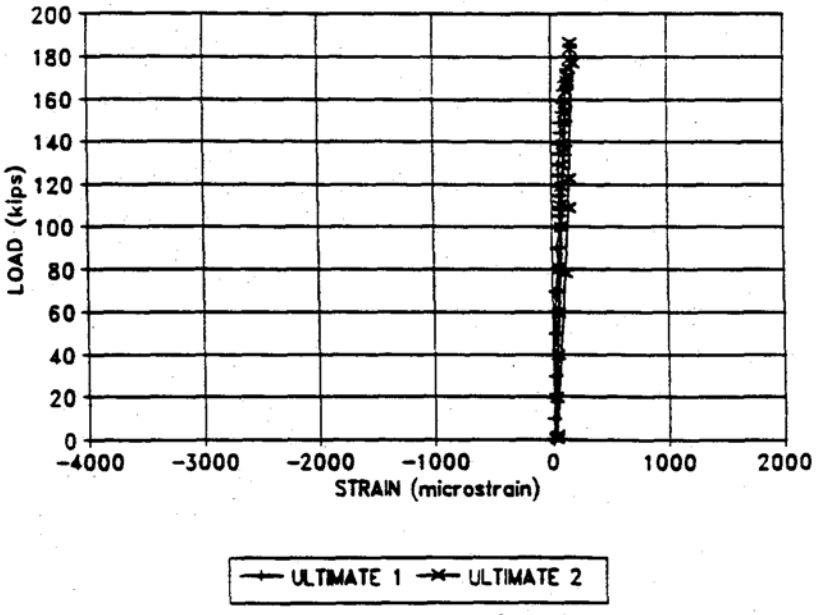

Figure C.20 Ultimate Load Test, Load vs. Strain, Gauge 4.

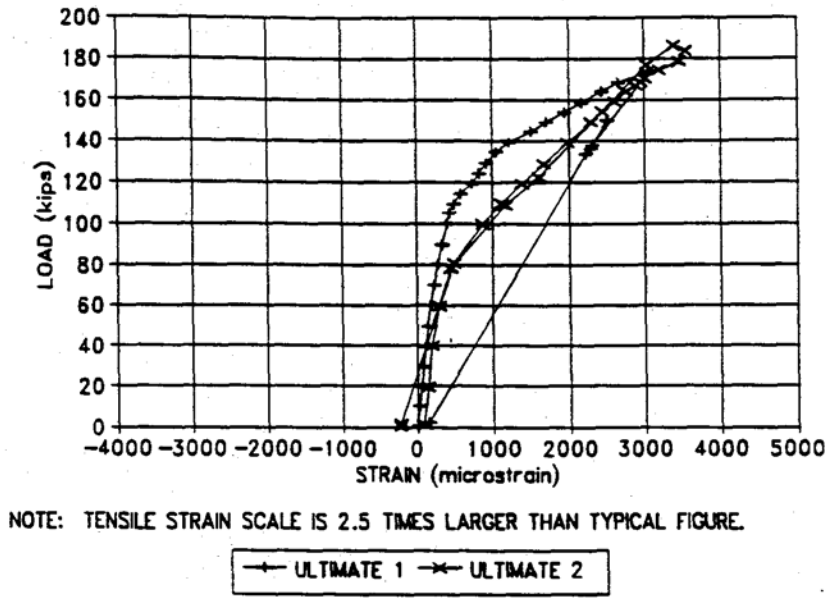

Figure C.21 Ultimate Load Test, Load vs. Strain, Gauge 5.

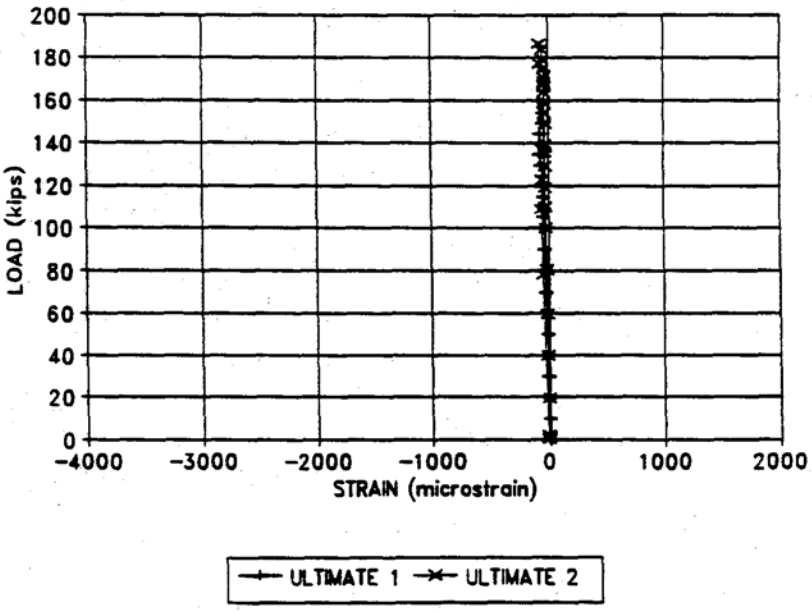

Figure C.22 Ultimate Load Test, Load vs. Strain, Gauge 6.

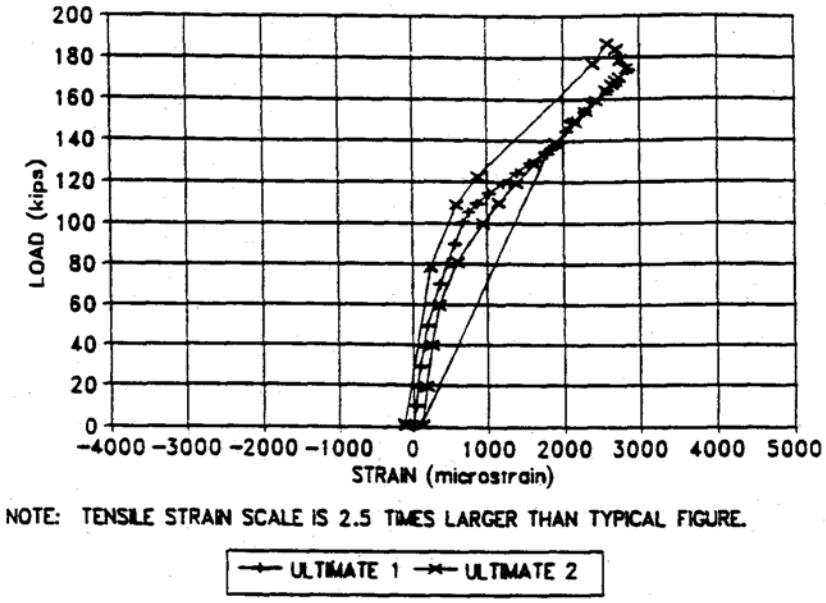

Figure C.23 Ultimate Load Test, Load vs. Strain, Gauge 7.

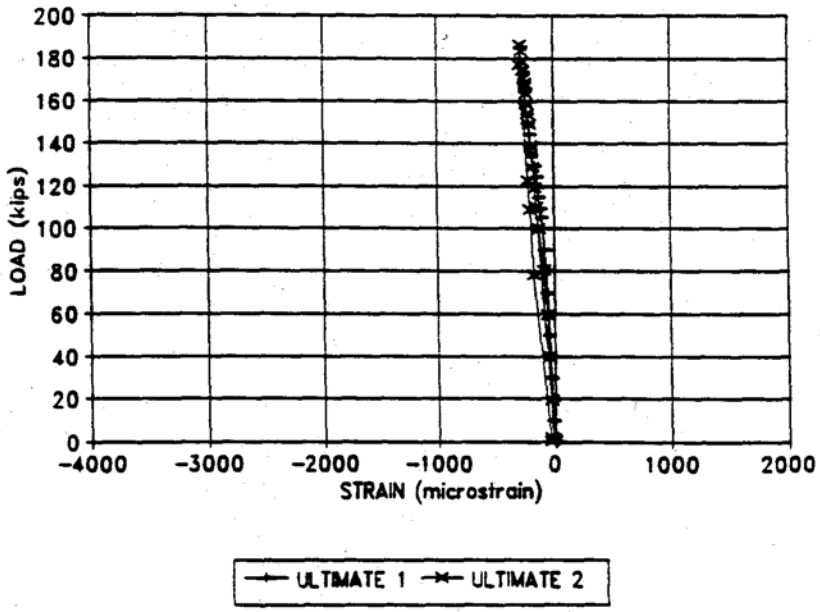

Figure C.24 Ultimate Load Test, Load vs. Strain, Gauge 8.

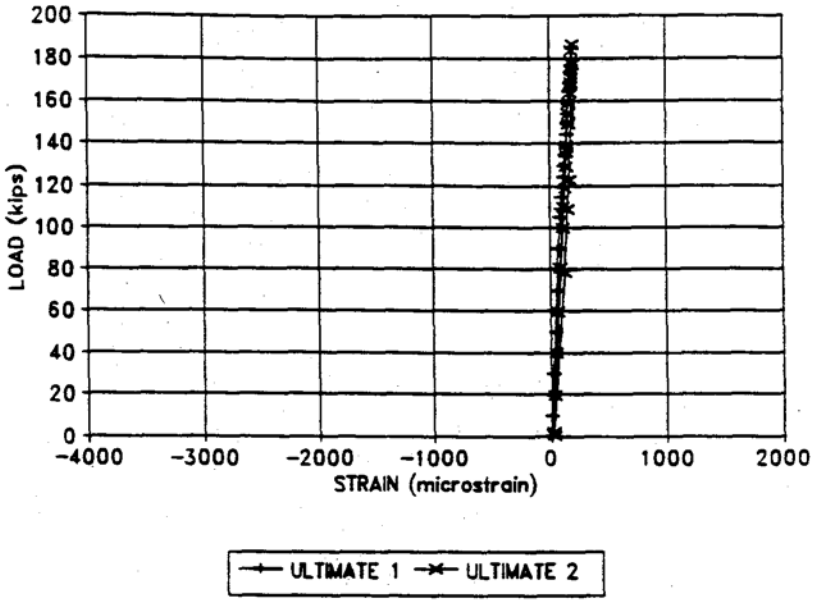

Figure C.25 Ultimate Load Test, Load vs. Strain, Gauge 9.

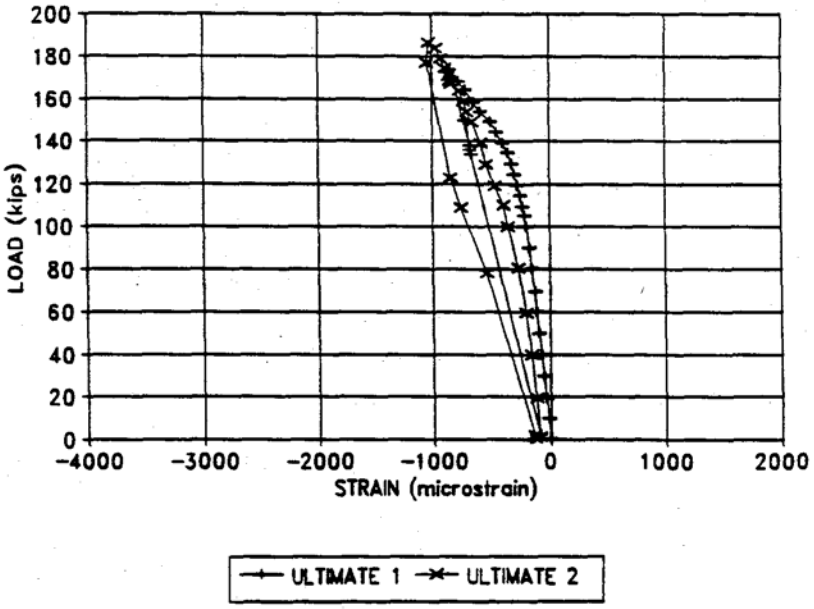

Figure C.26 Ultimate Load Test, Load vs. Strain, Gauge 18.

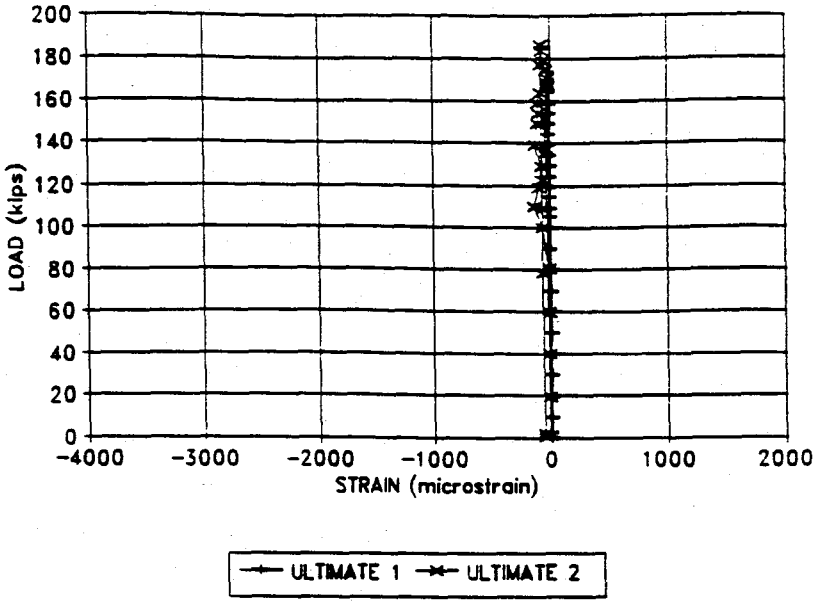

Figure C.27 Ultimate Load Test, Load vs. Strain, Gauge 31.

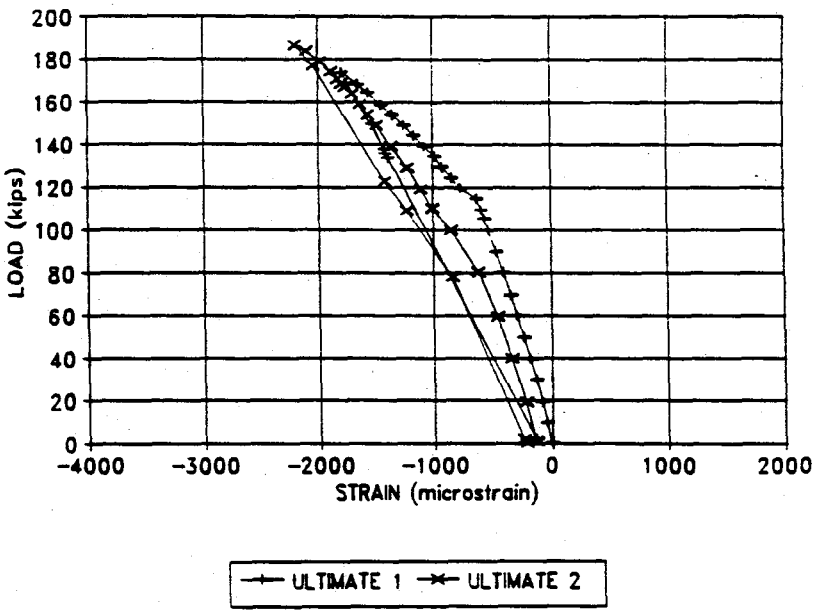

Figure C.28 Ultimate Load Test, Load vs. Strain, Gauge 32.

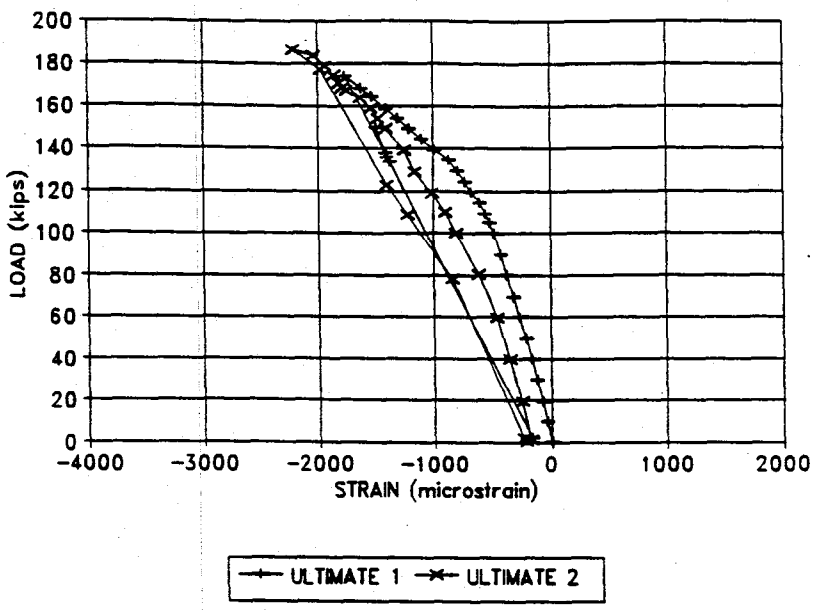

Figure C.29 Ultimate Load Test, Load vs. Strain, Gauge 33.

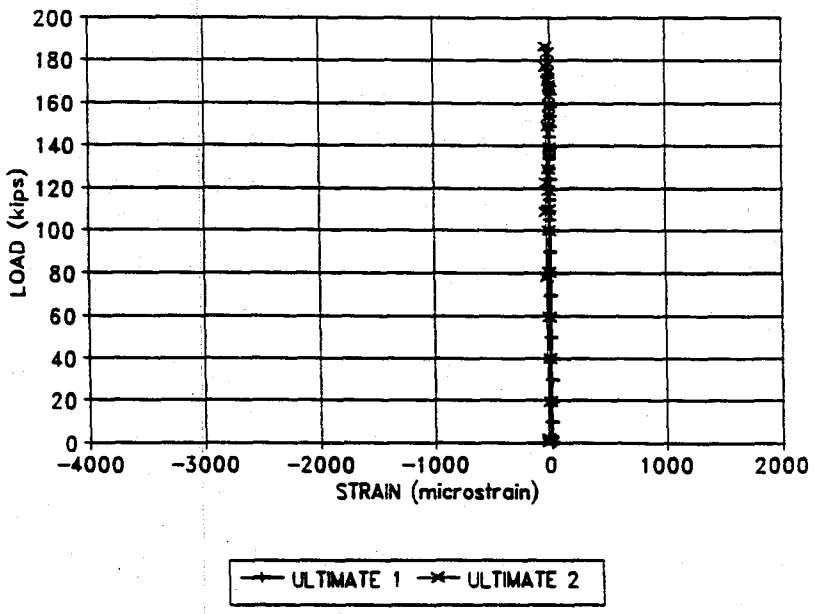

Figure C.30 Ultimate Load Test, Load vs. Strain, Gauge 34.

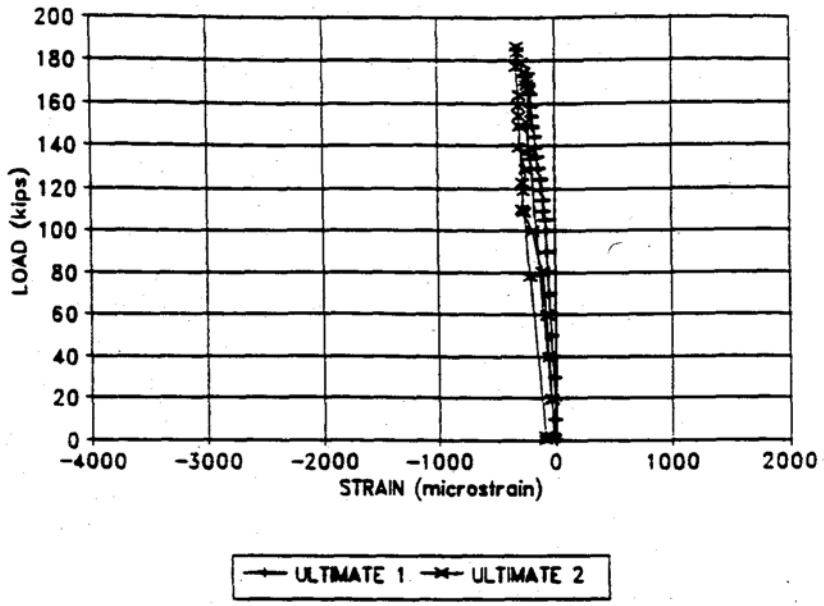

Figure C.31 Ultimate Load Test, Load vs. Strain, Gauge 35.

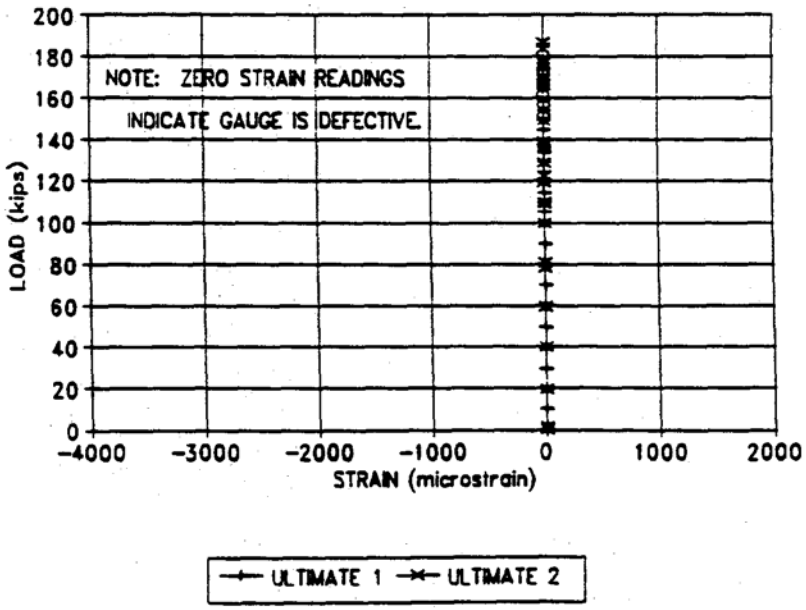

Figure C.32 Ultimate Load Test, Load vs. Strain, Gauge 36.

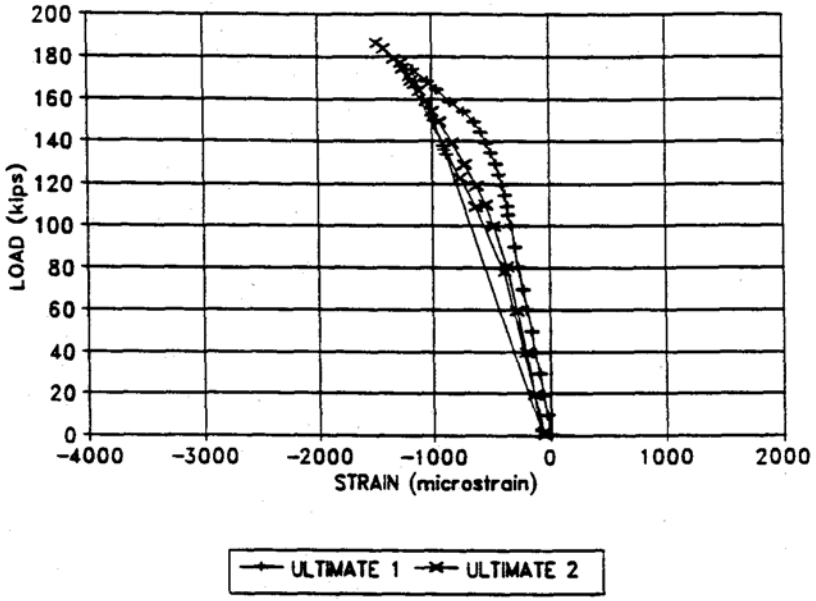

Figure C.33 Ultimate Load Test, Load vs. Strain, Gauge 37.

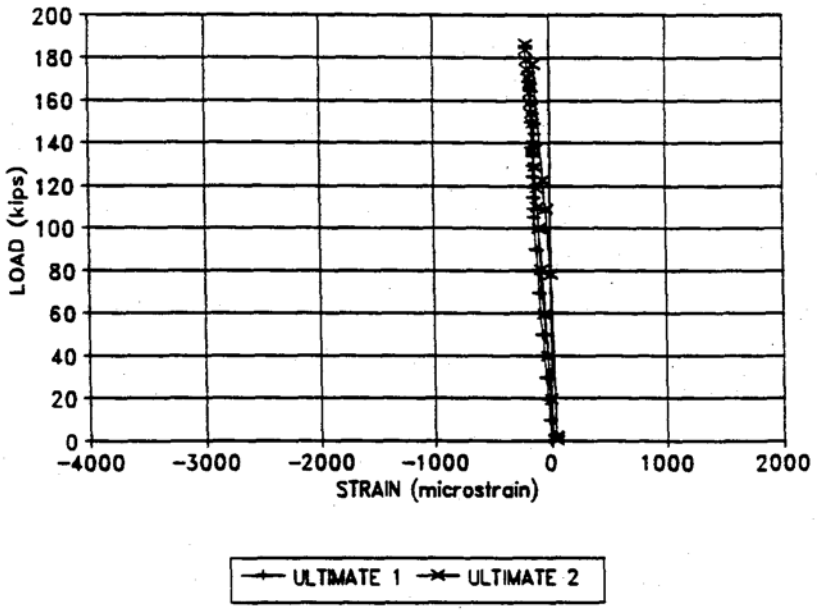

Figure C.34 Ultimate Load Test, Load vs. Strain, Gauge 38.

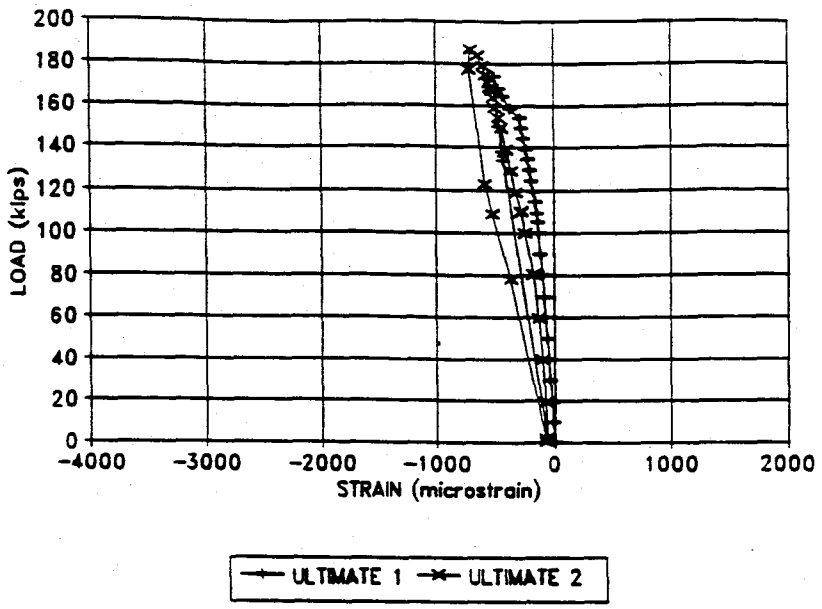

Figure C.35 Ultimate Load Test, Load vs. Strain, Gauge 39.

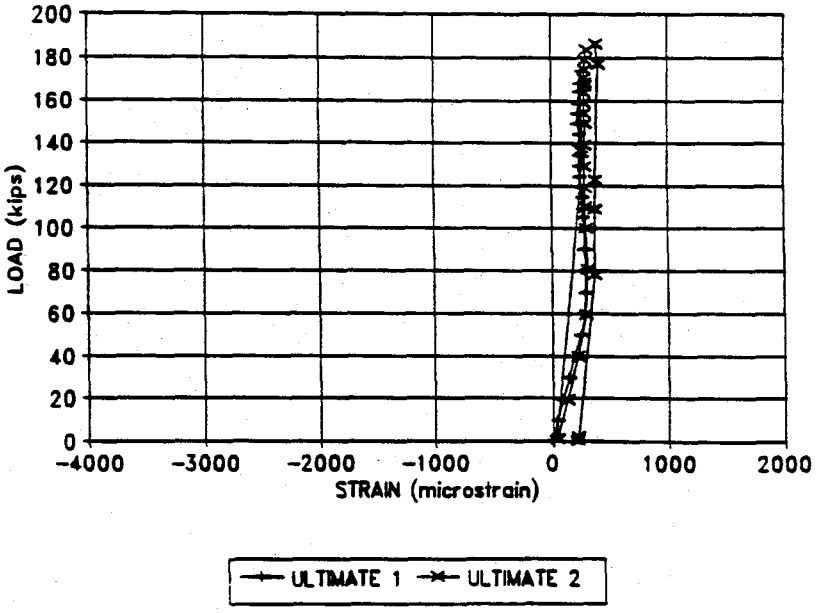

Figure C.36 Ultimate Load Test, Load vs. Strain, Gauge 40.

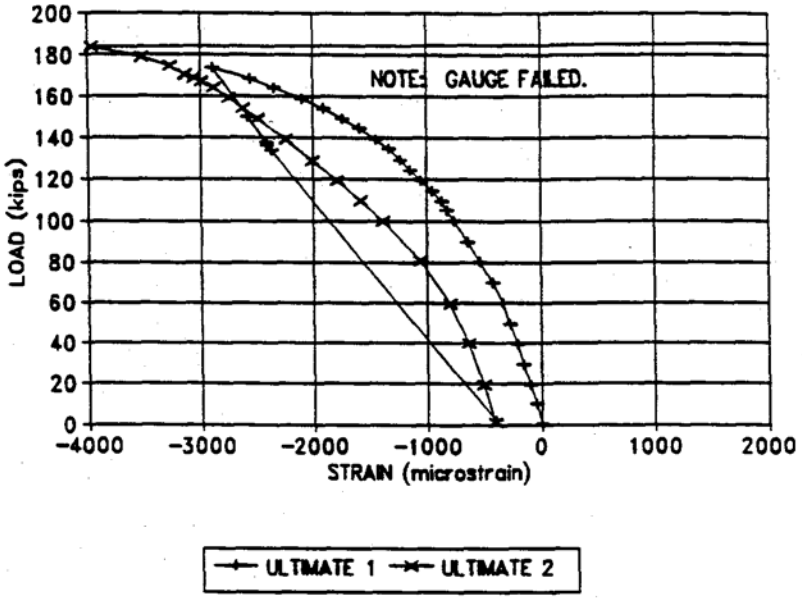

Figure C.37 Ultimate Load Test, Load vs. Strain, Gauge 42.

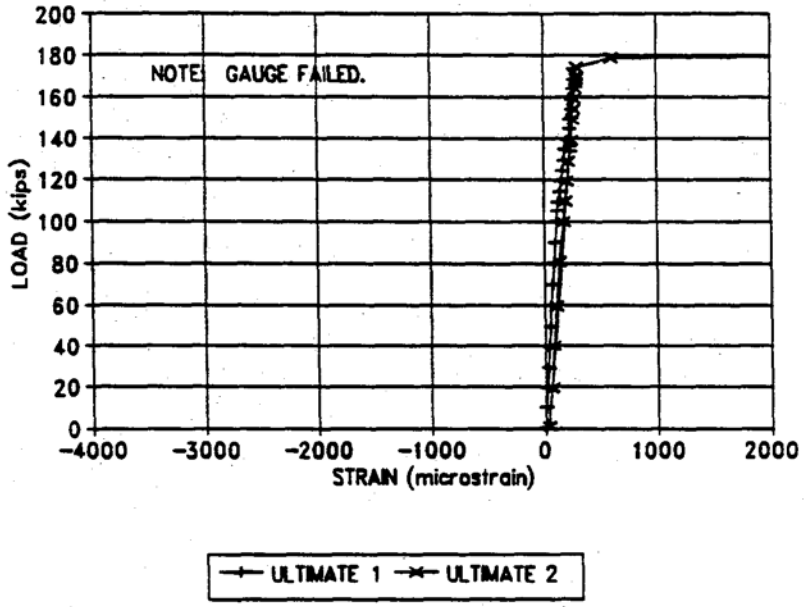

Figure C.38 Ultimate Load Test, Load vs. Strain, Gauge 43.

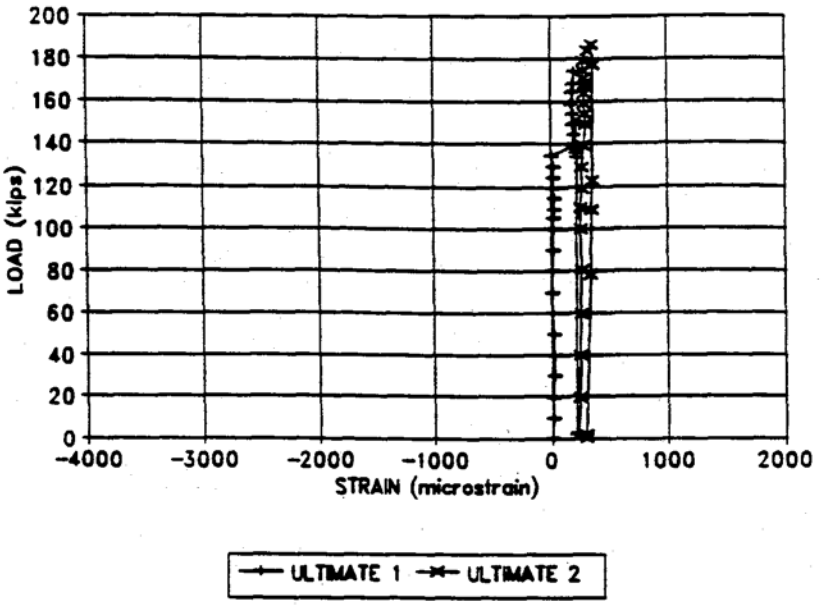

Figure C.39 Ultimate Load Test, Load vs. Strain, Gauge 44.

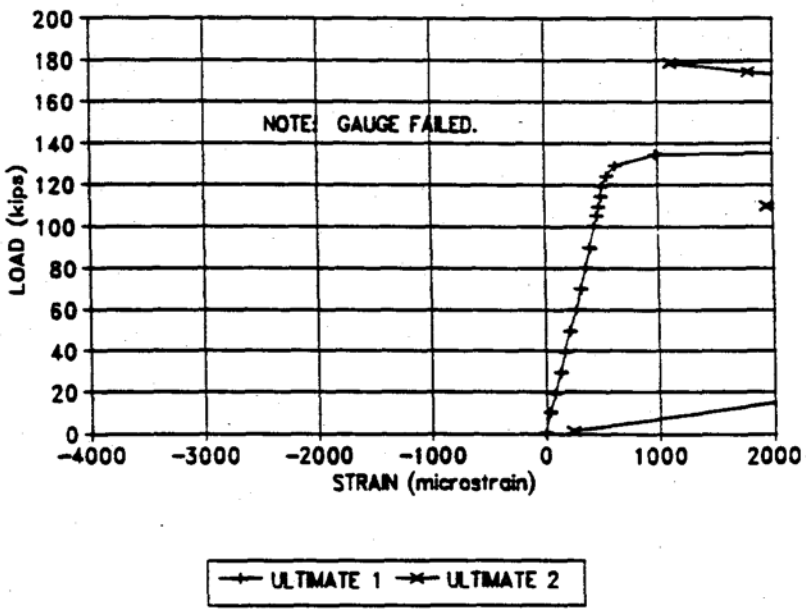

Figure C.40 Ultimate Load Test, Load vs. Strain, Gauge 45.

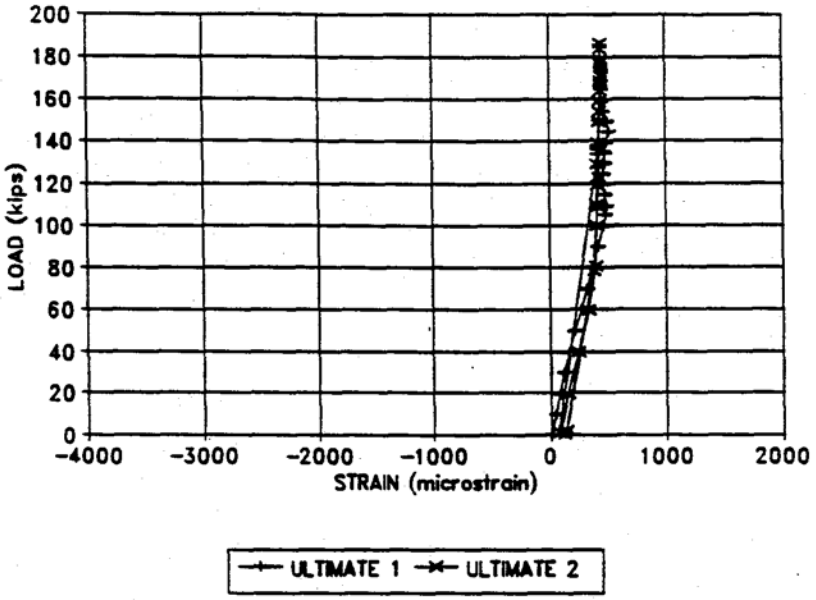

Figure C.41 Ultimate Load Test, Load vs. Strain, Gauge 46.

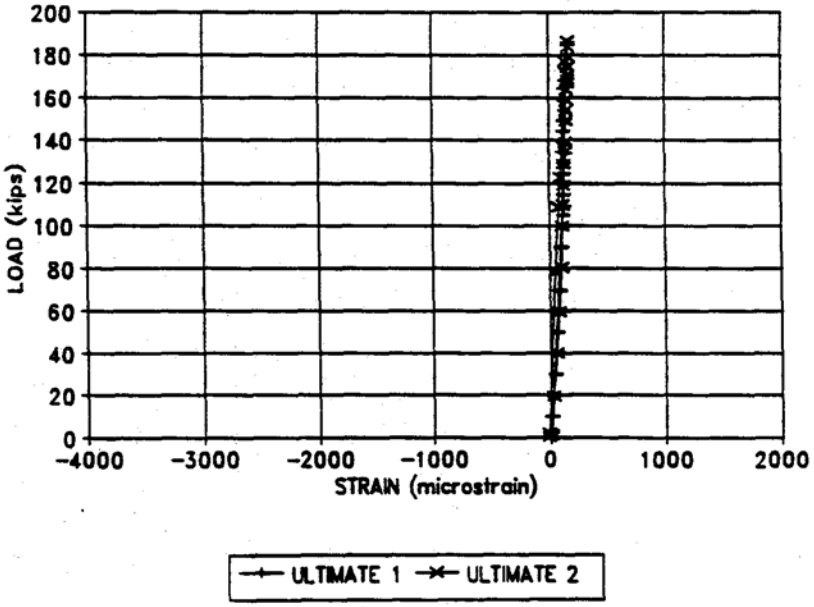

Figure C.42 Ultimate Load Test, Load vs. Strain, Gauge 47.

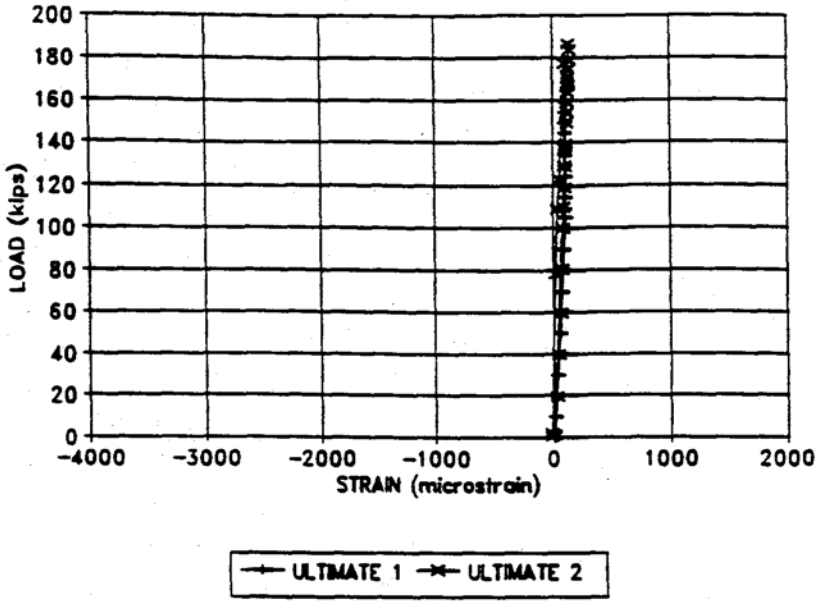

Figure C.43 Ultimate Load Test, Load vs. Strain, Gauge 48.

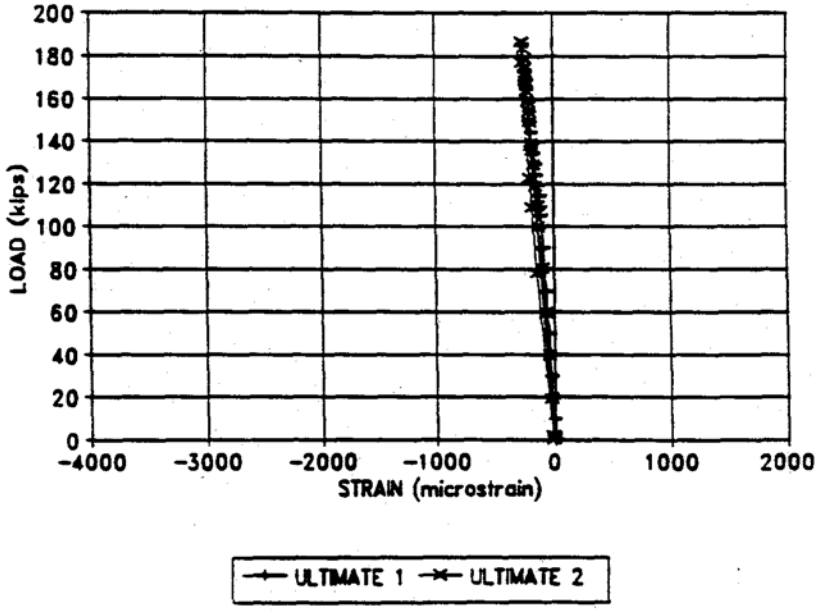

Figure C.44 Ultimate Load Test, Load vs. Strain, Gauge 49.

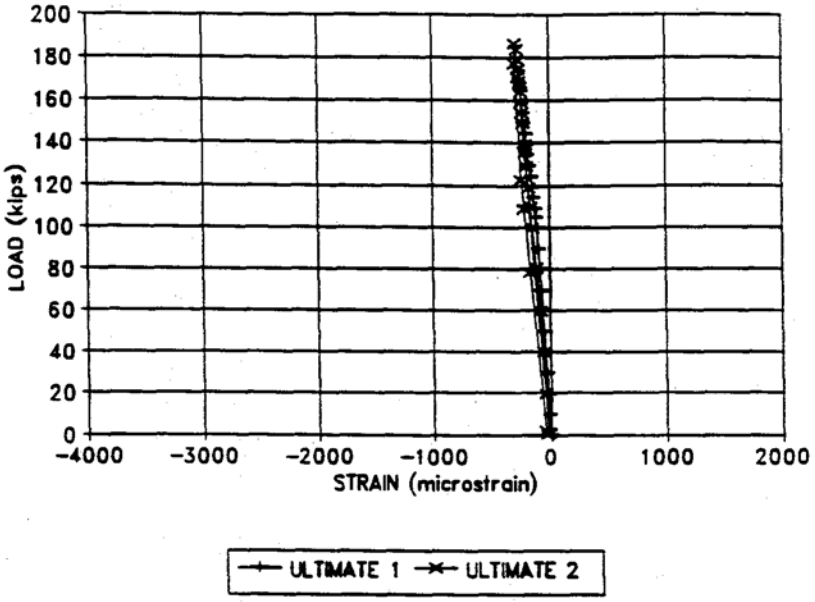

Figure C.45 Ultimate Load Test, Load vs. Strain, Gauge 50.

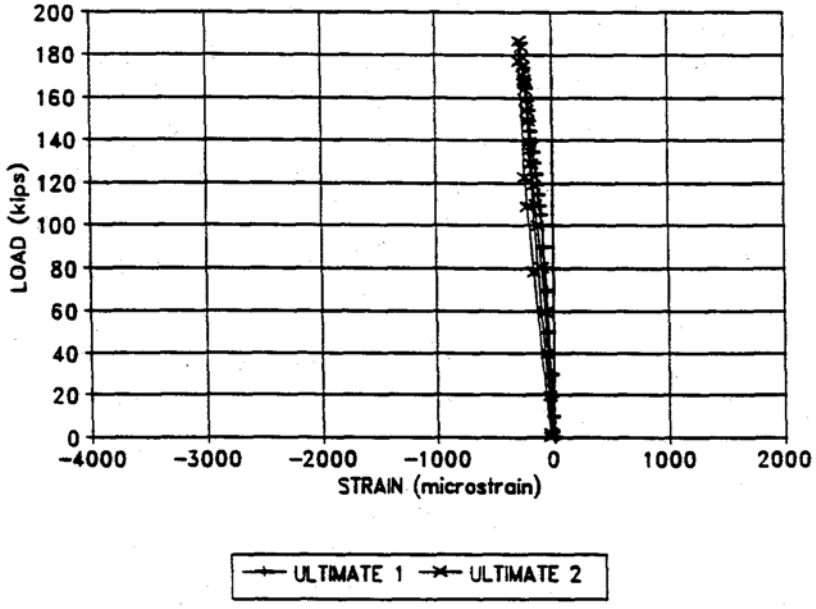

Figure C.46 Ultimate Load Test, Load vs. Strain, Gauge 51.

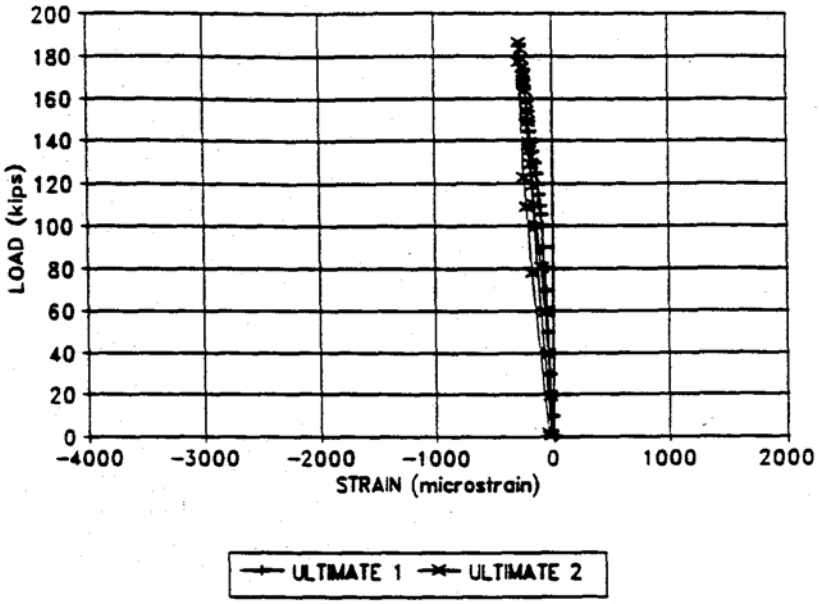

Figure C.47 Ultimate Load Test, Load vs. Strain, Gauge 52.

REFERENCES

1. H. Carr and M. May, "A Sound Investment: Trestle at $23 per Sq. Ft.," *Engineering News Record*, Vol. 221 No. 8, August 25, 1988, pp. 30-31.

2. R. A. Cook, F. E. Fagundo, B. A. Munson, B. M. Schafer, and D. E. Richardson, "Analytical and Experimental Evaluation of a Precast, Post-Tensioned, Segmental Flat Slab Bridge System for Service Loads," *Structures and Materials Research Report No. 91-2*, University of Florida, Gainesville, Florida, June 1991.

3. American Association of State Highway and Transportation Officials, *Standard Specifications for Highway Bridges: Interim Specifications-Bridges-1990*, Fourteenth Edition, Washington D. C., 1990.

4. E. L. Wilson and A. Habibullah, *SAP90 A Series of Computer Programs for the Static and Dynamic Finite Element Analysis of Structures*, Computers & Structures, Inc., Berkeley, California, 1989.

5. H. Mayer, "Analytical and Experimental Evaluation of a Precast, Post-Tensioned, Segmental Flat Slab Bridge System for Service Level Fatigue Loading," Master's Thesis presented to the Department of Civil Engineering, University of Florida, Gainesville, Florida, August 1992.

6. T. Y. Lin and N. H. Burns, *Design of Prestressed Concrete Structures*, Third Edition, John Wiley & Sons, New York, 1981.